Durham University

Durham E-Theses

The interactions of anti-nucleons in complex nuclei

Khan, Naseer Ahmad

How to cite:

Khan, Naseer Ahmad (1965) *The interactions of anti-nucleons in complex nuclei*, Durham theses, Durham University. Available at Durham E-Theses Online: http://etheses.dur.ac.uk/8726/

Use policy

The full-text may be used and/or reproduced, and given to third parties in any format or medium, without prior permission or charge, for personal research or study, educational, or not-for-profit purposes provided that:

- a full bibliographic reference is made to the original source
- a link is made to the metadata record in Durham E-Theses
- the full-text is not changed in any way

The full-text must not be sold in any format or medium without the formal permission of the copyright holders.

Please consult the full Durham E-Theses policy for further details.

Academic Support Office, The Palatine Centre, Durham University, Stockton Road, Durham, DH1 3LE
e-mail: e-theses.admin@durham.ac.uk Tel: +44 0191 334 6107
http://etheses.dur.ac.uk

The Interactions of Anti-Nucleons

in

Complex Nuclei

A thesis presented by

Naseer Ahmad Khan

for the

Degree of Doctor of Philosophy

at the

University of Durham

April 1965

16 FEB 1966
LIBRARY

CONTENTS

		Page
PREFACE		i
LIST OF FIGURES		ii
LIST OF TABLES		v
INTRODUCTION		1
CHAPTER 1	Review of the Interactions of Antinucleons	5
1.1	The Production of Antinucleons	5
1.1.1	Antiprotons	5
1.1.2	Antineutrons	6
1.2	The Properties of Antinucleons	7
1.3	The Interactions of Antinucleons	8
1.3.1	Interaction cross-sections of antiprotons	8
1.3.2	Antiproton-nucleus cross-sections	13
1.3.3	Antiproton-neutron cross-sections	13
1.4	The Charge Exchange of Antiprotons	15
1.5	The Annihilation Process	18
1.5.1	Pion multiplicities and energy spectra	22
1.5.2	Estimation of neutral pions emitted in $\bar{N}N$ annihilation	22
1.5.3	Strange particle production	25
1.5.4	Pion-pion correlations	27

Page

1.6 The Selection Rules involved in Annihilation 28

1.6.1 Selection rules for antiproton-nucleon annihilation and the multipion resonances 28

1.6.2 Selection rules and annihilation in complex nuclei 33

CHAPTER 2 The Antiproton-Nucleon Annihilation 35

2.1 The Interactions of Antiprotons in Flight 35

2.1.1 Annihilation in flight in nuclear emulsion 37

2.1.2 Relative probabilities of annihilation in flight on neutrons and protons of emulsion nuclei 38

2.2 The Annihilations of Antiprotons at Rest 39

2.2.1 Process of absorption and annihilation in complex nuclei 39

2.2.2 Relative probabilities of annihilation at rest on neutrons and protons 42

2.2.3 Annihilation at rest in deuterium 45

2.3 The Experimental Set-up 47

2.3.1 Exposure of the emulsion stack 47

2.3.2 Scanning for annihilation stars 48

2.3.3 The classification of annihilation stars 49

		Page
2.4	Annihilation in the Light Elements	49
	2.4.1 Probabilities of absorption by hydrogen in the emulsion	52
2.5	Results	54
	2.5.1 The neutron/proton ratio for white stars	55
	2.5.2 The relative importance of T = 1 and T = 0 channels	57
	2.5.3 Characteristics of black stars	58
2.6	The Calculation of the Effects of Secondary Interactions	59
	2.6.1 Effects of charge exchange	59
	2.6.2 Effects of absorption	60
	2.6.3 Comparison of observed and calculated multiplicities	61
2.7	Conclusions	62
CHAPTER 3	General Features of Antiproton Annihilation at Rest	63
3.1	Average Number of Secondary Pions Interacting Inside the Parent Nucleus	63
3.2	The Absorption Probability Calculated from the Number of Pions that have Interacted	64
3.3	Average Pion Multiplicity	67
3.4	Correlation of Charged Pion Multiplicity and the Number of Heavily Ionising Particles	67

Page

3.4.1 Relation between shower and grey tracks 67

3.4.2 Relation between shower and black tracks 68

3.4.3 Relation between grey and black tracks 69

3.4.4 Variation of mean number of pions with grey and black track multiplicity 70

3.5 Size Distribution of Annihilation Stars 72

3.6 Momentum Distribution of Recoiling Nuclei 73

3.6.1 Measurement of recoil tracks 75

3.6.2 Discussion and interpretation 78

3.7 Conclusions 80

CHAPTER 4 The Production and Annihilation of Anti-neutrons in an Emulsion Stack 81

4.1 Production 81

4.1.1 Production in hydrogen 81

4.1.2 Production in complex nuclei 82

4.1.3 Production in the emulsion stack 84

4.2 Scanning for Antineutron Stars 86

4.3 Contamination 86

4.3.1 Contamination from cosmic rays 88

4.4 Selection Criteria 89

4.5 Results 94

4.5.1 Multiplicity distribution of anti-neutron annihilations 95

Page

4.5.2 Measurements in the enriched sample of stars 96

4.5.3 Cross-section for charge exchange 97

4.6 Conclusions 98

CHAPTER 5 Comparison of Meson Multiplicities with the Predictions of Theories of Nucleon-Anti-nucleon Annihilation 99

5.1 General Features of Annihilation at Rest 99

5.2 Fermi's Statistical Theory 99

5.3 The Theory of Koba and Takeda 103

5.4 Summary of the Models of Meson Production 105

5.4.1 Multiplicity of charged pions in annihilation at rest 105

5.4.2 Variation of mean multiplicities of mesons with the energy of antiprotons 105

5.5 Comparison with Experimental Results 106

ACKNOWLEDGMENTS 110

APPENDIX A.1 111

APPENDIX A.2 113

APPENDIX A.3 116

APPENDIX A.4 117

REFERENCES 118

PUBLICATIONS BY THE AUTHOR 123

ABSTRACT

The interactions of antinucleons in complex nuclei of emulsion have been studied. The three main lines of investigation are the following:

1) The annihilation at rest of antiprotons in the complex nuclei of emulsion has been studied and a method has been devised of separating the annihilations in the light and the heavy elements. By identifying the annihilations on the neutrons and protons in light elements it is shown that the ratio of the probabilities of annihilation of antiprotons on the two nucleons is the same, in contrast to earlier work in this field. This implies that annihilation proceeds equally through the singlet and triplet isospin channels. The apparent departures from this result for heavy elements have been accounted for by the secondary interactions of the annihilation products in the parent nuclei.

2) The antiproton is used as a nuclear probe to determine the distribution of momenta of the nucleons of light elements such as carbon. It is found that the momenta follow the distribution expected from a harmonic oscillator model of the nucleus as found by other techniques and that these momenta extend up to about 400 MeV/c.

3) The interactions of antineutrons produced by the charge exchange of antiprotons with the emulsion nuclei have been studied and it has been shown that the general characteristics of the antineutron stars such as the sizes, the mean multiplicities of secondary mesons and their energy spectra are similar to those of antiproton stars. Finally, the charge exchange cross-section for antiprotons of mean energy 125 MeV has been determined and is found to be (17 ± 6) mb. This is close to the value expected from the calculations made for the charge exchange cross-section of antiprotons in complex nuclei.

PREFACE

This thesis is an account of the work carried out by the author whilst at the University of Durham. It is concerned with the interactions in nuclear emulsion of antiprotons at rest and antineutrons in flight. The exposure to the 700 MeV/c antiproton beam was carried out by the CERN Emulsion Group. The experiment was carried out with the collaboration of Dr. A.J. Apostolakis Mr. G.A. Briggs and Dr. J.V. Major.

The author has been responsible for a considerable part of the measurements, reduction of data and analyses of the results. In particular the work on the interaction of antineutrons and of the mechanism of meson production on annihilation has been the sole responsibility of the author.

LIST OF FIGURES

		Following page
Figure 1	Total $\bar{p}p$ and pp cross-sections	10
Figure 2	Annihilation cross-sections in complex nuclei	13
Figure 3	Total and partial $\bar{p}p$ cross-sections	13
Figure 4	Energy variation of the charged and total multiplicities of antiproton annihilation	22
Figure 5	Mean number of neutral pions accompanying particular charged multiplicities	24
Figure 6	Ratio of the isotopic spin channels T = 1 and T = 0 in the annihilation of anti-protons on nucleons	39
Figure 7	The calculated variation of the odd/even ratio with the probability of absorption of secondary mesons	60
Figure 8	The calculated variation of the mean charged multiplicity with the probability of absorption of secondary mesons	61
Figure 9	The comparison of observed and calculated charged multiplicities	62
Figure 10	The variation of the mean number of grey tracks with the charged pion multiplicity	68
Figure 11	The variation of the mean number of black tracks with the charged pion multiplicity	69

		Following page
Figure 12	The variation of the mean number of black tracks with the number of grey tracks	70
Figure 13	The variation of the mean number of shower tracks with the grey track multiplicity	72
Figure 14	The variation of the mean number of shower tracks with the black track multiplicity	72
Figure 15	Size distribution for $\bar{p}$ stars of $n_s = 2$	72
Figure 16	Size distribution for $\bar{p}$ stars of $n_s = 3$	72
Figure 17	Size distribution for $\bar{p}$ stars of all n_s curves for heavy ions in G5 emulsion	72
Figure 18	Range momentum curves in G5 emulsion	75
Figure 19	Momentum distribution of nucleons	78
Figure 20	The variation of charge exchange cross-sections with the absorption coefficient	83
Figure 21	Size distribution for selected anti-neutron stars of $n_s = 2$	92
Figure 22	Size distribution for selected antiproton stars of $n_s = 2$	92
Figure 23	Size distribution for antineutron stars of $n_s = 3$	94
Figure 24	The comparison of charged multiplicities	96

		Following page
Figure 25	The kinetic energy spectrum of pions from antiproton annihilation	97
Figure 26	The kinetic energy spectrum of pions from antineutron annihilations	97
Figure 27	Size distribution for selected antineutron stars	97
Figure 28	The energy dependence of charge exchange cross-sections	98
Figure 29	Multiplicities of charged pions predicted by various models of annihilation	105
Figure 30	The variation of average pion multiplicity with $W/2M_p$	106
Figure 31	Comparison of experimental and predicted multiplicities	106
Figure 32	The parameters of a complex nucleus	113

LIST OF TABLES

Table		Page
1	Properties of Antinucleons	7
2(a)	$\bar{p}p$ cross-section from 0.575 to 5.35 GeV/c	
2(b)	Antiproton-proton cross-sections	
3	$\bar{p}$-complex nuclei cross-sections	14
4	Charge exchange cross-sections for antiprotons in hydrogen and complex nuclei	19
5	Charged and total pion multiplicities for $\bar{p}p$ and $\bar{p}$-nucleus annihilation	23
6	Number of neutral mesons accompanying charged mesons in the annihilation of antiprotons	25
7(a)	Selection rules for $\bar{p} + n \longrightarrow m\pi$	30
7(b)	Selection rules for $\bar{p} + p \longrightarrow m\pi$ or $\bar{n} + n \longrightarrow m\pi$	31
8	Resonance particles in $N\bar{N}$ annihilation and their properties	32
9	Comparison of $\bar{p}p$ and $\bar{p}n$ cross-sections	36
10	Effect of secondary interactions of pions on the final products of $\bar{p}$-D annihilation	46
11	Relative probabilities of capture by each element of the gelatine matrix of emulsion	52
12	Characteristics of white stars	54
13	Characteristics of black stars	55

Table		Page
14	Mean number of grey tracks versus charged pion multiplicity	68
15	Number of shower tracks versus mean number of black tracks	69
16	Mean number of shower tracks versus grey track multiplicity	70
17	Mean number of shower tracks versus black track multiplicity	71
18	Frequency distribution of track length of recoiling nuclei	76
19	Momentum distribution of recoiling nuclei	77
20	Breakdown of original sample of stars recorded on scanning for antineutrons	87
21	Star size distribution for 300 MeV pions in G5 emulsion	90
22	Size distribution for antiproton stars of $n_s = 1$ in G5 emulsion	91
23	Size distribution for antiproton stars of $n_s = 3$ in K5 emulsion	93
24	Comparison of the multiplicity distribution of mesons from the annihilation of antineutrons and antiprotons	95

INTRODUCTION

Anderson's discovery of positrons among the particles produced by cosmic rays in a cloud chamber, not only confirmed Dirac's prediction about antiparticles of electronic mass and of charge +e, but also brought about the search for the "charge conjugates" of nucleons. Although Bridge et al. (1954) and Amaldi et al. (1955), using the Wilson Cloud Chamber and photographic plates respectively, had each observed a cosmic ray event which they attributed to the annihilation of an antiproton with a nucleon, the evidence was not conclusive.

The Bevatron at the University of California was built to produce antiprotons, it being designed to accelerate protons to energies greater than the threshold energy needed for the production of nucleon-antinucleon pairs. After the first successful detection of the antiproton in 1955, at the Berkeley Laboratory, the main properties of the antiproton were established such as its mass, charge and stability against spontaneous decay. Since then, a number of experiments with improved yield of antiprotons for a given flux of accelerated protons have been carried out at Berkeley as well as at Brookhaven, Cern and Dubna. Whereas in the first experiment at Berkeley, the ratio of antiprotons to contamination pions was of the order of 1 to 50,000, in

1961, with the Cern Proton Synchrotron, employing refined optics and using electrostatic separators, this ratio was increased to 3 to 1 at lower and to almost pure antiproton beam at higher momenta (Amaldi et al. (1964)). In the experiment of Amaldi et al., the average yield was from two to six antiprotons per pulse (1 pulse equivalent to 10^{11} circulating protons).

With antiprotons available in such copious numbers, a large variety of experiments has been performed to study the interaction of antinucleons with nucleons. All the modern techniques for the detection of elementary particles have been employed in determining the elastic, inelastic, charge exchange and total cross-sections of these particles. The present investigation is limited to the annihilation and charge exchange properties of antinucleons employing the emulsion technique.

In Chapter 1 are summarised the main properties of antinucleons as well as the antinucleon-nucleon and antinucleon-nucleus cross-sections at various energies of the incident antinucleons. These are compared with the corresponding N-N cross-sections.

In Chapter 2, annihilation of antiprotons in flight and at rest is discussed and the relative probabilities of annihilation on protons and neutrons as found by different workers is given, along with their explanation

for the discrepancy between results in flight and at rest In the same chapter there is also described work to resolve the difficulty mentioned above. On the basis of statistics larger than those of previous experiments, it is found that the annihilation of antiprotons proceeds equally through the singlet and triplet isospin channels. The apparent lack of equality of probabilities of annihilation on protons and neutrons found in heavy elements is accounted for by the interactions of the annihilation products in the parent nuclei for which detailed calculations are given.

The general features of the antiproton-nucleon annihilation are described in Chapter 3. The mean charged and total multiplicities, the star size distributions, and the number of mesons absorbed per annihilation star, are all determined. The stopping antiproton is used as a probe of nuclear structure. This technique is employed to study the distribution of momenta of the nucleons of light elements of emulsion.

In Chapter 4 there is outlined a method for the determination of the charge exchange cross-section of antiprotons in an emulsion stack. The cross-section for production of antineutrons for a mean antiproton energy of 125 MeV is found to be (17 ± 6)mb. The annihilations of antineutrons thus produced are studied and the mean energy of the secondary mesons and the star sizes of the annihilations determined. These are found to be very similar to those for antiprotons.

In the last chapter, the more important theories of nucleon-antinucleon annihilation are described and the experimental results about multiplicity distributions are compared with the predicted values. It is concluded that the Koba and Takeda model gives a satisfactory picture of the $N\bar{N}$ annihilation phenomenon.

CHAPTER 1

Review of the Interactions of Antinucleons

1.1 The Production of Antinucleons

1.1.1 Antiprotons

Antiprotons are usually produced in an accelerating machine by the bombardment of the nucleons in a target consisting of complex nuclei, (such as beryllium or copper), by energetic protons. The principal process is

$$p + N \rightarrow \bar{p} + 3N + \text{mesons}$$

For stationary target nucleons the threshold energy in the laboratory system for the incident protons is about 6 GeV. However, the threshold is reduced on account of the motion of the nucleons inside a complex nucleus. For a nucleonic momentum of 200 MeV/c, for example, the threshold is reduced to 5.3 GeV.

A comparison between different targets shows that for the same conditions, light nuclei are as effective for the production of antiprotons as heavy nuclei. Since the probability of collision of an incident proton with a nucleon is greater for a heavy than for a light nucleus, the equality of the cross-section of production for antiprotons in different elements indicates that the absorption of antiprotons in heavy nuclei is considerable.

1.1.2 Antineutrons

Antineutrons are also produced by the process mentioned above but it is difficult to recognise them in the neutral beam emerging from the accelerator. An attempt was made, without success, by Youtz (1958) to detect antineutrons formed in the reaction

$$p + p \rightarrow \bar{n} + He^3$$

However, the most convenient and practical way of producing antineutrons is by the charge exchange of antiprotons. Although the cross-section for charge exchange is small, experiments have been successfully performed, both by counter and bubble chamber techniques, and with emulsions (this thesis), to study the annihilation properties of antineutrons. The charge exchange reactions are the following:

$\bar{p} + p \rightarrow \bar{n} + n$ .... Elastic charge exchange

$\bar{p} + N \rightarrow \bar{n} + N$ + mesons .... Inelastic charge exchange

The second reaction, however, competes poorly with the elastic charge exchange. At an antiproton momentum of 1.61 GeV/c, for example, Xuong et al. (1961) have found the cross-sections for

$\bar{p} + p \rightarrow p + \bar{n} + \pi^-$ to be (0.96 ± 0.22)mb, and for

$\bar{p} + p \rightarrow n + \bar{n} + \pi^o$ to be (1.6 ± 0.3)mb.

The latter cross-section was not directly measured but was deduced from the reaction

$$\bar{p} + p \rightarrow \bar{p} + p + \pi^{o}$$

The value for the elastic charge exchange of antiprotons at the same energy is about 6 mb (Hinrichs et al. (1962)) and (Elioff et al. 1962). The ratio of inelastic to elastic charge exchange decreases with the decrease in the antiproton energy.

1.2 The Properties of Antinucleons

The main properties of antinucleons, some found directly since the discovery of antiproton in 1955, and others inferred from the known properties of nucleons, are summarised in Table 1.

Table 1

Properties of Antinucleons

Property	Antiproton	Antineutron	Remarks
Mass	$(1.004 \pm 0.025) M_p$	Same as M_N	Directly measured
Charge	-e	zero	"
Lifetime	stable	(1050 ± 200) sec	Inferred
Decay mode	"	$\bar{n} \rightarrow e^{+} + \bar{p} + \nu$	"
Magnetic moment	-2.79	+1.91	Directly determined for the antiproton
Spin	$\frac{1}{2}$	$\frac{1}{2}$	Inferred
Isotopic spin	$\frac{1}{2}$	$\frac{1}{2}$	"
3rd component of I spin	$-\frac{1}{2}$	$\frac{1}{2}$	"
Parity	odd	odd	"
Intrinsic Parity	-1	-1	"
Creation	in pairs	in pairs	Directly observed
Annihilation	"	"	"

1.3 The Interactions of Antinucleons

The study of the interactions of antinucleons with protons and complex nuclei is of importance for the proper understanding of nuclear forces, and can give valuable information about the structure of complex nuclei. The annihilation of the antiproton-proton system to mesons affords an opportunity of studying the $\pi - \pi$ interactions without the complicating presence of a nucleon in the final state.

A large number of experiments on the interactions of antinucleons with nucleons have been performed, notably at Berkeley and Cern, and cross-sections for various processes have been measured. Although interactions of both antiprotons and antineutrons have been studied, the experiments with the latter are fewer in number on account of the obvious difficulty of their production and detection. These experiments will be briefly described in a separate section. Experiments on antiprotons, on the other hand, are too many to permit detailed description of each. Only general features will be described. Moreover, it will be assumed that the interactions of antiprotons are typical of all antinucleons.

1.3.1 Interaction cross-sections of antiprotons

Collisions of antiprotons with nuclei may lead to elastic scattering, inelastic scattering, charge exchange or annihilation as is shown in the following reactions:

1 ..... $\bar{p} + N \longrightarrow \bar{p} + N$ .... elastic scattering

2 ..... $\bar{p} + N \longrightarrow \bar{p} + N$ + mesons .... inelastic scattering

3 ..... $\bar{p} + p \longrightarrow \bar{n} + n$ .... charge exchange

4 ..... $\bar{p} + N \longrightarrow \bar{n} + N$ + mesons .... inelastic charge exchange

5 ..... $\bar{p} + N \longrightarrow$ mesons .... Annihilation

Annihilation may also lead to hyperon production but the cross-section for this process is very small.

The term "total cross-section" will be used for the sum of the cross-sections for reactions 1 to 5. Some counter experiments have been performed to measure total cross-sections up to as high an antiproton momentum as 24 GeV/c. The most recent measurement of the total cross-section is by Amaldi et al. (1964) in the momentum range (0.575 - 5.35)GeV/c. The total cross-section decreases monotonically with increasing momentum of the antiprotons and is given by the empirical formula,

$$\sigma_{tot} = (85.8 \pm 0.4)\ (\tfrac{1}{\beta})\text{mb},$$

(where β is the antiproton velocity in the laboratory system,) up to a momentum of 1.6 GeV/c. Beyond this momentum the formula

$$\sigma_{tot} = \sigma_{\infty} \cdot \frac{1}{\beta}\left(1 + \frac{a}{\gamma^{\lambda}}\right)$$

holds. Here, σ_{∞} is the asymptotic value of the total cross-section at high energy and is taken to be 40 mb. The constants a and λ have values 2.1 and 0.8; $\gamma = (1-\beta^2)^{-\frac{1}{2}}$. The results are summarised in Tables 2(a) and 2(b).

Table 2(a)

$\bar{p}p$ cross-sections from 0.575 to 5.35 GeV/c

(Amaldi et al., 1964)

Momentum (MeV/c)	Total cross-section
575	167.4 ± 7.8
629	156.3 ± 7.3
681	144.3 ± 3.7
733	142.1 ± 3.3
785	132.7 ± 3.0
837	128.0 ± 2.9
867	120.7 ± 1.3
888	116.8 ± 3.3
972	120.5 ± 0.9
972	119.0 ± 1.1
972	121.5 ± 1.5
1074	113.3 ± 0.9
1178	111.6 ± 0.6
1380	103.3 ± 0.4
1380	103.3 ± 0.6
1380	103.9 ± 1.1
1380	103.1 ± 1.1
1380	103.5 ± 0.6
1688	96.17 ± 0.39
1888	87.83 ± 0.24
2082	88.48 ± 0.20
2283	83.78 ± 0.43
2485	78.04 ± 0.52
2686	79.33 ± 0.25
2886	77.82 ± 0.28
2940	74.3 ± 6.1
3088	75.24 ± 0.70
3240	72.9 ± 1.0
3540	69.7 ± 0.5
3860	67.7 ± 0.9
4015	66.84 ± 0.32
4300	60.6 ± 0.8
4760	65.8 ± 0.9
5350	57.9 ± 2.6

Table 2(b)

Antiproton-proton cross-sections (Millibarns)

Kinetic Energy (MeV)	Momentum (MeV/c)	Cross-section (mb)				Reference
		Elastic	Inelastic	Charge Exchange	Total	
Substance Hydrogen						
45±20	290	80±10	175±45	27±6	281±46	Cork et al. 1962
90±20	420	66±6	101±9	19±3	185±13	
145±17	535	52±6	99±8	12±3	163±12	
245±20	725	45±5	66±6	7±2	118±9	
75±137.5	458	66±17	112±23			Agnew et al. 1960
137±200	588	56±14	60±18			
470	1050		51±10			Goldhaber et al. 1961
534±25	1134	42±5	70±3	.0±1.3	118±6	Elioff et al. 1962
700±33	1343	42±4	66±3	7.2±1.5	116±5	
816±37	1515	38±4	63±3	7.1±1.2	108±5	
948±42	1637	33±3	56±2	6.8±1.0	96±3	
1068±46	1773	30±2	60±2	5.7±1.1	96±3	
925	1610			7.82±0.55		Hinrichs et al. 1962
1000	1696	33±2	62±3	$5^{+1}_{-1.5}$	100±3	Armenteros et al. 1960
1250	1977	28±2	57±4	4±1	89±4	
2000	2784	25±4	49±6	3^{+2}_{-3}	80±6	
	3000	21.2±1.0			72.3±1.9	Goldschmidt-Clermont et al. 1962
2445	3250	20.7±1.6	35.8±3	1.6±0.8	72.5±1.9	Ferbel, 1963
6320	7200	13.79±1.0				Foley et al., 1963
8010	8900	13.89±0.35				
9060	10000	14.6±3.3				
11060	12000	11.59±0.41				

The variation of the total $\bar{p}p$ cross-section with the antiproton momentum is shown in Figure 1. Also shown in the same figure are the proton-proton cross-sections at various momenta. It can be seen that although the total antiproton-proton cross-sections are much larger than the corresponding proton-proton cross-sections at low and medium energies, the difference between them is much smaller at higher energies. According to Pomeranchuk, dispersion relations indicate that the two cross-sections should converge to the same constant value at sufficiently high energies. Very high energies are required to test this prediction.

Measurements of angular distributions in the centre of mass system for the elastic scattering of antiprotons in the energy range (0.02 - 2.5) GeV show that the differential cross-section decreases rapidly with the centre of mass scattering angle. [(20-40) MeV, Hossain and Shaukat (1964), (75-200) MeV, Agnew et al. (1960), (1-2) GeV, Armenteros, et al. (1960), 2 GeV, Goldschmidt-Clermont et al. and 2.45 GeV, Ferbel (1963)]. This is similar to proton and pion scattering and implies a small momentum transfer to the target nucleon.

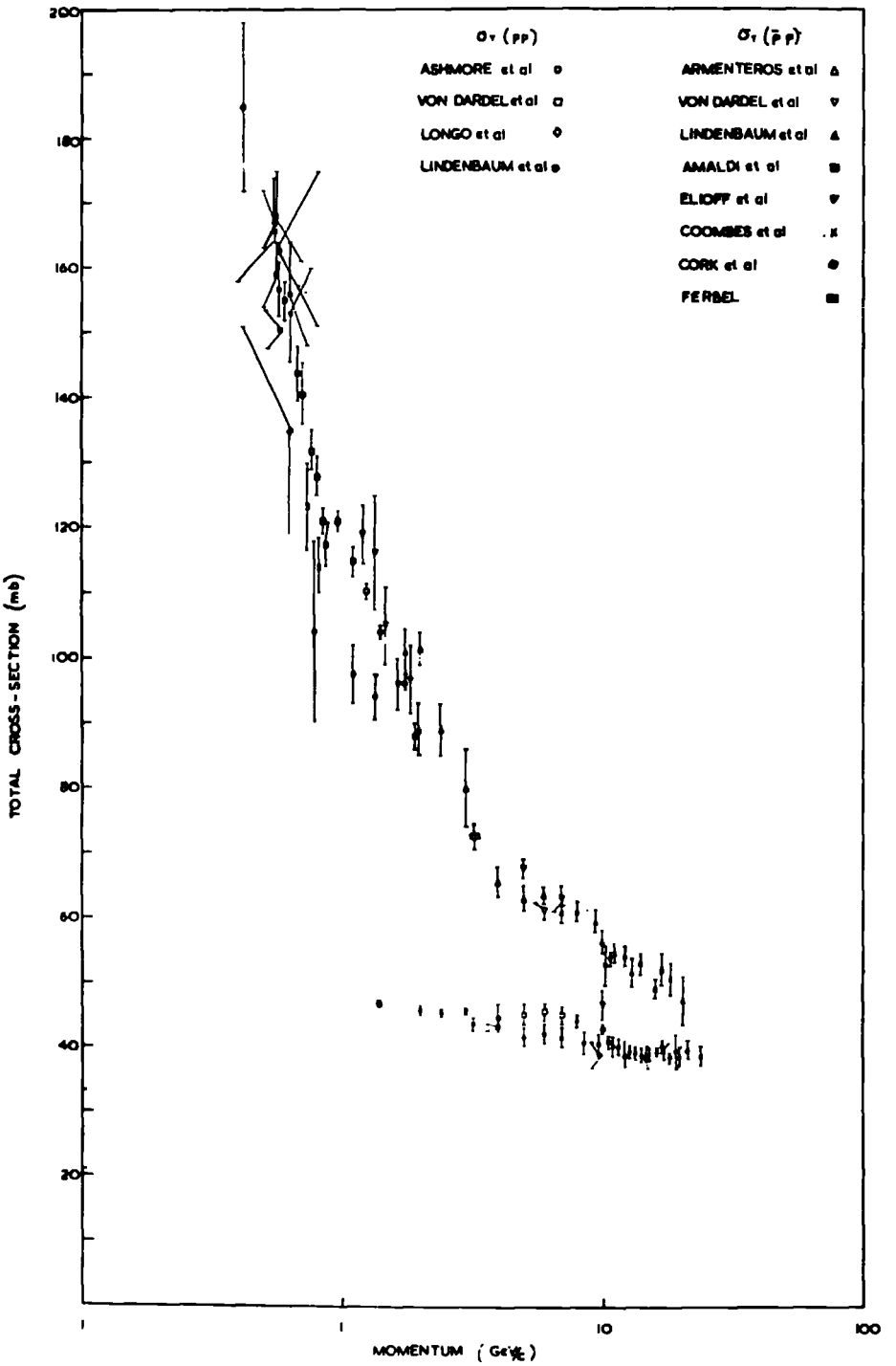

FIG. 1 Total $\bar{p}p$ and pp cross-sections

In spite of the small differential cross-sections at large angles, the antiproton-proton collisions have the advantage compared with the p-p scattering that angles of scattering up to 180^{o} can be investigated. In p-p scattering, for example, only angles up to 90^{o} in the centre of mass can be determined because it is not possible to distinguish between the primary and the target protons.

The large $\bar{p}p$ cross-sections have been explained by Ball and Chew (1958) by a theory which rests on an analogy with the nucleon-nucleon scattering, where the nucleon is thought of as a hard repulsive core of radius ($\frac{1}{2}\frac{\hbar}{m c}$), surrounded by a pion cloud. For a nucleon-antinucleon system, the hard repulsive core is replaced by an absorbing core to account for the large annihilation cross-section. The pion cloud surrounding an antinucleon must be the charge conjugate of the cloud surrounding a nucleon. With these assumptions, the interaction cross-section between a proton and an antiproton can be calculated in the same way as for the proton-proton interaction. These calculations refer to

antiproton energies of up to 200 MeV, and the results fit the experimental cross-sections quite well. Fulco (1958) has computed the angular distributions in the $\bar{p}p$ centre of mass system for elastic scattering of anti-protons on the Ball and Chew model and finds a peak in the forward direction. As mentioned before, the experimental distribution shows a similar behaviour.

It is found that the cross-sections for elastic scattering and inelastic interaction are approximately equal. Thus the Ball-Chew model is essentially like a classical black-sphere region of size $\lambda\!\!\!^{-}_{\pi}$ (pion Compton wavelength). In the opinion of Elioff et al., this is explained by the effectiveness of the outer potential due to the pion cloud which draws the anti-proton into the core region where it annihilates.

For higher energies, the method of Ball and Chew is not applicable, and a model has been proposed by Koba and Takeda which accords very well with the measured cross-sections. This will be described in Chapter 5.

1.3.2 Antiproton-nucleus cross-sections

The interactions of antiprotons in complex nuclei are also characterised by their large cross-sections. As for the antiproton-proton interactions, the cross-section increases rapidly as the antiproton slows down. The major contribution to this increase comes from the annihilation process. The results at various energies for different targets are summarised in Table 3. The annihilation cross-section for deuterium, carbon and emulsion are displayed in Figure 2. The total and partial $\bar{p}p$ cross-sections are displayed in Figure 3. It can be seen that the charge exchange, elastic and inelastic cross-sections all increase with the decrease in antiproton energy. The curves in the figure have been drawn to show this trend. The cross-sections for antiprotons in complex nuclei follow a similar variation.

1.3.3 Antiproton-neutron cross-sections

The direct determination of antiproton-neutron cross-section is difficult because the neutron is always bound in complex nuclei. Indirect methods have, therefore, to be used. The cross-sections for neutrons (given in Table 3) have been determined by Elioff et al. by the subtraction of $\bar{p}p$ cross-sections from $\bar{p}$-d measurements. In this determination of the $\bar{p}$-n cross-sections the correction for the

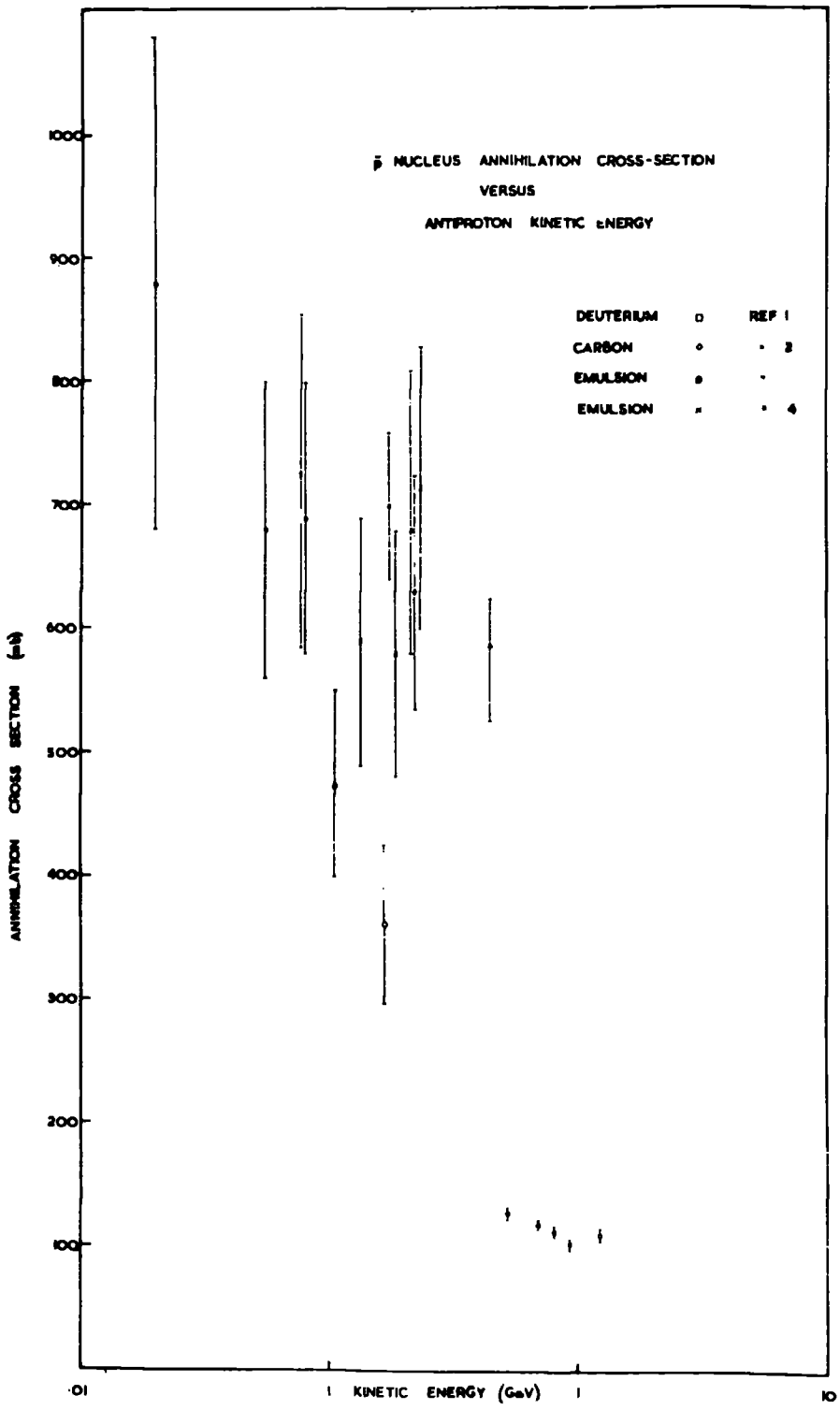

FIG. 2 Annihilation cross sections in complex nuclei

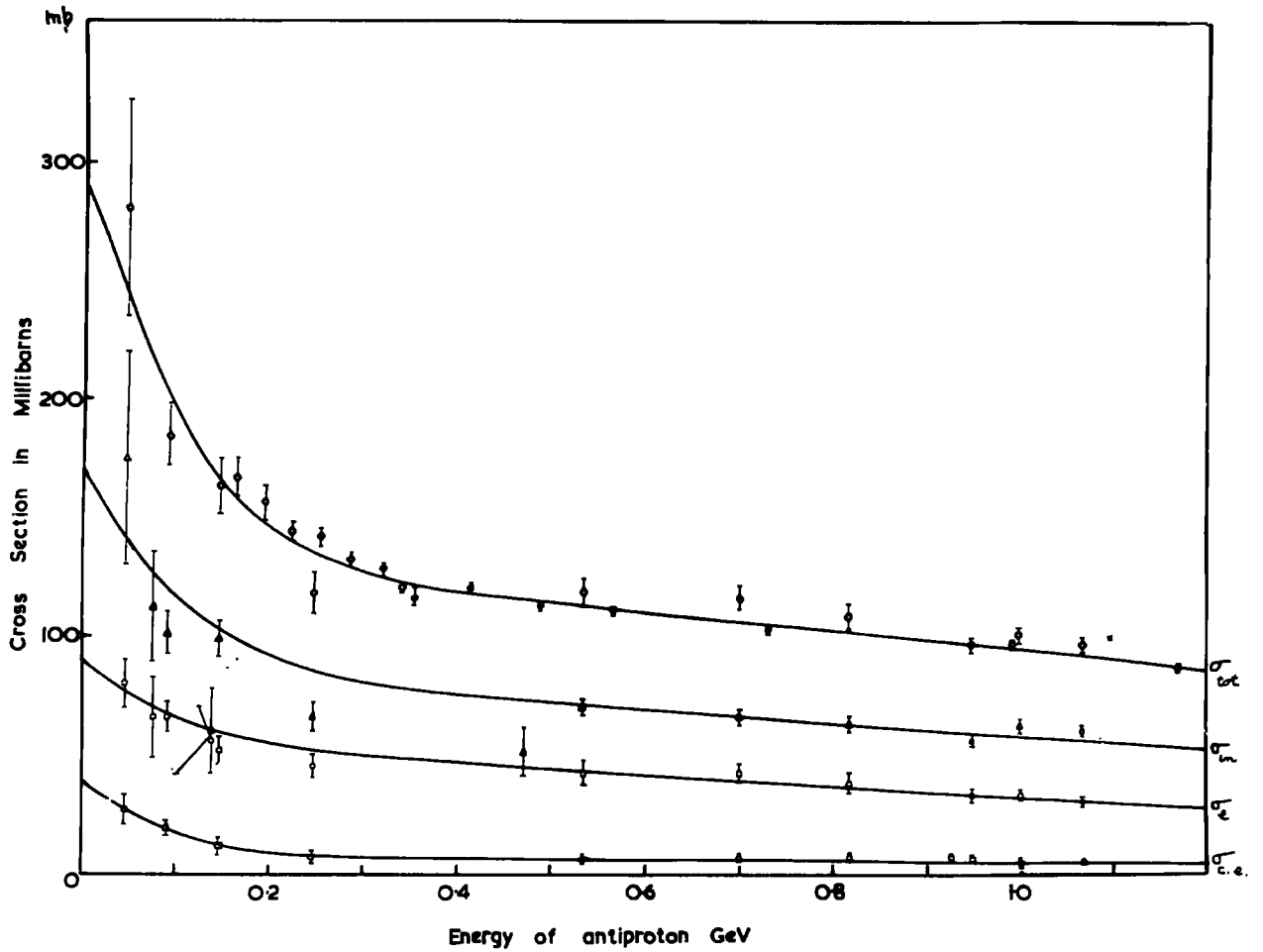

FIG. 3 Total and partial $\bar{p}p$ cross-sections

Table 3

Antiproton-complex nuclei cross-sections (millibarns)

Target	$\bar{p}$ Kinetic Energy (MeV)	$\bar{p}$ Momentum (MeV/c)	Cross-section mb. Elastic	Inelastic	Charge Exchange	Total	Reference
'Neutron' (by the difference technique from $\bar{p}$-D cross-sections)	534	1134	40±10	79±6		119±8	Elioff et al. 1962
	700	1343	25±8	71±5		96±7	
	816	1482	44±9	68±5		112±8	
	948	1636	39±7	63±4		102±6	
	1068	1773	42±6	67±5		109±4	
Deuterium	534		80±6	126±5	3.3±1.3	210±5	Elioff et al. 1962
	700	1343	67±5	117±4	5.4±1.4	189±5	
	816	1482	78±5	112±4	6.5±1.5	195±6	
	948	1636	71±5	102±4	4.4±1.1	178±5	
	1068	1773	68±4	109±5	5.6±1.0	184±3	
Beryllium	320	838	297±40		10^{+6}_{-7}	730±40	Wenzel Proc. Aix-en-Provence Conference
Carbon	75±137.5	458	345±60	474±76			Agnew et al. 1960
	137.5±200	588	255±45	360±65			
	96	434			$40^{+1.6}_{-1.5}$		Button et al. 1957
	320	838	270±23		11^{+4}_{-5}	670±30	Wenzel
	470	1050		368±60			Goldhaber et al. 1960
Lead	92	426			$3.8^{+4.2}_{-2.5}$		Button et al. 1957
Emulsion Nuclei	5-20	150	93.7±20				Hossain et al. 1964
	20-40	239	85.0±15				
	40-60	310	86.5±16				

Target	Kinetic Energy (MeV)	Momentum (MeV/c)	Cross-section (mb) Annihilation and charge exchange	Inelastic	Total	Reference
Emulsion nuclei	140	531	1485	143	1650	Amaldi et al. 1959
	140	531	1045	60.5	-	
	150	551	984	41.8	1045	
	150	551	1133	85.3	1216	
	Average 125	Average 479	C.E. (17±6)			Khan and Major 1965

shielding of one nucleon by the other in the deuterium nucleus is to be applied. Blair (1958) has made special calculations for the antinucleon-nucleon case where the range of interaction is comparable to the radius of the deuteron. Another way of studying the antiproton-neutron interaction is to obtain an antineutron beam and look for their interactions in a liquid hydrogen bubble chamber. This process is charge symmetric to $\bar{p}$-n and has been investigated by Hinrichs et al. (1962) in the 72-inch hydrogen bubble chamber. This is mentioned in section 1.4 under charge exchange of antiprotons. Experimentally it is found that the cross-section for inelastic interaction of antiprotons in hydrogen ($\sigma_{\bar{p}p}$) is equal to the antiproton-neutron cross-section ($\sigma_{\bar{p}n}$). The consequences of this are discussed in Chapter 2.

1.4 The Charge Exchange of Antiprotons

An early experiment to demonstrate the charge exchange production of antineutrons was carried out by Button et al. (1957). An antiproton selected from a beam entered an absorber. If no charged particle was recorded by a counter immediately behind the absorber but an annihilation pulse was observed in a calibrated scintillation counter further down stream, it was concluded that the antiproton had undergone charge exchange in the absorber and that the resultant antineutron had been annihilated in the

scintillator. The cross-sections for the charge exchange of antiprotons in lead, carbon and hydrogen were determined and were found to be the same within statistical limits. Assuming that the angular distribution of the $\bar{p}p$ charge exchange cross-section was the same as that for the p-n charge exchange, it was found that the differential cross-section at 0^{o} in the laboratory system was (38 ± 20)mb/st. At the same energy and laboratory angle the p-n charge exchange is 54 mb.

In addition to the counter technique, bubble chambers have been employed to determine the charge exchange cross-sections of antiprotons as well as to study the subsequent annihilation of antineutrons. In the hydrogen bubble chamber, the charge exchange is recognised by the disappearance in flight of an antiproton accompanied by an interaction, further downstream, which has been produced by a neutral particle. This secondary star is required to distinguish charge exchange from the annihilation of an antiproton in which no charged particles are emitted. The number of such stars is limited by the size of the chamber and in estimating the cross-section for charge exchange, corrections for the geometry of the chamber must be made.

The main contribution to this investigation comes from the Berkeley Laboratory where the process has been studied up to an antiproton momentum of about 2 GeV/c. Hinrichs et al. (1962) measured the angular distribution of the produced antineutrons as well as the antineutron-proton annihilation cross-section. The energy to which this cross-section refers was estimated by assuming that the production is elastic; the momentum of an antineutron was determined from its angle of production. For an energy of 930 MeV for the incident antiprotons, it was found that 80% of the antineutrons produced by charge exchange had energies between 800 and 930 MeV.

The cross-section for charge exchange was found to be strongly peaked forward, thus confirming the result obtained previously by Goldhaber et al. (1961) who reported the absence of charge exchange events at centre of mass angles greater than 60°. This is not unexpected since large-momentum-transfer collisions lead principally to annihilations, leaving the possibility of charge exchange to low momentum transfers only. Wenzel pointed out that the optical theorem relating the $\bar{p}p$ charge exchange forward scattering cross-section and the total $\bar{p}p$ and $\bar{p}n$ cross-sections is satisfied by the results of these experiments. The theorem states that:

$$\left(\frac{d\sigma_{\bar{p}p}}{d\Omega}\right)_{\theta=0^\circ} \geq \left[\frac{K\{\sigma_T(\bar{p}p)-\sigma_T(\bar{p}n)\}}{4\pi}\right]^2$$

where K is the wave number for the antiproton. This formula is independent of any models for nucleon-antinucleon interaction and is based only on the charge independence of nuclear forces. (Segre, 1958).

A summary of the various experiments performed so far to determine the charge exchange cross-sections at various antiproton energies is given in Table 4.

Since the charge exchange cross-sections in hydrogen and heavier elements at similar energies are approximately equal, it follows that the effective charge exchange cross-section per proton of a target nucleus decreases with increasing Z. This is not unexpected since the antineutrons are readily absorbed in the parent complex nuclei. It can thus be concluded that in complex nuclei interactions the observable antineutrons are produced only when the incident antiprotons make grazing collisions with the nuclei. (Button et al., 1957).

1.5 The Annihilation Process

The property of antinucleons to annihilate on nucleons finally establishes their identity beyond any doubt. The first detailed work on the annihilation process was carried out by Barkas et al., (1957) using the emulsion technique.

Table 4

Charge Exchange Cross-sections for Antiprotons in Hydrogen and Complex Nuclei

Substance	K.Energy of Antiproton (MeV)	Charge Exchange cross-section mb.	Technique employed	Reference
Hydrogen	45 99 145 245	27 ± 6 19 ± 3 12 ± 3 7 ± 2	15-inch hydrogen bubble chamber (Berkeley)	Cork et al. 1962
Hydrogen	133 ± 13 197 ± 16 265 ± 17 333 ± 17	10^{+2}_{-3} 11^{+2}_{-4} 8^{+2}_{-3} 7 ± 2	Scintillation counter	Coombes et al. 1958
Hydrogen	534 ± 25 700 ± 33 816 ± 37 948 ± 42 1068 ± 46	6.0 ± 1.3 7.2 ± 1.5 7.1 ± 1.2 6.8 ± 1.0 5.7 ± 1.1	Counter system (Berkeley)	Elioff et al. 1962
Hydrogen	2172	1.6 ± 0.8	20-inch liquid-hydrogen bubble chamber	Ferbel, 1963
Hydrogen	930	7.82 ± 0.55	72-inch liquid hydrogen bubble chamber (Berkeley)	Hinrichs et al. 1962

Table 4 cont.

Substance	K.Energy of Antiproton	Charge Exchange cross-section mb.	Technique employed	Reference
Deuterium	534 ± 25 700 ± 33 816 ± 37 948 ± 42 1068 ± 46	3.3 ± 1.3 5.4 ± 1.4 6.5 ± 1.5 4.4 ± 1.1 5.6 ± 1.0	Counter system (Berkeley)	Elioff et al, 1962
Beryllium	320	11^{+4}_{-5}	Counter	Cork, et al., 1957
Carbon	320	10^{+6}_{-7}		
Carbon	400	8		Cork et al. 1956.
Carbon	434	$4.0^{+1.6}_{-1.5}$	Counter	Button et al. 1957
Lead	426	$3.8^{+4.2}_{-2.5}$		
Emulsion	150	(17 ± 6)		Khan and Major 1965.

Measurements were made to establish the identity and energy of the products of annihilation. A difficulty arises in the interpretation of these observations from the fact that in emulsions, the antiproton annihilates usually in a complex nucleus. The secondary particles may interact with the nucleus in escaping from the centre of annihilation leading to changes in multiplicity and energies of the secondary particles. From this point of view, hydrogen bubble chambers are more useful than emulsions and have been therefore widely employed. However, the antiproton can be used as a nuclear probe to investigate the properties of complex nuclei. A study of the interactions in emulsions and proper recognition of the secondary processes, therefore, becomes of importance. This point is discussed in detail in Chapters 2 and 3. As an example, the region of the nucleus where annihilation takes place may be discussed now. The energy of the escaping mesons is about 200 MeV for which the mean free path in nuclear matter is about 10^{-13} cm (Lindenbaum, 1957). For annihilation at rest about 20% of the pions are absorbed before escaping whereas for annihilation in flight, about 40% are absorbed. These numbers can be understood if the annihilation at rest occurs in the surface of the nucleus where the escape probability is high and the annihilation in flight takes place within the body of the nucleus.

1.5.1 Pion multiplicities and energy spectra

The average charged multiplicity for antiproton-nucleon annihilation at rest is three and the total multiplicity is about five (see section 1.5.2). Even for annihilations in flight, the multiplicity is relatively independent of energy as can be seen from Figure 4, which summarises the results in the energy range (0-1)GeV given in Table 5.

The energy spectra of the secondary mesons have been determined for annihilations at rest and in flight. Ekspong et al. (1961) have computed the combined values by taking the weighted averages of the results from Uppsala, Berkeley, Rome and Saclay groups. The mean total energies at rest and in flight are (365±8) MeV and (356±11) MeV respectively.

1.5.2 Estimation of Neutral pions emitted in $\bar{N}N$ annihilation

There are two methods by which the number of neutral mesons accompanying a given charged particle multiplicity can be estimated:

a) From missing energy: for a given multiplicity of charged particles, the mean energy of the charged pions in the centre of mass system is determined. Assuming that the neutral mesons have the same mean energy, their number is estimated from

$$\text{Number of neutral mesons} = \frac{\text{Non-visible energy}}{\text{Mean total energy of charged pions}}$$

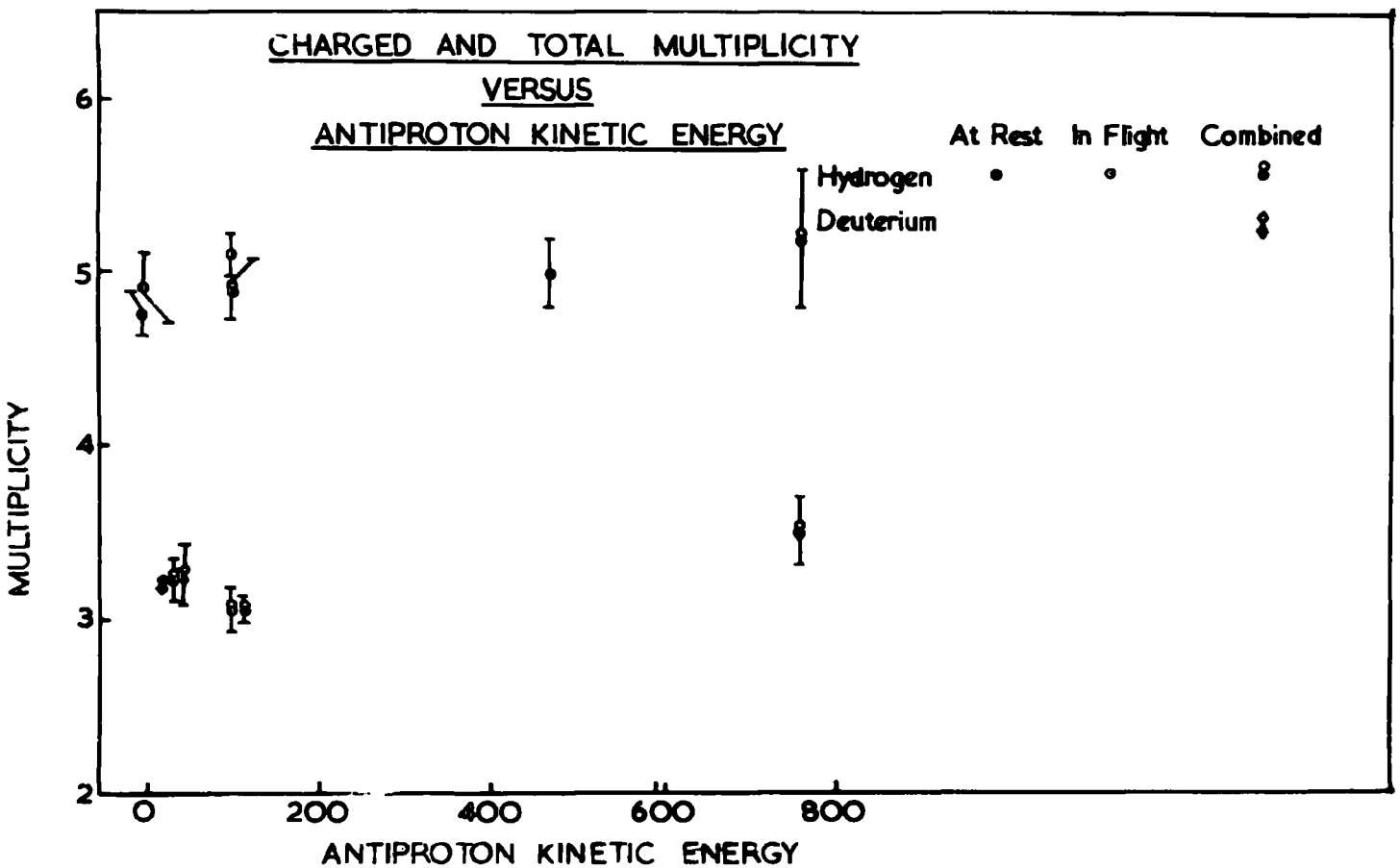

FIG. 4 Energy variation of the charged & total multiplicities of antiproton annihilation

Table 5

/ Charged and total pion multiplicities for $\bar{p}p$ and $\bar{p}$-nucleus annihilations

Substance	Charged multiplicity			Total multiplicity			Energy MeV	Reference	Remarks
	At rest	In flight	combined	At rest	In flight	combined			
Hydrogen			3.06±0.12 (3.06±0.08)			4.88±0.18 (4.66±0.5)	Aver. 100 Max. 200	Agnew et al. 1960	
			3.21±0.12			4.94±0.31	Aver. 32 Max. 63	Horwitz et al. 1959	
			3.5 ± 0.2			5.2 ± 0.4	Aver. 765 Max. 1100	Hinrichs et al. 1962	$\bar{n}p$ annihilations
				4.9±0.2	5.0±0.2	4.95±0.2	Aver. 470	W.A. Wenzel, 1962	
				4.72±0.11	5.1±0.12	4.89±0.12	Aver. 100 Max. 250	Agnew, 1959	
Deuterium			**3.23±0.18			5.03±0.44	Aver. 32	Horwitz et al. 1959	**this value may include K-mesons
			3.19±0.02				~zero (20MeV)	Barnes et al. 1964	
Carbon	2.85±0.12	2.96±0.1	2.91±0.12	3.99±0.4	4.12±0.4	4.06±0.4	Aver. 100 Max. 200	Agnew et al. 1960	
Emulsion	2.64±0.14	2.34±0.13	2.49±0.10	*4.77±0.14	*5.12±0.22	*4.92±0.13	Aver. 150 Max. 250	Amaldi et al. 1959	*these values are combined Rome and Berkeley data
	2.38±0.11	2.19±0.11	2.29±0.08	4.77±0.9 (4.68±0.12)	5.11±0.12 (5.12±0.15)	4.9±0.1	Aver. 166 Max. 215	Ekspong et al. 1961	
			3.5 ± 0.5			5.3±0.4		Barkas et al. 1957	
	2.36±0.03							This work	Values obtained from heavy elements of emulsion
	2.90±0.04					4.92±0.15	125	This work	Values obtained from light elements of emulsion

/ The combined multiplicity in column 7 has been corrected for loss of mesons by secondary interactions.

b) From the decay of $\pi^0 \rightarrow 2\gamma \rightarrow 4e$. In heavy liquid chambers, the decay of neutral pions into pairs of gamma rays which materialise into electrons, occurs with fair probability, thus making a direct observation possible.

Both methods have been used over a wide range of energies. It is found that the average value of total multiplicity remains constant. The extra energy available in energetic antinucleon annihilations appears to result in an increased average energy of the pions rather than an increase in multiplicity. The mean number of neutral mesons accompanying charged mesons as estimated by the above mentioned two methods are given in Table 6 and are shown in Figure 5.

The dotted lines have been drawn from the following simple viewpoint. The sum of the neutral and charged mesons is constant and equal to the mean total multiplicity. Obviously this does not hold for large values of the charged particle multiplicity but it should be valid enough at low values to enable approximate extrapolation to be made.

The ratio of the mean values of the neutral and charged particle multiplicities thus found is consistent with charge independence. Conversely, if charge independence is assumed to hold in antiproton-nucleon annihilation, it can be concluded that the energy going into electromagnetic radiation or neutrinos must be small. (Barkas

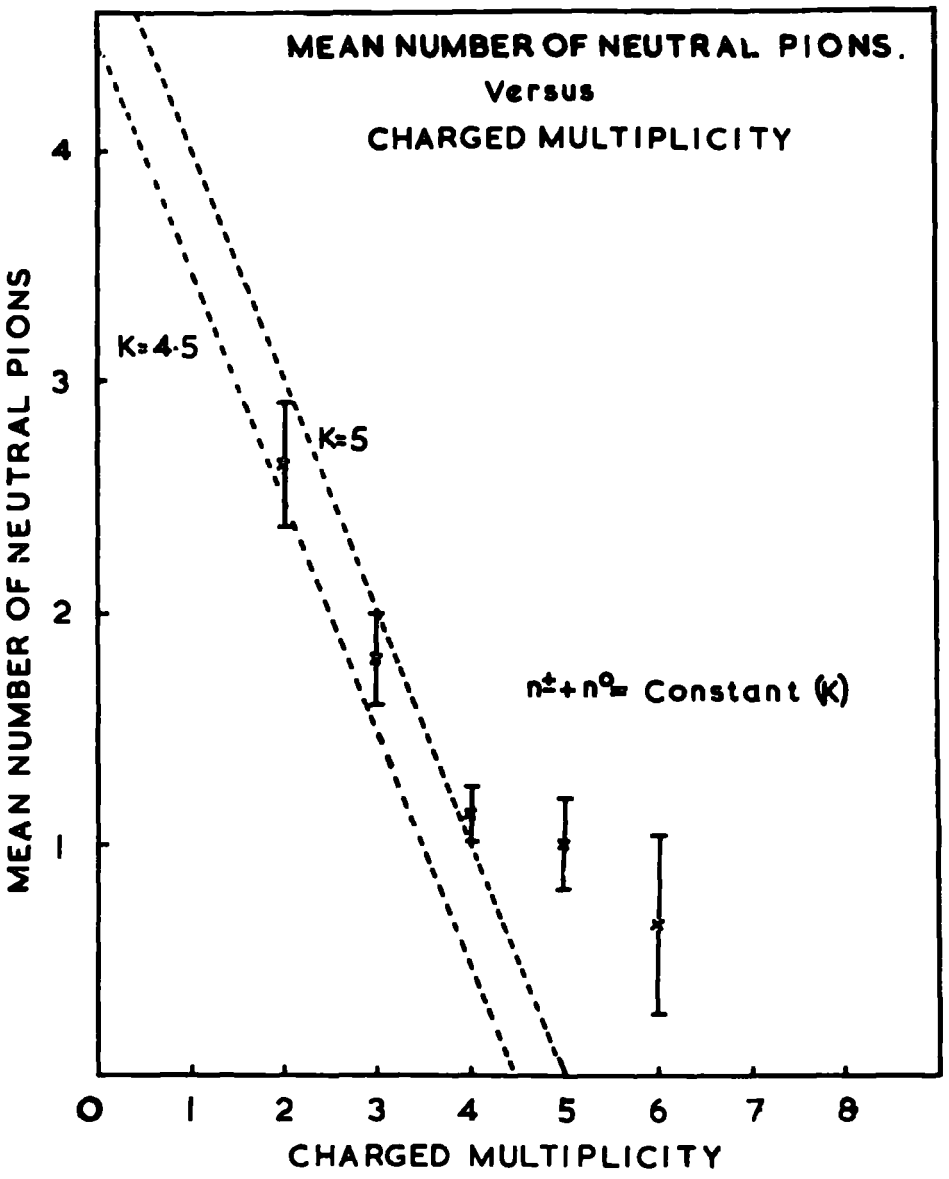

FIG. 5 Mean number of neutral pions accompanying particular charged multiplicities

Table 6

Number of neutral mesons accompanying charged mesons in the annihilation of antiprotons

$n_{\pi^\pm}$	n_{π^0}	Weighted mean	Method employed	*Reference	Total Multiplicity
2	3.0 ± 0.2		energy balance	1	
	2.5 ± 0.5		π^0 decay	2	
	$2.4^{+1.2}_{-0.9}$		π^0 decay	1	(4.64 ± 0.27)
	1.9 ± 0.3	2.64 ± 0.27	energy balance	3	
3	1.8 ± 0.2	1.8 ± 0.2	energy balance	4	(4.8 ± 0.2)
4	1.5 ± 0.3		energy balance	1	
	1.3 ± 0.4		energy balance	3	
	$1.1^{+0.9}_{-0.5}$		π^0 decay	1	(5.13 ± 0.12)
	1.1 ± 0.1		energy balance	2	
	1.1 ± 0.1	1.13 ± 0.12	π^0 decay	2	
5	1.0 ± 0.2	1.0 ± 0.2	energy balance	4	(6.0 ± 0.2)
6	0.8 ± 0.4		π^0 decay	2	
	0.7 ± 1.3		energy balance	1	
	0.5 ± 0.3		energy balance	2	(6.65 ± 0.39)
	0.5 ± 1.5	0.65 ± 0.39	energy balance	3	

* 1 - Agnew et al. (1960) 2 - Goldhaber et al. (1961)
3 - Horwitz et al. (1959) 4 - Hinrichs (1961)

et al., 1957).

1.5.3 Strange particle production

In addition to the pions, K-mesons are also created as a result of $\bar{N}N$ annihilation. To conserve strangeness they must be produced in pairs. The combinations $K^+\bar{K}^0$, K^+K^-,

$K^o, \bar{K}^o$ and $K^o K^-$ may be expected.

In emulsion, $K^o \bar{K}^o$ pairs will escape detection. Moreover, it has been estimated by Nilsson and Frisk (1958) that about 44% of negative K-mesons will be reabsorbed in parent nuclei. According to Ekspong et al., (1961) the $K\bar{K}$-pairs not detectable in emulsion constitute about 40% of all charge states. Allowing for this they conclude from their observations that $(3 \pm 2)\%$ of the antiproton stars emit $K\bar{K}$-pairs, and that the average total energy carried by them per annihilation star is $E_{K\bar{K}} = (33 \pm 22)$ MeV. Heavy liquid bubble chambers are highly efficient for the observation of short-lived neutral K-mesons. Charged K-mesons can also be detected in good ionisation conditions. This makes the bubble chamber a much more suitable instrument for the study of strange particle production in $N\bar{N}$ annihilation than emulsion.

A detailed study of this process has been carried out by Kalbfleisch (1961) with the Lawrence Radiation Laboratory's 72-inch liquid-hydrogen bubble chamber at antiproton momenta of 1.61 GeV/c and 1.99 GeV/c. The average multiplicity is found to be $(2K + 2.4\pi)$ at 1.61 GeV/c and $(2K + 2.6\pi)$ at 1.99 GeV/c and the fractions of annihilation yielding $K\bar{K}\, n\pi$ final states are (0.103 ± 0.011) and (0.13 ± 0.03) respectively. The fraction of annihilation yielding $K\bar{K}\, n\pi$ is smaller still for annihilation of antiprotons at rest. The values found are 4% (Kalogeropoulous, 1959) and $\sim 5\%$

(Agnew et al., 1960). At an antiproton momentum of 1.05 GeV/c, Goldhaber et al. (1961) find K-meson production to be 8% of all annihilation. These values are very much lower than the values predicted by the statistical theory. (See Chapter 5). At an antiproton momentum of about 2 GeV/c, the production of $\Lambda\bar{\Lambda}$, $\Sigma\bar{\Sigma}$, $\bar{\Sigma}^{0}\Lambda$, $\Sigma^{0}\bar{\Lambda}$ also becomes possible. Such pairs have been detected but the cross-sections for their production are of the order of a few microbarns only.

1.5.4 Pion-pion correlations

The angular distribution of pairs of pions from $\bar{p}$-p annihilation at 1.05 GeV/c momentum was measured by Goldhaber et al. (1959) from 2500 "hydrogen like" annihilation events observed in the 30-inch propane bubble chamber. It was found that pairs of like pions (i.e. pions in the isotopic spin state I = 2) and unlike pions (i.e. pions in the isotopic spin states I = 0, 1 or 2) have different distributions of angles in the centre of mass of the antinucleon-nucleon system. The ratio α between the number of pion pairs emitted in the backward hemisphere to those in the forward was found to be 1.23 ± 0.10 for like pions and 2.18 ± 0.12 for unlike pions. It was pointed out that the value of α for like pion-pairs differed from that predicted by the Lorentz-Invariant-Phase-Space Model of the statistical theory by about four standard deviations. This was ascribed

to the presence of additional pion-pion correlations. These strong asymmetries in the production angular distributions of the charged π-mesons are, however, found to be in general agreement with the predictions of the Koba-Takeda model which assumes that the peripheral pion clouds surrounding the nuclear cores are free to move in their original direction after the annihilation of the cores. A brief description of this model will be made in Chapter 5. It is, however, relevant here to mention that contrary to the isotropic distribution of mesons of all charges as predicted by the statistical theory, annihilations into K^+K^- pairs suggest forward peaking for K^-. (Lynch 1961). A similar asymmetry for pions is reported by Maglic et al. (1961) at 1.6 GeV/c for the reactions

$$\bar{p} + p \rightarrow 2\pi^- + 2\pi^+ + \pi^o$$

$$\rightarrow 2\pi^- + 2\pi^+$$

$$\text{and} \quad \rightarrow 2\pi^- + 2\pi^+ + n\pi^o ,$$

where π^--distribution displays a forward peak and π^+ a backward peak. The observation of Goldhaber et al. of an angular asymmetry between like and unlike pion pairs is also confirmed.

1.6 The Selection Rules Involved in Annihilation

1.6.1 Selection rules for antiproton-nucleon annihilation and the multipion resonances

The initial $\bar{p}$-N state can result in a final state con-

taining either an even or an odd number of charged mesons, if the annihilation is purely mesic. Selection rules for the various mesic states can be established on the basis of the conservation of angular momentum, parity, charge conjugation, and isotopic spin. Lee and Yang (1956) have compiled tables giving strictly forbidden states and states forbidden so far as isotopic spin is a good quantum number (see Tables 7(a) and 7(b).

Selection rules for the emission of K-particles as well as for the formation of pions in non-annihilating collisions of antiprotons and nuclei have also been established. The situation, however, has become much more complex since it has been discovered that the final states may also be reached through the production of multipion resonances as a result of nucleon-antinucleon annihilation. These new particles have been studied in great detail and work is going on for the determination of their quantum numbers. The various resonance particles which have been observed in $N\bar{N}$ annihilation and their known properties are summarised in Table 8.

The complexities become manyfold when it is realised that the same final state configuration may be reached through several alternative resonant states. As an example the following annihilation process may be quoted:

Table 7(a)

Selection Rules for $\bar{p} + n \rightarrow m\pi$

State	Spin Parity	I	G	$\pi^- + \pi^o$	$2\pi^- + \pi^+$	$\pi^- + 2\pi^o$	$2\pi^- + \pi^+ + \pi^o$	$\pi^- + 3\pi^o$	$3\pi^- + 2\pi^+$	$2\pi^- + \pi^+ + 2\pi^o$	$\pi^- + 4\pi^o$
^1S_o	0^-	1	-	X			-	-			
$^3S_1$	1^-	1	+		-	-			-	-	-
$^1P_1$	1^+	1	+	X	-	-			-	-	-
^3P_o	0^+	1	-	-	X	X	-	-			
$^3P_1$	1^+	1	-	X			-	-			
$^3P_2$	2^+	1	-	-			-	-			

X means strictly forbidden and - means forbidden so far as the isotopic spin is a good quantum number.

Table 7(b)

Selection Rules for $\bar{p} + p \rightarrow m\pi$ or $\bar{n} + n \rightarrow m\pi$

State	Spin parity	C	I	G	$2\pi^o$	$\pi^+ + \pi^-$	$3\pi^o$	$\pi^+ + \pi^- + \pi^o$	$4\pi^o$	$\pi^+ + \pi^- + 2\pi^o$	$2\pi^+ + 2\pi^-$	$5\pi^o$	$\pi^+ + \pi^- + 3\pi^o$	$2\pi^+ + 2\pi^- + \pi^o$
^1S_o	D^-	+	0	+	X	X	-	-				-	-	-
			1	-	X	X			-	-				
$^3S_1$	1^-	-	0	-	X	-	X		X	-	-	X		
			1	+	X		X	-	X			X	-	-
$^1P_1$	1^+	-	0	-	X	X	X		X	-	-	X		
			1	+	X	X	X	-	X			X	-	-
^3P_o	0^+	+	0	+			X	X				-	-	-
			1	-	-	-	X	X	-	-	-			
$^3P_1$	1^+	+	0	+	X	X	-	-				-	-	-
			1	-	X	X			-	-	-			
$^3P_2$	2^+	+	0	+			-	-				-	-	-
			1	-	-	-			-	-	-			

X means strictly forbidden

- means forbidden so far as the isotopic spin is a good quantum number.

Table 8

Resonance Particles in $N\bar{N}$ Annihilation and their properties

Particle	I	G	J	P	$N\bar{N}$	M	Γ	S
η	0	+	0	-1	$^1S_0$	548.5 $\pm$ 0.6	?	0
ρ	1	+	1	-1	$^3S_\phi$	751 $\pm$ 6	100$\pm$10	0
w	0	-	1	-1	$^3S_1$	781 $\pm$ 1 782.8$\pm$0.5	$4<\Gamma<11$	0
K^{*0}	$\frac{1}{2}$		1	-		891 $\pm$ 1	50 $\pm$ 2	$\pm$1
K_c	$\frac{3}{2}$		1?	+?		1215 $\pm$ 15	60 $\pm$ 10	$\pm$1

$$\bar{p} + p \rightarrow \left\{ \begin{matrix} \rho^+ + \pi^- \\ \rho^0 + \pi^0 \\ \rho^- + \pi^+ \end{matrix} \right\} \rightarrow \pi^+ + \pi^- + \pi^0$$

For stopping antiprotons, it has been shown by Chadwick et al. (1962) that all the three resonance bands appear strongly in the phase space plot with comparable strength. The presence of these bands not only controls the initial capture butalso affects the total amplitude for the process. Dalitz (1963) has discussed the effects of the different configurations on the initial states from which capture can take place for annihilation at rest. For absorption from the $^1S_0$ $\bar{p}p$ state, for example, G-parity conservation roquires I = 1 for the final state which then has the charge structure ($\rho^+\pi^-$ or $\rho^-\pi^+$). For $^3S_1$ capture,

G-parity conservation requires I = 0, which corresponds to the charge structure ($\rho^+\pi^-$, $\rho^0\pi^0$ or $\rho^-\pi^+$). Since the three bands observed have nearly the same strength, it can be concluded that the ρ-production is dominantly from the $^3S_1$ state. The $^1S_0$ capture, however, can lead directly to the emission of three s-wave pions in a I = 1 state. This is a much more dominant mode than ρ-production.

1.6.2 Selection rules and annihilation in complex nuclei

The states $^1S_0$, $^3S_1$, etc. mentioned in connection with the discussion of 1.6 refer to the relative orbital angular momentum of the antiproton and the annihilated nucleon. For protonium and deuterium, S, P, D, ... also represent the angular momenta of the antiprotons in their "atomic" orbits. In heavier elements, the nucleon to be annihilated has angular momentum ℓ about the centre of the nucleus. The relative angular momentum of the nucleon-antinucleon pair is given by the sum of the 'atomic' and the 'nucleonic' orbital angular momenta ($\vec{L} + \vec{\ell}$). For example, annihilation from an S state atomic orbit need no longer imply a relative angular momentum of zero. Thus, even if Stark mixing (see paragraph below) leads to absorption from nS atomic states in complex nuclei, because of the 'nucleonic' angular momenta, the appropriate selection rules correspond to 0, 1, 2, .. etc. units of angular momentum.

For annihilation both in hydrogen and in complex nuclei, because of the thermal motion and recoil from capture, the $\bar{p}$-nucleus system will move into the vicinity of other atoms and experience their partially shielded electric fields. An interaction can take place between the antiproton and the neighbouring atom via the electric field and angular momentum is transferred from or to the antiproton. Consequently, an antiproton captured into (n,L) may be transferred into (n,S) which is a more favourable state for annihilation. This result of the Stark effect may not be very predominant in heavy nuclei since the stray electric fields are comparatively small and absorption may be from atomic states other than the S-states, which leads to further mixing of the selection rules. Moreover, especially in deuterium, a coulomb effect will be an additional complication, since the antiproton is attracted by the electric field of the proton.

The above discussion shows that the factors controlling the annihilation of antiprotons in complex nuclei are many and varied and that proper consideration should be given to each before any conclusion is drawn from the selection rules. This aspect of annihilation at rest is discussed again in Chapter 2.

CHAPTER 2

The Antiproton-Nucleon Annihilation

2.1 The Interactions of Antiprotons in Flight

Antiprotons in flight may interact with nucleons by elastic and inelastic processes. In the latter, the interaction may involve the inelastic scattering of the antiproton or the mutual annihilation of the antiproton and the target nucleon. In both processes, mesons are produced. Thus,

$\bar{p} + p(n) \longrightarrow \bar{p} + p(n) + \text{mesons}$		Inelastic scattering
$\bar{p} + p \longrightarrow \bar{n} + n + \text{mesons}$		Inelastic charge exchange
$\longrightarrow \bar{n} + n$		Elastic charge exchange
$\longrightarrow \text{mesons}$		Annihilation

The interaction with the proton involves the T = 1 and the T = 0 isospin channels whereas the interaction with the neutron involves only the T = 1 isospin state. Thus,

$$\sigma(\bar{p}p) = \tfrac{1}{2}\left[\sigma(0) + \sigma(1)\right]$$

$$\sigma(\bar{p}n) = \sigma(1)$$

where $\sigma(0)$ and $\sigma(1)$ are the cross-sections for the two isospin channels. By measuring the interaction cross-sections, the cross-sections $\sigma(0)$ and $\sigma(1)$ can be determined.

The elastic and inelastic interaction cross-sections for antiprotons have been measured by Elioff et al. (1962) in the energy range 0.5 to 1 GeV, both in hydrogen and in deuterium. It is found that the anti-proton-deuteron total and inelastic cross-sections are 1.8 times as large as the antiproton-proton cross-sections. Correction has, however, to be made for the shielding of one nucleon by the other in the deuterium nucleus. Experimental information on nucleon-deuteron and nucleon-nucleon cross-sections indicates that the sum of free-nucleon cross-sections is 10% greater than the deuteron cross-section. Using the calculations of Blair (1958) for the shadow effect in the deuteron on the antinucleon interactions, Elioff et al. obtain the anti-proton-neutron cross-sections by subtracting $\bar{p}$-p from the corrected $\bar{p}$-d cross-sections at the corresponding energies. Their results are summarised in Table 9.

Table 9

Comparison of $\bar{p}p$ and $\bar{p}n$ cross-sections (mb)

$\bar{p}$ energy (MeV)	Total		Elastic		Inelastic		Charge Exchange
	$\bar{p}p$	$\bar{p}n$	$\bar{p}p$	$\bar{p}n$	$\bar{p}p$	$\bar{p}n$	$\bar{p}p$
534±25	118±6	119±8	42±5	40±10	70±3	79±6	6.0±1.3
700±33	116±5	96±7	42±4	25±8	66±3	71±5	7.2±1.5
816±37	108±5	112±7	38±4	44±9	63±3	68±5	7.1±1.2
948±42	96±3	102±6	33±3	39±7	56±2	63±4	6.8±1.0
1068±46	96±3	109±4	30±2	42±6	60±2	67±5	5.7±1.1

A comparison of $\bar{p}p$ and $\bar{p}n$ cross-sections shows that within experimental errors, the cross-section for interaction with protons is the same as that for neutrons. Since the $\bar{p}$-p system may interact through the isotopic spin states T = 1 and T = 0 while the $\bar{p}n$ system can interact only through the state T = 1, the equality of these cross-sections shows that the two states are equally effective. This conclusion is further supported by the experiment of Hinrichs et al. (1962) on the antineutron-proton interaction which is charge symmetric to the antiproton-neutron interaction and should take place with the same cross-section. The observed value of $\sigma(\bar{n}p)$ is (45.2 ± 5.4) mb which compares very well with $\sigma(\bar{p}p)$ of (51 ± 3)mb at similar energies.

2.1.1 Annihilation in flight in nuclear emulsion

In emulsions, where the interactions take place in complex nuclei, the annihilation on a proton is distinguished from that on a neutron by the number of mesons produced, which should be even in the case of a proton and odd in the case of a neutron. The ratio of the number of events with odd to the number of events with even number of mesons gives the ratio of the relative frequencies of annihilation on neutrons and protons. This odd/even ratio, when compared with the neutron/proton ratio for the emulsion nuclei, gives the ratio of the

relative probabilities of annihilation on neutrons and protons. However, confusion arises by the secondary interactions of the mesons within the parent nuclei. Proper allowance has, therefore, to be made for cases where secondary interactions do take place and the odd/even ratio is modified accordingly. If the two isospin channels are in fact equally operative, the modified ratio should be consistent with the neutron/proton ratio of the emulsion nuclei. The mesons comprise both pions and kaons but in the present work kaons have not been distinguished from pions since they constitute only a small fraction (4%) of the total.

2.1.2 Relative probabilities of annihilation in flight on neutrons and protons in emulsion

The relative probabilities of annihilation of anti-protons in the energy region (0-250 MeV) on neutrons and protons have been inferred by Ekspong and Ronne (1959) from the annihilation cross-section per nucleon measured by them for emulsion. They have compared their value of annihilation cross-section per nucleon of (98^{+30}_{-25})mb with the value of the annihilation cross-section per proton of (80 ± 13)mb found directly on protons by Coombes et al. (1958), and have concluded that the $\bar{p}$-n cross-sections are at least as large as, if not larger than, the corresponding $\bar{p}$-p cross-sections.

The evidence quoted from the counter experiment of Elioff et al., the Bubble Chamber results of Hinrichs et al., and the emulsion data of Ekspong and Ronne all point towards equal probability of inelastic interaction of an antiproton in flight with neutrons and protons and when interpreted in terms of isospin, show that interaction takes place equally through the T = 1 and T = 0 channels. This is shown in Figure 6 where the ratio of the two channels is plotted against the kinetic energy of the antiproton.

2.2 The Annihilation of Antiprotons at Rest

2.2.1 Process of absorption and annihilation in complex nuclei

As the antiproton slows down and reaches the end of its range, it may be captured in a Bohr orbit of the nucleus and make many radiative or Auger transitions to lower orbits until it is finally absorbed on the surface of a nucleus and annihilates on a nucleon. The de-excitation by these radiative and Auger transitions may, however, be affected by the electric fields of the neighbouring atoms and the antiproton may undergo Stark transitions which increase the probability of the antiproton populating the low angular momentum states. Whether the nuclear capture takes place from a particular angular momentum state will depend upon the relative values of the

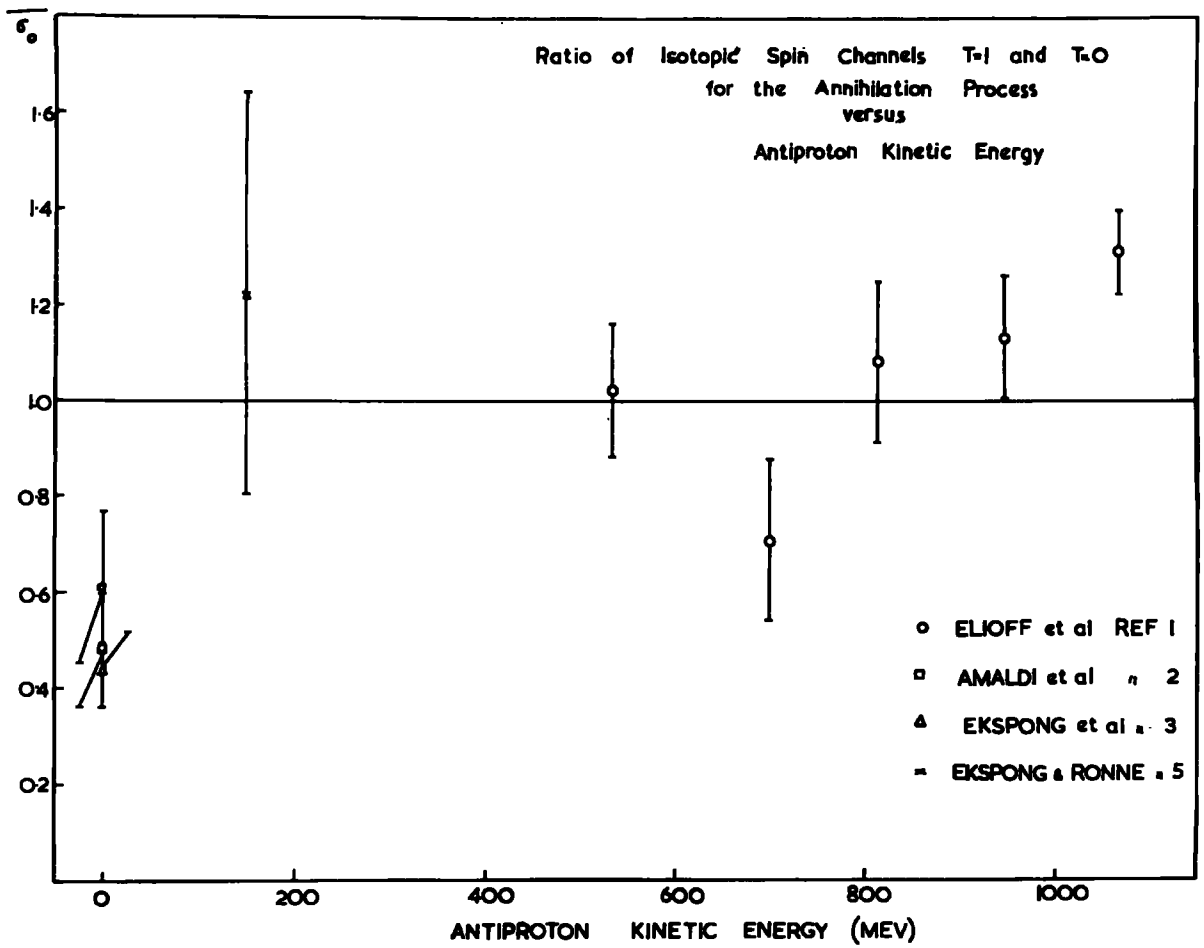

FIG. 6 Ratio of the I spin channels T=1 & T=0 in the annihilation of antiprotons on nucleons

electromagnetic transition rates and the capture rate from that state. For example, Desai (1960) has calculated the relative capture rates for antiprotons in protonium as well as the Stark transition rates and finds the following values:

i) Capture rates for S and P states

$$\Gamma_c(nS) = 5.3\ 10^{18}/n^3 \text{ sec}^{-1}$$

$$\Gamma_c(nP) = 4.3\ 10^{14}/n^3 \text{ sec}^{-1}$$

ii) Stark Transition rate

$$\Gamma_s(nP\text{-}nS) = \Gamma_s(nS\text{-}nP) \sim n^2\ 4.2\text{x}10^{13}\ \frac{a_o}{R(t)}\ \exp -\frac{R(t)}{a_o}$$

where R(t) is the distance of a hydrogen atom from protonium at time t and a_o is the radius of the first Bohr orbit for the electron. For $5 < n < 20$ and $R(t) \sim a_o$,

$$\Gamma_s(nP\text{-}nS) \gg 10^{13} \text{ sec}^{-1} \propto n^2$$

$$\Gamma_c(nS) > 10^{13} \text{ sec}^{-1} \propto 1/n^3$$

$$\Gamma_c(nP) > 10^{13} \text{ sec}^{-1} \propto 1/n^3$$

For protonium , therefore, P state capture becomes comparable to the S state capture only for values of n smaller than 10. Much before the antiproton reaches such low values of n, the Stark effect collisions become effective and the capture takes place predominantly from S-states of orbit $n \sim 5\text{-}20$. The absorption of antiprotons in deuterium may also take place from n S states where S refers to the angular momentum of the antiproton in its atomic orbit. Corresponding

calculations for the annihilation of antiprotons in complex nuclei have not been made. However, for the entirely similar process of the absorption of negative K-mesons by emulsion nuclei, calculations by Martin (1962) and Condo et al. (1964) indicate that the nuclear capture of the meson occurs dominantly from states of $\ell = 3,4$ for the heavy nuclei and from $\ell = 2$ for the light elements. For antiprotons the capture will be favoured from higher values of ℓ because of the increased mass, for example, $\ell \sim 5$ for heavy and $\ell \sim 3$ for light elements. (Martin, private communication). Thus, contrary to the case of hydrogen and deuterium, on account of the motion of the nucleons in the nucleus, the capture will not occur from a specific state of $\bar{p}$-nucleon angular momentum.

Selection rules (Tables 7a,b Chapter 1) which determine the probability of annihilation on nucleons on the basis of the relative angular momentum of the antiproton and the absorbing nucleon can be verified only for the case of hydrogen and deuterium where the initial angular momentum state of the $\bar{p}$-N system is unique.

For annihilation in emulsions, complications arise for two reasons. Firstly, the angular momentum of the absorbing nucleon makes the relative $\bar{p}$-nucleon angular momentum on capture non-unique so it is not possible to apply selection rules. Secondly, although the probability of atomic capture

of an antiproton on a given constituent of emulsion is proportional to the number of atoms/c.c. of that element, not much is known about the relative probability of capture on different constituents of the emulsion.

Fermi-Teller (1947) predict that capture obeys the Z-rule, which is valid separately for Ag Br and the light elements (CNO) but may not be valid for the emulsion as a whole. Experiments with muons show that their absorption lies between an N-rule and an NZ rule. A similar conclusion has been reached from observations on pion annihilation. The absorption of antiprotons may also be governed by some intermediate rule. Moreover, in heavy nuclei, the composition of the nuclear surface may be different from the core composition. The relative proton and neutron densities in the nuclear surface being unknown, the comparison between the probabilities of annihilation on neutrons and protons becomes difficult. Even when the relative number of different nucleons in the nuclear surface can be accurately determined, the annihilation products cannot be used unambiguously to identify the annihilated nucleon since the secondary pions confuse the original characteristics by their interactions with other nucleons of the nucleus.

2.2.2 Relative probabilities of annihilation at rest on neutrons and protons

The relative probabilities of annihilation of antiprotons

at rest on neutrons and protons of emulsion nuclei have been determined by Amaldi et al. (1959). The experimental value of the odd/even ratio which is the ratio of the frequencies of annihilations on neutrons and protons is found to be (0.91 ± 0.15), which value, when corrected for the efficiency of detection of pions, the dip angle of grey tracks, the production of charged secondaries and for the charge exchange of neutral and charged pions, becomes (0.78 ± 13). The correction for charge exchange is arbitrary and inadequate, and is allowed for by increasing the value of the probability of absorption of pions without allowing for the charge exchange of neutral and charged mesons separately. From this ratio of relative frequencies, taking into account the secondary interactions of pions with the nucleons of the parent nuclei, a modified value of (0.64±0.26) is obtained. This is then compared with the neutron/proton ratio of 1.2 which is derived after weighting according to the frequency distribution of nuclei in the emulsion.

From the apparently much smaller role played by the neutron than the proton, it is concluded that the probability of annihilation is larger in the T = 0 than in the T = 1 state. Another interpretation by Amaldi et al. is based on the assumption that the annihilation takes place mainly from the S and P states relative to the absorbing nucleon. Imposing the selection rules of tables

7a and b, annihilation on a proton is much more probable than on a neutron because for the S and P states, there are twice as many allowed transitions for the $\bar{p}p$ as for the $\bar{p}n$ system. However in view of the discussion of section 2.2.1, this interpretation cannot be justified.

The experiment has been repeated by Ekspong et al. who give a value of (0.73 ± 0.09) for the odd/even ratio. Their experimental result has been derived in the following way. The multiplicity distribution of charged pions predicted by the statistical theory of Fermi is assumed to be the original distribution on annihilation subsequently modified by the absorption due to secondary interactions of the pions. For various degrees of absorption, a series of curves corresponding to different ratios of probabilities of annihilation on neutrons and protons is obtained, and it is found that the experimental value corresponds to a one to four probability of annihilation on neutrons as compared to protons. It is, therefore, concluded that the $T = 0$ isospin channel predominates over the $T = 1$ channel. Figure 6 summarises the results of the experiments referred to above. Whereas at finite energies, the experiments show the ratio of the probability of interaction through the isospin channel $T = 1$ to that for $T = 0$ to be unity, the points corresponding to zero energy of antiprotons fall well below. The points due to Amaldi

et al. and Ekspong et al. correspond to the observed and the corrected experimental values.

2.2.3 Annihilation at rest in deuterium

The experiments on annihilation of antiprotons at rest in emulsion indicate that the neutron is less effective in the annihilation process than the proton. This is in contradiction to the results at finite energies where the two have been found to be equally effective. If the selection rules are operative, their effect should become apparent in the annihilation of antiprotons in deuterium, which will take place mainly from the S-states of the $\bar{p}$-D system. The effect will, however, be masked by the Coulomb attraction between the proton and the antiproton which is bound to enhance the probability of annihilation on protons. Moreover, allowance must be made for the secondary interactions of pions with the second nucleon in the deuteron before any final conclusion about relative probabilities of annihilation on neutrons and protons can be reached.

If the average kinetic energy of the secondary pions is about 200 MeV, the cross-sections for elastic scattering and charge exchange can be estimated from the pion-nucleon scattering data. The cross-section for elastic scattering of neutral pions is twice its charge exchange cross-section. The maximum effects of the secondary interactions of pions on the final products of antiproton-deuteron annihilation can be estimated and are summarised in Table 10.

Table 10

Effect of secondary interactions of pions on the final products of $\bar{p}D$ annihilation

Secondary Interaction of pions	x-section (mb)	Number of pions per annihilation	Total contribution	Charge	
$\pi^- p \longrightarrow \pi^- p$	23	2	46	odd	
$\pi^- p \longrightarrow \pi^o p$	46	2	92	even	$\frac{\text{even}}{\text{total}}$
$\pi^+ p \longrightarrow \pi^+ p$	210	1	210	odd	$\frac{162.5}{559.5}$
$\pi^o p \longrightarrow \pi^o p$	94	1.5	141	odd	$=0.290$
$\pi^o p \longrightarrow \pi^+ n$	47	1.5	70.5	even	
$\pi^- n \longrightarrow \pi^- n$	210	1.5	315	even	
$\pi^+ n \longrightarrow \pi^+ n$	23	1.5	36	even	$\frac{\text{odd}}{\text{total}}$
$\pi^+ n \longrightarrow \pi^o p$	46	1.5	69	odd	$\frac{139.5}{631.5}$
$\pi^o n \longrightarrow \pi^o n$	94	1.5	141	even	$=0.221$
$\pi^o n \longrightarrow \pi^- p$	47	1.5	70.5	odd	

Diff. $=0.069$

$$\frac{\text{odd}}{\text{even}} \quad \frac{1-0.069}{1+0.069} = 0.87$$

The approximate calculation summarised in Table 10 is based on the extreme assumption that the spectator nucleon is always struck by one of the secondary pions. Since the secondary interaction and the coulomb effect both lead to the reduction of the odd/even ratio, it is difficult to come to any firm conclusion concerning the effect of the

selection rules on the odd/even ratio observed for deuterium. This ratio has been found to be (0.763±.019) by Barnes et al. (1964) (private communication).

To decide whether or not the probability of annihilation at rest on neutrons and protons is the same, some other method has to be devised which will take into proper account the various processes involved. To avoid the biases that result from selection rules and from Coulomb effect in deuterium, the relative probabilities of annihilation on neutrons and protons are best determined in large nuclei. Firstly, annihilation takes place from orbitsof high angular momentum which leads to mixing of the selection rules. Secondly, the spherically symmetric Coulomb field ensures that there is no preferential absorption by protons. However, there is the disadvantage that with large nuclei, secondary interactions of the products of annihilation will destroy the relationship between odd (even) multiplicities and annihilations on neutron (proton). Consequently a compromise must be made to nuclei of intermediate size. To this end the following experiment has been carried out in which the annihilations of antiprotons in the light elements (CNO) and the heavy elements of emulsion have been separately examined.

2.3 The Experimental Set-up

2.3.1 Exposure of the emulsion stack

A stack of K5 emulsion of size (25 cm x 15 cm x 600μ)

was exposed at the Cern Proton Synchrotron to a separated beam of antiprotons of momentum 700 MeV/c, developed by Amaldi et al. Tho diameter of the beam was 5 cms and in seven and a half hours a total of 96,000 antiprotons and 33,000 negative pions (contamination) passed through the stack, thus yielding fluxes of 0.49×10^4 $\bar{p}/cm^2$ and $0.17 \times 10^4 \pi^-/cm^2$ respectively.

2.3.2 Scanning for annihilation stars

Scanning was carried out under X20 x1.5x15 on Cooke microscopes in a region about 10 cms from the edge of the plates and tracks were followed until the antiprotons annihilated or escaped from the plate. Annihilations in flight were rejected. Initially 929 stars were recorded of which 223 were accompanied by lightly ionising secondaries only. A further 499 such stars were found in a scan exclusively made for this purpose, giving a total of 722. Single tracks were not included in this sample because of the possibility of confusion with protons. The number of annihilations with zero prongs was assumed to be 3% of all events of even multiplicity (Horwitz et al. (1959)), thus bringing the total number of such stars to 733 and of all interactions to 1439.

2.3.3 The classification of annihilation stars

The annihilation of an antiproton at rest takes place on a nucleon in the surface of a nucleus with the production, chiefly, of about five pions. If the pions escape from the nucleus without making any interactions with its nucleons, it may recoil intact and give rise to a short black track whose length will depend on the mass of the nucleus and its momentum. The possibility of a nucleus remaining intact and giving rise to a visible recoil track after one of its nucleons is annihilated is greater for the light than for the heavy elements of the emulsion. Interactions consisting of lightly ionising secondaries and none or one short black track are, therefore, assumed to take place predominantly in the light elements of emulsion and are termed "white stars". All others are called "black stars" since they are accompanied by one or more heavily ionising secondary particles. The method used here is similar to the one followed by Barbaro-Galtieri et al. (1963) for the negative K-mesons in emulsion.

2.4 Annihilation in the Light Elements

Carbon, nitrogen, oxygen and hydrogen form the group of light elements in the emulsion. Annihilation of an antiproton on hydrogen can lead to even multiplicity only whereas annihilations in the other members of the group

may lead to both odd and even multiplicities, depending on whether the capture is on a neutron or a proton. The annihilation of a nucleon leaves the rest of the nucleus in an excited state. To estimate the excitation of the recoiling nucleus, we can assume that the process consists of

i) the separation of the parent nucleus into the excited daughter nucleus and a nucleon, and

ii) the annihilation of the nucleon.

Thus, for a nucleus N of mass A and charge Z, the annihilation on a neutron or a proton unaccompanied by secondary interactions can be represented as

$$\bar{p} + N(A,Z) \longrightarrow N(A-1,Z)^{*} + \text{mesons}$$

and

$$\bar{p} + N(A,Z) \longrightarrow N(A-1,Z-1)^{*} + \text{mesons},$$

respectively, where * indicates the excited state of the daughter nucleus.

It is difficult to estimate the excitation energy but a value has been calculated on the basis of assumption (i) above. The excitation energy is then the excitation produced when a nucleon is removed from the nucleus.

Considering annihilations on neutrons and protons of the nuclei of carbon, nitrogen and oxygen respectively, the following reactions are obtained:

$$\bar{p} + n\ (C_6^{12}) \longrightarrow C_6^{11} + 10.3\ \text{MeV} + \text{ann}^{n}\ \text{products}$$

$$n\ (N_7^{14}) \longrightarrow N_7^{13} + 2.2\ \text{MeV} + \text{ann}^{n}\ \text{products}$$

$$n\ (O_8^{16}) \longrightarrow O_7^{15} + 7.2\ \text{MeV} + \text{ann}^{n} \text{ products}$$

$$\bar{p} + p\ (C_6^{12}) \longrightarrow B_5^{11} + 8.4\ \text{MeV} + \text{ann}^{n} \text{ products}$$

$$p\ (N_7^{14}) \longrightarrow C_6^{13} + 0\ \text{MeV} + \text{ann}^{n} \text{ products}$$

$$p\ (O_8^{16}) \longrightarrow N_7^{15} + 4.5\ \text{MeV} + \text{ann}^{n} \text{ products}$$

From the energy levels of light nuclei, (Ajzenberg et al. (1955)), the following transitions are possible for the excited nuclei of C^{11}, N^{13} and O^{15} produced as a result of antiproton annihilation on neutrons:

(i) $(C_6^{11} + 10.3\ \text{MeV}) \longrightarrow Be^{7} + \alpha^{4}$ or $Be^{8} + \alpha^{3}$ (2 MeV)
$\longrightarrow C_6^{11} + \gamma$ to ground state and
$C_6^{11} \quad B_5^{11} + \beta^{+}$

(ii) $(N_7^{13} + 2.2\ \text{MeV}) \longrightarrow C^{12} + p(0.2\ \text{MeV})$
$\longrightarrow N_7^{13} + \gamma$ to ground state and
$N_7^{13} \quad C^{13} + \beta^{+}$

(iii) $(O_8^{15} + 7.2\ \text{MeV}) \longrightarrow O_8^{15} + \gamma$ to ground and
$O_8^{15} \quad N_7^{15} + \beta^{+}$

It can be seen that β-emission nearly always takes place. In the case of annihilations on protons, the excited nuclei B^{11}, C^{13} and N^{15} can undergo only γ-emission as given below:

(i) $(B_5^{11} + 8.4\ \text{MeV}) \longrightarrow B_5^{11} + \gamma$ to ground level

(ii) $(C_6^{13} + \sim 0\ \text{MeV}) \longrightarrow C_6^{13} + \gamma$ to ground level

(iii) $(N_7^{15} + 4.5\ \text{MeV}) \longrightarrow N_7^{15} + \gamma$ to ground level

Summarising, the antiproton-neutron annihilation will nearly always be followed by β-emission and antiproton-proton annihilation only by γ-emission. Since neutron annihilation leads to odd and proton annihilation to even multiplicity, β- emission may accompany odd but not even multiplicity.

2.4.1 Probability of absorption by hydrogen in the emulsion

The Fermi-Teller Z-rule for pion and muon absorption depends on energy loss being uniform in the absorbing medium, i.e., a uniformly mixed medium. Since K5 emulsion is in the form of crystals of Ag Br in a gelatine matrix, the Z-rule breaks down though it may be expected to hold separately for the crystals and the gelatine. In the CNOH group, i.e., in the gelatine, the relative contribution of hydrogen should be 0.17 as shown in Table 11.

Table 11

Relative Probabilities of Capture by each Element of the Gelatine Matrix of Emulsion

Element	N($\times 10^{22}$)	Z	NZ($\times 10^{22}$)	Relative contribution on Z-rule
C	1	6	6	0.316
N	0.3	7	2.1	0.111
O	1	8	8	0.421
H	3	1	3	0.169

Now the relative probability of absorption of pions by hydrogen in paraffin (CH_2) and lithium hydride (Li H) is found to be 1:1000 rather than 1:3 as expected from the Z-rule. As pointed out in Section 2.2.2, the molecular collisions lead to the transfer of the pion from hydrogen to carbon or lithium since its transitions through the optical levels of pionium are relatively slow. Baker (1960) has estimated that for negative K-mesons, less than 10% of the mesons which form mesic atoms in hydrogen are finally absorbed by the proton. If a similar process occurs for antiprotons, there should be only a small contribution from hydrogen. This has indeed been found to be the case by Agnew et al. (1960) who studied the antiproton interactions in propane and discovered that the stopping antiprotons preferentially annihilate on carbon. The explanation is that the relatively few antiprotons originally captured on hydrogen are subsequently transferred to carbon by the collisions of protonium (about 10^{11} collisions per sec) with the neighbouring carbon atoms in propane. They assume this transfer mechanism to be so efficient as to make all annihilations of stopped antiprotons to occur on carbon nuclei.

The neutron/proton ratio for CNOH group of emulsion, in view of the very low possible contribution from hydrogen can therefore be taken as unity instead of 0.73

which will be expected if hydrogen contributed according to the Z-rule.

2.5 Results

Of the 1428 stars recorded in scanning, each has been scutinised twice to determine the number of secondary mesons and to identify associated low energy electrons. The data are summarised in Tables 12 and 13 for the two categories of white and black stars. The charged particle multiplicity distribution, the mean multiplicity and the odd/even ratio for each group are given. The proportion of white stars with and without accompanying low energy electrons and with and without visible recoiling nuclei is also shown in Table 12.

Table 12

Characteristics of White Stars

a) Multiplicity distribution

n_s =	0	1	2	3	4	5	6	7	8
	11*	82	187	231	159	45	14	3	1

$\bar{n}_s = (2.90 \pm 0.04)$

b)	n_s odd	n_s even
Total number of events	361	372
Proportion with recoils	(41±3)%	(34±3)%
Proportion with electrons	(57±4)%	(13±2)%
Mean multiplicity	(2.84±0.06)	(2.97±0.06)
c) Odd/even ratio is (0.97 ± 0.05)		

* This number has been calculated from the data of Horwitz et al. (1959).

Table 13

Characteristics of Black Stars

a) Multiplicity distribution

n_s =	0	1	2	3	4	5	6	7
	44	153	196	171	111	22	6	3

$\bar{n}_s = (2.36 \pm 0.03)$

b)	n_s odd	n_s even
Total number of events	349	357
Mean multiplicity*	(2.28±0.04)	(2.44±0.05)

c) Odd/even ratio is (0.98 ± 0.05)

* The observed multiplicity distributions for white and black stars are not Poissonian. To estimate the error on the mean, the procedure adopted is to take n_s odd and n_s even separately in small groups (of 36 each) and to determine the mean n_s for each group. These means are supposed to be distributed as a Gaussian, the standard deviation of which is determined and hence the error on the mean.

2.5.1 The neutron/proton ratio for white stars

Before the relative probabilities of annihilation on neutrons and protons could be determined, the neutron/proton ratio to which the odd/even ratio is to be compared, must be known.

As pointed out in Section 2.4.1, this is expected to be unity if no annihilations occur in hydrogen. From Table 12 the role of hydrogen can be estimated from the

proportion of annihilations without visible recoiling nuclei for even multiplicity which is 66% compared to 59% for the odd multiplicity. Thus, only (9 ± 8)% of all multiplicities can be considered to have arisen in hydrogen. Considering the large error, this result is not inconsistent with a zero contribution from hydrogen.

The assumption of sections 2.3.3 and 2.4, namely, that the white stars represent annihilation in the light elements of emulsion (carbon, nitrogen and oxygen) do seem to be confirmed by the experimental results in view of the following:

i) Odd multiplicity is usually accompanied by low energy electrons whereas even multiplicity is not. The 13% of even multiplicity events which are accompanied by low energy electrons may be cases of Auger electron emission. Background electrons may also be present though their contribution should be the same for even as well as for odd multiplicity events. For the latter, it is generally observed that where both an electron and a recoiling nucleus are found, the electron does appear to be emitted from the end of the recoil, thus confirming its identity definitely as β -emission from the excited daughter nucleus of one of the CNO group.

ii) The mean multiplicity, (2.97 ± 0.06), of the even-pronged stars compares well with the value of (3.21 ± 0.35) obtained by Horwitz et al. (1959) for annihilations of

antiprotons at rest in hydrogen and also with that of (3.06 ± 0.26) found by Agnew et al. (1960) at an antiproton kinetic energy of 80 MeV. This shows that there have been few secondary interactions between the mesons and the nucleons inside the absorbing nuclei. Moreover, the mean multiplicity of the black stars (Table 13) is appreciably lower than its value for the white stars, indicating the absence of secondary collisions in the latter and their presence in the former.

iii) An analysis of the recoil tracks of white stars shows that their length distribution is consistent with annihilation in the light elements. This is discussed in greater detail in Section 3.6 of Chapter 3.

To summarise, the events given in Table 5 represent annihilations, unaccompanied by secondary collisions, occurring predominantly in carbon, nitrogen and oxygen, for which the neutron/proton ratio is unity.

2.5.2 The relative importance of T = 1 and T = 0 channels

It has been shown above that the neutron/proton ratio for light elements which give rise to white stars is close to unity. The odd/even ratio for this group is (0.97±0.03). The close agreement between these two means that the probability of annihilation of an antiproton at rest is the same as the probability of annihilation on a proton. Hence

the amplitudes for annihilation of the T = 1 and T = 0 channels are equal, in agreement with the results found at finite energies, but in disagreement with the results of Amaldi et al. (1959) and Ekspong et al. (1961) at zero energy. This is not surprising in view of the fact that the results in the latter cases are derived from annihilations in all elements of the emulsion for which corrections for absorption have been made but charge exchange has either been ignored altogether or inadequately allowed for.

In the work described here, the results are derived from the group of light elements of the emulsion for which no corrections for secondary interactions need to be made.

2.5.3 Characteristics of black stars

The results for the black stars are given in Table 13. The mean multiplicity is (2.36 ± 0.03) and the odd/even ratio is (0.98 ± 0.05) which is to be compared with a n/p ratio of 1.29. Since the black stars are characterised by the secondary interactions of the pions within the nuclei, the mean multiplicity and the odd/even ratio will be modified by the extent of these interactions, involving the absorption and the charge exchange of a meson. The multiplicity of a particular annihilation as well as the mean multiplicity of the group is reduced on the absorption of a meson. The charge exchange of a charged meson reduces, and the charge exchange of a neutral meson increases, the multiplicity of a particular annihilation

although the mean multiplicity may remain unaffected. The mean multiplicity of (2.36 ± 0.03) found for black stars when compared with (2.90 ± 0.04) for the white stars shows the extent to which it has been modified by absorption and charge exchange.

2.6 The Calculation of the Effects of Secondary Interactions

There are two main assumptions on which the detailed calculations for the secondary effects are based:

i) that the probability of annihilation on a neutron is the same as the probability of annihilation of an antiproton at rest on a proton, and

ii) the multiplicity distribution of the white stars, after adjustment for a neutron/proton ratio of 1.29 which is typical of heavy elements, is the true distribution resulting from annihilation. This is modified subsequently by the secondary interactions of mesons. Both these assumptions are borne out by the experimental results mentioned earlier. Hence there is an advantage over previous calculations which are based on theoretical values of absorption and distribution of pions. The details of the calculation are given in the appendix.

2.6.1 Effects of charge exchange

To calculate the effect of charge exchange of mesons it is necessary first to know the number of neutral mesons which accompany each charged particle multiplicity. A

summary of the previous estimates based on the observation of pair production in heavy liquid chambers and on the method of energy balance has already been given in Table 6, of Chapter 1. These include charged multiplicities of 2 and upwards. Extrapolation to n_s values of 1 and 0 is uncertain but the number of zero and one pronged stars entering the calculation is small. Figure 5 (Chapter 1) shows the variation of mean number of neutral pions with each charged multiplicity. The mean number of neutral mesons averaged over various values of charged multiplicity is (2.02 ± 0.15).

The relative probability for the charge exchange of a neutral meson on a neutron or a proton in the energy range of the secondary pions has been estimated from the isospin amplitudes and is twice the corresponding probability for the charge exchange of a charged pion. From the known cross-section for charge exchange and the mean path length in large nuclei, the expected probability is about 0.1. At this value the effect of charge exchange is to increase the mean multiplicity by about 5% and reduce the odd/even ratio by about 20%.

2.6.2 Effects of absorption

The absorption of mesons will tend to reduce the mean multiplicity and the odd/even ratio. This can be observed from curve 1 in figures 7 and 8. The probability of absorption can be estimated from the observed charged

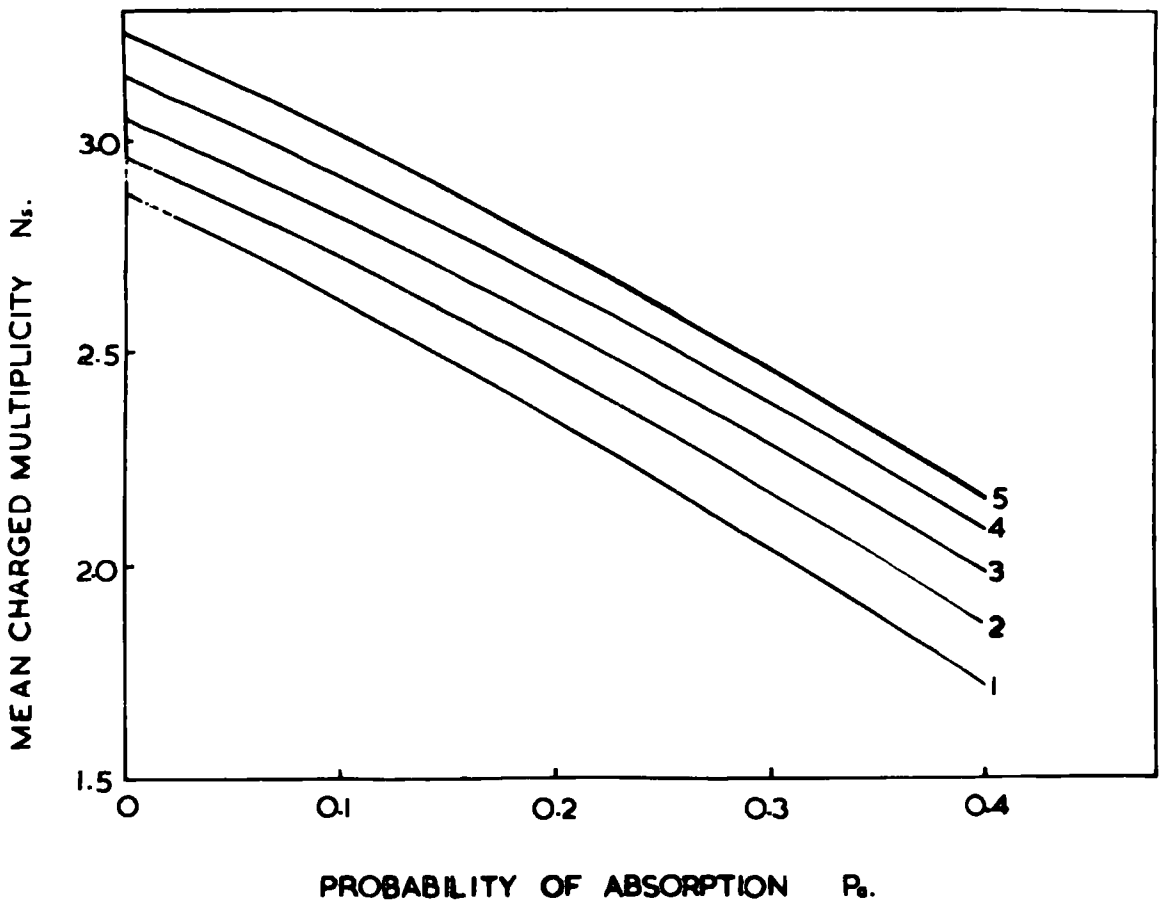

FIG. 7 The calculated variation of the mean charged multiplicity due to absorption and charge exchange of the secondary mesons

particle multiplicity from Figure 7. It is found to be 0.27 , a rather high but not unexpected value since it corresponds to annihilations in the heavy elements of emulsion.

The observed odd/even ratio for the black stars is shown in Figure 8 for the value of absorption probability corresponding to the mean multiplicity of (2.36 ± 0.03), and is in good agreement with the calculated value.

If the effect of charge exchange is ignored (curve 1 of Figure 8) the probability of absorption is reduced to 0.19 and the agreement between the expected and the observed odd/even ratios can be brought about only if the probability of annihilation on the neutrons is reduced to about 0.75 of the probability of annihilation on the protons. Both Amaldi and Ekspong find a ratio close to this value.

2.6.3 Comparison of observed and expected charged particle multiplicities

The charged particle multiplicity for the white stars when normalised to the neutron/proton ratio of 1.29 for the heavy elements of emulsion gives the multiplicity expected before any secondary interactions take place. This is modified by charge exchange and absorption. The final distribution is computed for the values of charge exchange and absorption expected in the experiment and

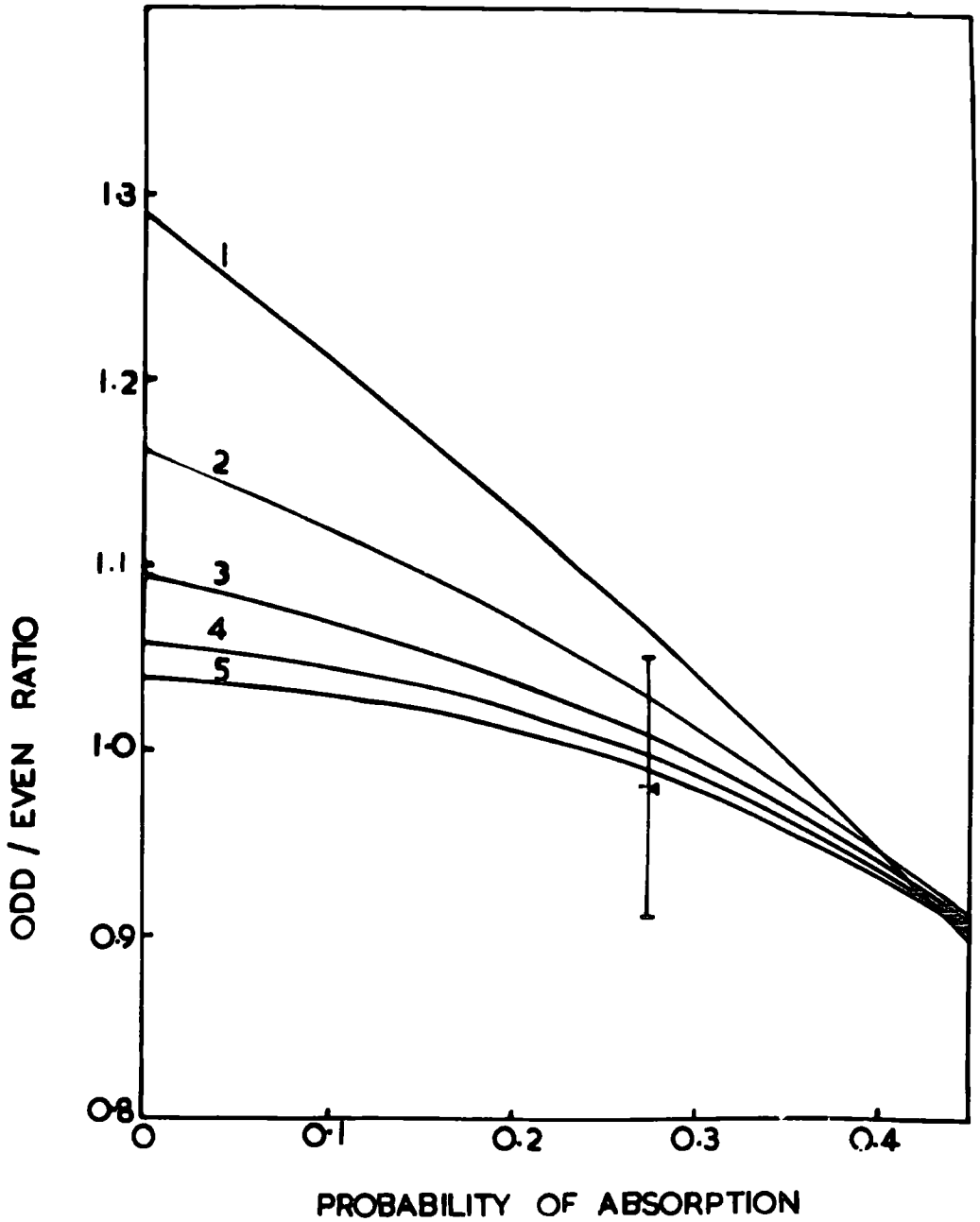

FIG. 8 The calculated variation of odd even ratio due to absorption and charge exchange of secondary mesons

is shown in Figure 9. Also shown in the same figure is the observed distribution for the sample of black stars. There is good agreement between the computed and the observed distributions.

2.7 Conclusions

The mean multiplicities, the multiplicity distributions and the odd/even ratios have been determined for the annihilation in the light and heavy elements of emulsion of stopping antiprotons. The isospin amplitudes for the $T = 0$ and $T = 1$ channels are found to be the same for annihilations in the light elements of emulsion. The apparent lack of equality of the probabilities of annihilation on neutrons and protons found in heavy elements results from the interactions of the annihilation products in the parent nuclei.

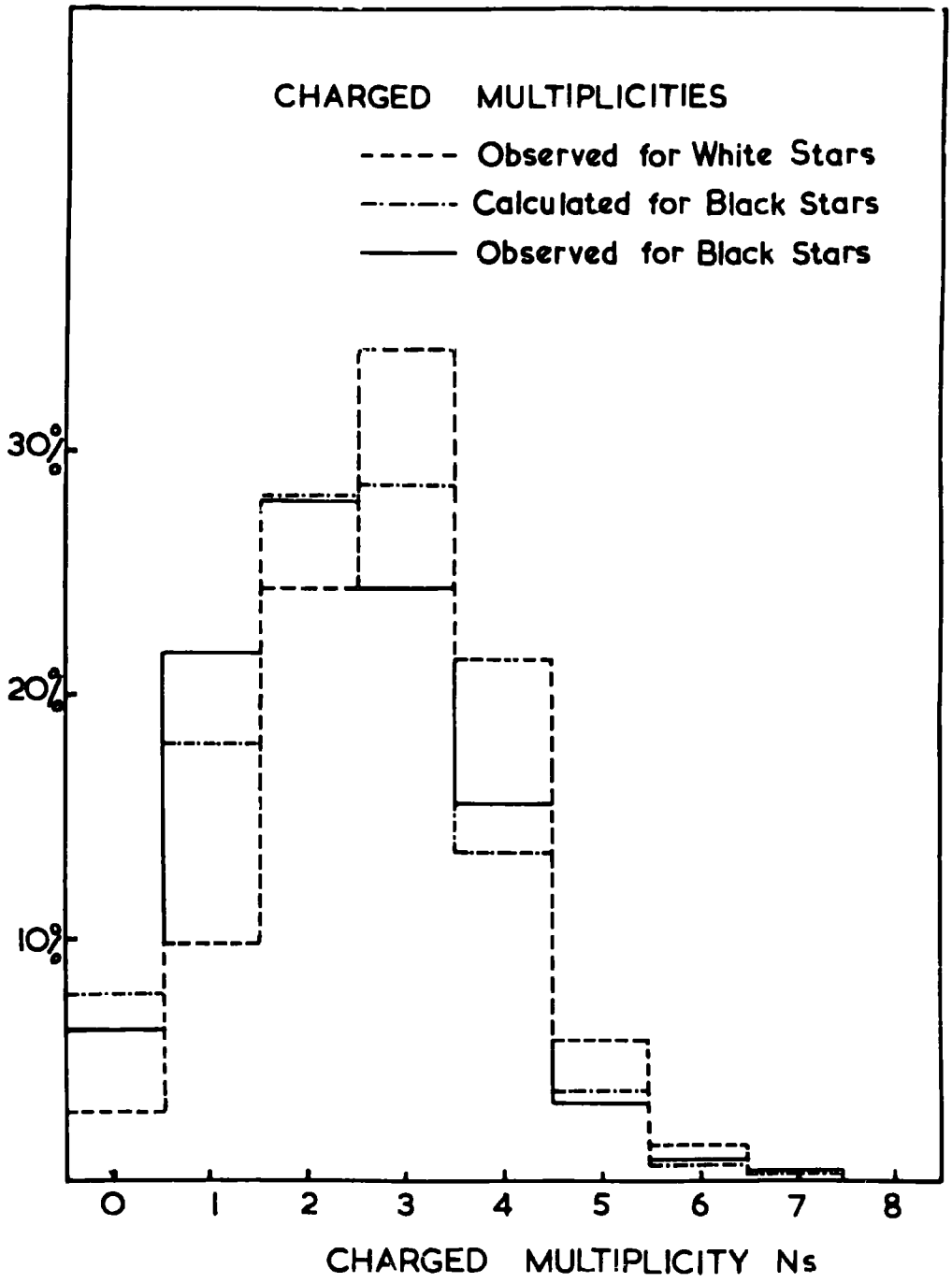

FIG. 9 The comparison of observed and calculated charged particle multiplicities

CHAPTER 3

General Features of Antiproton Annihilation At Rest

3.1 Average Number of Secondary Pions Interacting Inside the Parent Nucleus

After the annihilation of an antiproton on a nucleon at the surface of a nucleus, some of the mesons created pass through the nucleus and may interact with its nucleons. A part of the energy of these interacting mesons is given to the nucleus and manifests itself in the form of knock-on and evaporation tracks in the emulsion. These nucleonic tracks indicate the extent to which secondary interactions of the mesons have taken place. In the absence of any such collisions there are no heavily ionising particles and the annihilation event is called a white star.

The number of pions interacting within the parent nucleus, after the antiproton has annihilated on one of its nucleons, can therefore be determined from the relative frequency of white stars. This method of analysis is derived from Amaldi et al. (1959). The probability of observing N_w white stars out of a total number N_{tot} of all type of stars is given by

$$\frac{N_w}{N_{tot}} = \eta^{\langle N_\pi \rangle} \qquad \ldots\ldots (1)$$

where η is the probability that a secondary pion escapes from the nucleus without interaction and $\langle N_\pi \rangle$ is the

average number of charged and neutral mesons produced in annihilation. It is expected that there will be a contribution to white stars from interactions in hydrogen and from stars in emulsion nuclei in which all nucleonic secondaries are neutral. The latter will be small and the former has already been shown in Chapter 2 to be negligible. Relation (i) is, therefore, valid.

In the present experiment the fraction of white stars is (0.24 ± 0.01) and the total multiplicity is (4.92 ± 0.15) (see section 3.31). Substituting in (i) gives a value (0.75 ± 0.01) for . Now η is related to the number ν, of pions interacting within the nucleus by

$$\eta = 1 - \frac{\nu}{\langle N_\pi \rangle} \qquad \ldots\ldots \text{(ii)}$$

Hence the number of interacting pions, ν, is (1.23 ± 0.05). This number is not very sensitive to the value of N_π. It comprises the number of pions which has been absorbed and those which have been scattered. In the next section their relative proportions are determined.

3.2 The Absorption Probability Calculated from the Number of Pions that have Interacted

The value of charged multiplicity found for black stars is (2.36 ± 0.03). Following the methods of Barkas et al. (1957) and Amaldi et al. (1959), if we denote by "a" the fraction of interacting pions absorbed in the emulsion nucleus, we have

$$\langle N_{\pi} \rangle = \frac{1}{e_{\pi}} \frac{N_{\pi}}{N_{\pi^{\pm}}} \langle N_{\pi^{\pm}} \rangle + aV$$

where

$\langle N_{\pi} \rangle$ = Average total multiplicity

$\langle N_{\pi^{\pm}} \rangle$ = Average charged particle multiplicity

V = Number of pions which interact within the parent nucleus,

and e_{π} = is the efficiency of detection of pions.

This expression is valid if absorption is the only mechanism by which secondary mesons interact. However, as was pointed out in Chapter 2, charge exchange may be an important process by which charged particle multiplicities are altered. The expression would still be valid under the following restrictions:

a) the charged particle ratio $N_{\pi}/N_{\pi^{\pm}} = 3/2$

b) the probability of charge exchange of neutral mesons by a proton or a neutron is twice that of charged mesons, and

c) the neutron/proton ratio is unity.

In the energy range of the experiment restriction (b) holds whereas restrictions (a) and (c) hold only approximately.

The application of the expression must be understood to lead only to an approximate estimate of the relative numbers of secondary mesons which are absorbed and are charge exchanged or scattered. It is now applied with the assumption that the three restrictions hold.

The efficiency of detection is defined as the ratio of the number of pions found to the true number of pions present. Besides the emulsion and microscope properties, it depends on the energy and angle of dip of the track and on the distance of the star from the glass surface. This last factor can, however, be easily avoided by excluding stars very near the top and the bottom of the emulsion surface. In the present work each star was examined by two physicists after its initial detection by the scanners; it is considered that the efficiency of detection of pions is almost 100%. The detection efficiency in previous work has been estimated and found to be quite high. [(Barkas et al. (1957) - 90%, Amaldi et al. (1959) - 93%, Ekspong et al. (1969) - 98%).] Assuming that the ratio $\frac{N_{\pi^0}}{N_{\pi^\pm}}$ is 3/2 and taking the value (2.90 $\pm$ 0.04) for the charged particle multiplicity from section 3.31, the number of pions absorbed, aν, is (0.81 $\pm$ 0.08), a value which compares quite well with that of unity found by previous workers. (Barkas et al., 1957, Amaldi et al., 1959). The number of interacting pions is 1.23 $\pm$ 0.05 (ν) made up of (0.81 $\pm$ 0.08) pions which are absorbed and (0.42 $\pm$ 0.09) pions which are charged exchanged or scattered. These average numbers refer to the total sample of white and black stars and are representative to the extent that the restrictions mentioned earlier hold.

3.3 Average Pion Multiplicity

The mean charged multiplicity from white stars is (2.90 ± 0.04) from Table 12 of Chapter 2. The neutral multiplicity corresponding to this is (2.02 ± 0.15) giving an average total multiplicity of (4.92 ± 0.15). The charged particle and total multiplicities for anti-proton annihilation at rest and in flight obtained by different workers have been summarised in Table 5.

3.4 Correlation of Charged Pion Multiplicity and the Number of Heavily Ionising Particles

From the considerations of section 3.1 it is clear that there must be a correlation between the number of charged pions observed and the corresponding average energy shown by the heavily ionising nucleons. On the average a high pion multiplicity probably implies few secondary collisions and should be associated with a small number of heavy tracks and vice versa. If such a correlation does actually exist, it will confirm the assumption that nuclear excitation depends chiefly on the secondary interactions.

3.4.1 Relation between shower and grey tracks

On account of the inelastic and charge exchange interactions of mesons produced on annihilation, the nucleons of the parent nucleus will be knocked out and the protons will give rise to grey tracks emerging from

the star. From the sample of black stars, the mean number of grey tracks was determined corresponding to different values of charged particle multiplicity. The results are summarised in Table 14.

Table 14

Mean Number of Grey Tracks

versus

Charged Pion Multiplicity

Number of Shower Tracks	0	1	2	3	4	5
Mean Number of Grey Tracks	1.7 ± 0.17	1.44 ± 0.09	1.47 ± 0.09	1.08 ± 0.08	0.88 ± 0.1	0.73 ± 0.21

The results of Table 14 are shown in Figure 10. The dotted line corresponds to the average number of grey tracks per annihilation star and the full line is the best straight line through the experimental points.

3.4.2 Relation between shower and black tracks

Whereas the number of grey tracks associated with a star reflect, by and large, direct collisions between the mesons and the nucleons, the emission of evaporation prongs is a more indirect phenomenon. Nevertheless, the energy release in the form of black tracks does represent the excitation produced in the nucleus on account of mesonic interactions. A correlation between the two should, therefore, be observed. This is shown in Table 15,

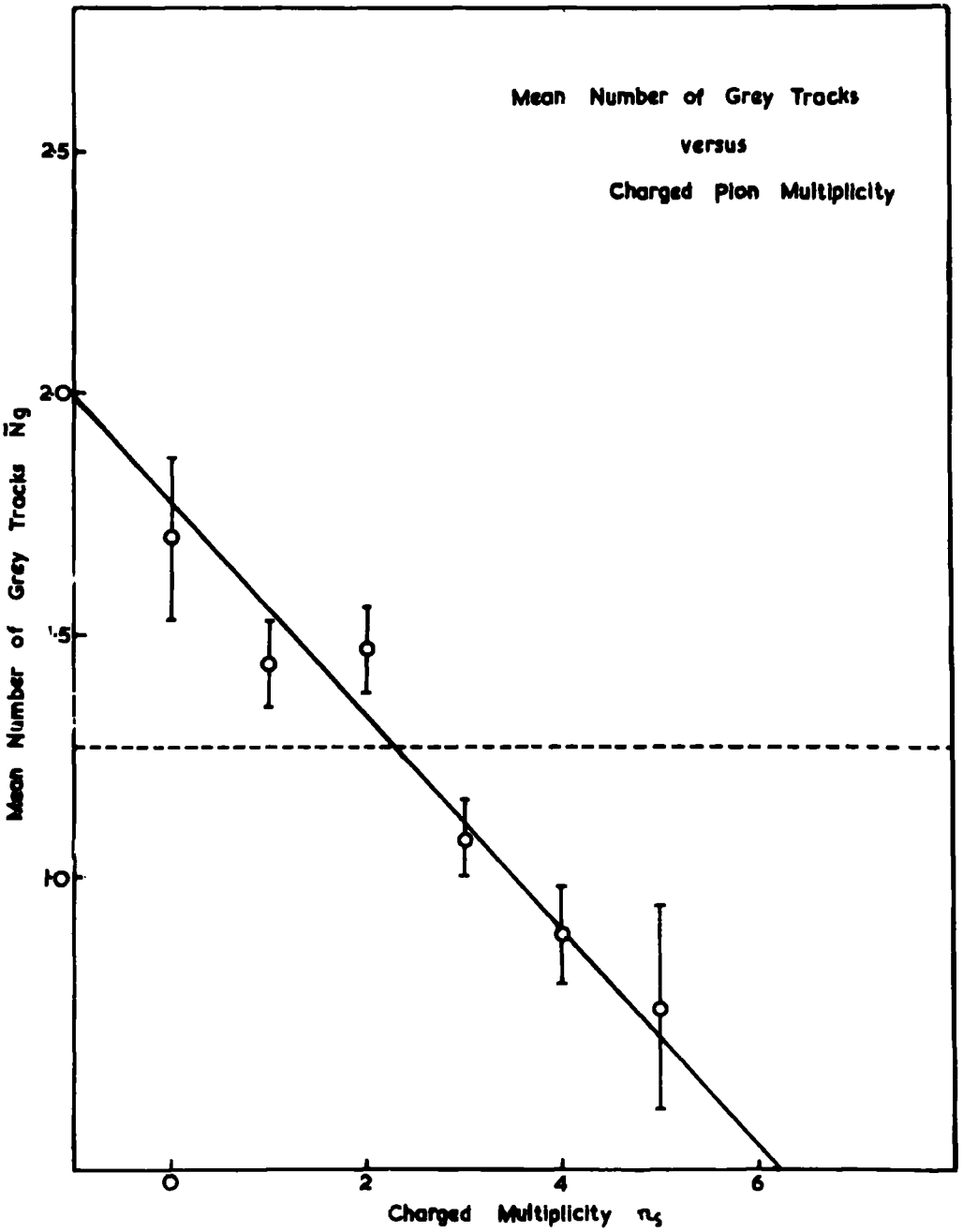

FIG. 10 The variation of the mean number of grey tracks with the charged pion multiplicity

from the mean number of black tracks associated with different charged particle multiplicity.

Table 15

Number of Shower Tracks Versus

Mean Number of Black Tracks

Number of Shower Tracks	0	1	2	3	4	5	6
Mean Number of Black Tracks	4.14 ± 0.45	3.81 ± 0.16	3.50 ± 0.17	2.93 ± 0.15	2.90 ± 0.19	2.90 ± 0.34	2.2 ± 0.45

In Figure 11, the mean numbers of black tracks are plotted against each value of the charged particle multiplicity and a linear relationship similar to that of grey tracks is found. The dotted line represents the average number of black tracks per star. The full line is the best straight line through the experimental points.

3.4.3 Relation between grey and black tracks

It has been explained before that the number of grey tracks represents the extent to which the secondary mesons have interacted with the nucleons. The excitation energy of the nucleus should therefore be large or small according as there are more or less grey tracks. Since the energy of excitation is released in the form of evaporation particles, the number of black tracks should vary as the number of grey tracks. Thus a linear relationship, similar to the previous two cases, ought to be observed if the mean

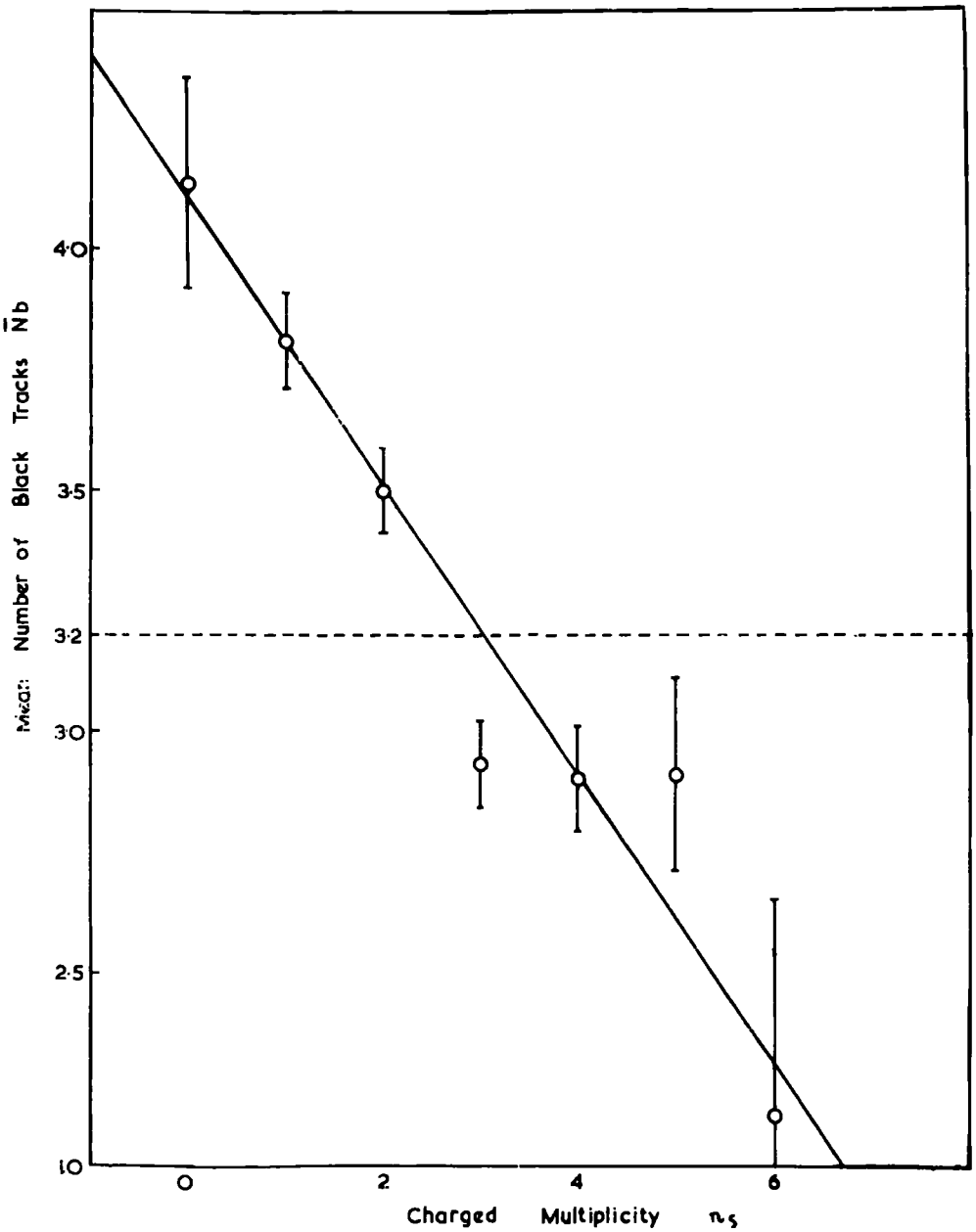

FIG. 11 The variation of the mean number of black tracks

numbers of black tracks are plotted against each grey multiplicity. This is confirmed by Figure 12 and shows that the mechanism of annihilation proceeds through the primary production of about 5 mesons which may interact with, and transfer some of their energy to, the nucleons which escape from the nucleus, leaving it excited. On de-excitation the heavily ionising particles are emitted. Some of the energy is shared by neutrals which do not leave any visible tracks in the emulsion.

3.4.4 Variation of mean number of pions with grey and black track multiplicity

Another way of looking at the correlation of shower and heavy prongs in the annihilation stars would be to find out the mean number of shower tracks corresponding to a particular grey or black track multiplicity. This is just the reverse of what has been done in the previous sections. The results of this analysis are given in Tables 16 and 17.

Table 16

Mean Number of Shower Tracks versus Grey Track Multiplicity

Number of Grey Tracks	0	1	2	3	4	5	6	-7	8
Mean Number of Shower Tracks	2.61 ± 0.17	2.39 ± 0.17	2.13 ± 0.18	2.13 ± 0.30	1.67 ± 0.33	1.84 ± 0.67	1.17 ± 0.59	-	0.5 ± 0.5

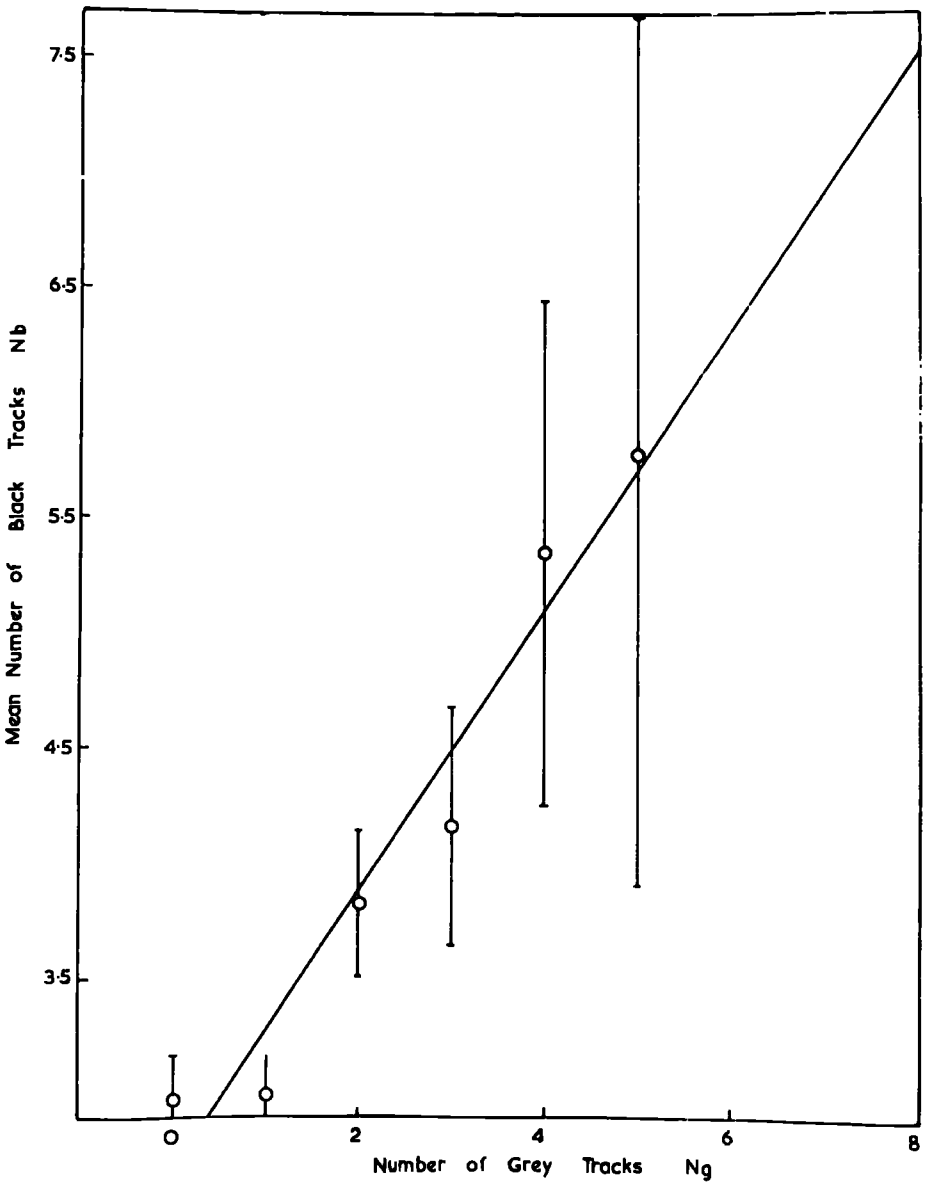

FIG. 12 The variation of mean number of black tracks with number of grey tracks.

Table 17

Mean Number of Shower Tracks versus Black Track Multiplicity

Number of Black Tracks	0	1	2	3	4	5	6	7	8	9	10	11	12
Mean Number of Shower Tracks	2.66 ± 0.53	2.53 ± 0.25	2.59 ± 0.14	2.39 ± 0.20	2.23 ± 0.25	2.26 ± 0.29	2.18 ± 0.44	1.80 ± 0.45	1.66 ± 0.42	2.34 ± 0.48	1.00 ± 0.33	2.00 ± 1.00	0.75 ± 0.38

Figures 13 and 14 give in a graphical form the relationship expressed by the results of Tables 16 and 17. In both cases the variation is linear as expected from the considerations of sections 3.4.1 and 3.4.2. From the slopes of the best straight lines through the experimental points it can be seen that approximately,

mean number of shower tracks = 0.85 Ng = 0.53 Nb

3.5 Size Distribution of Annihilation Stars

The size distribution for the total sample of white and black stars has been determined. The average number of grey tracks is (0.95 ± 0.03) and that of blacks tracks is (2.43 ± 0.05) giving an average size of (3.38 ± 0.06). The results of Ekspong et al. (1961) show that the mean number of heavy prongs (grey and black) is for annihilation

at rest $\langle N_H \rangle = (3.18 \pm 0.24)$

in flight $\langle N_H \rangle = (5.77 \pm 0.34)$

combined $\langle N_H \rangle = (4.51 \pm 0.22)$

The average number of heavy prongs per star for annihilation at rest (3.18 ± 0.24) thus compares very well with the number found in the present work (3.38 ± 0.06).

The size distributions for the sample of black stars with n_s = 2 and 3, and for the whole group containing all multiplicities are displayed in figures 15, 16 and 17 respectively. They bring out the general characteristics

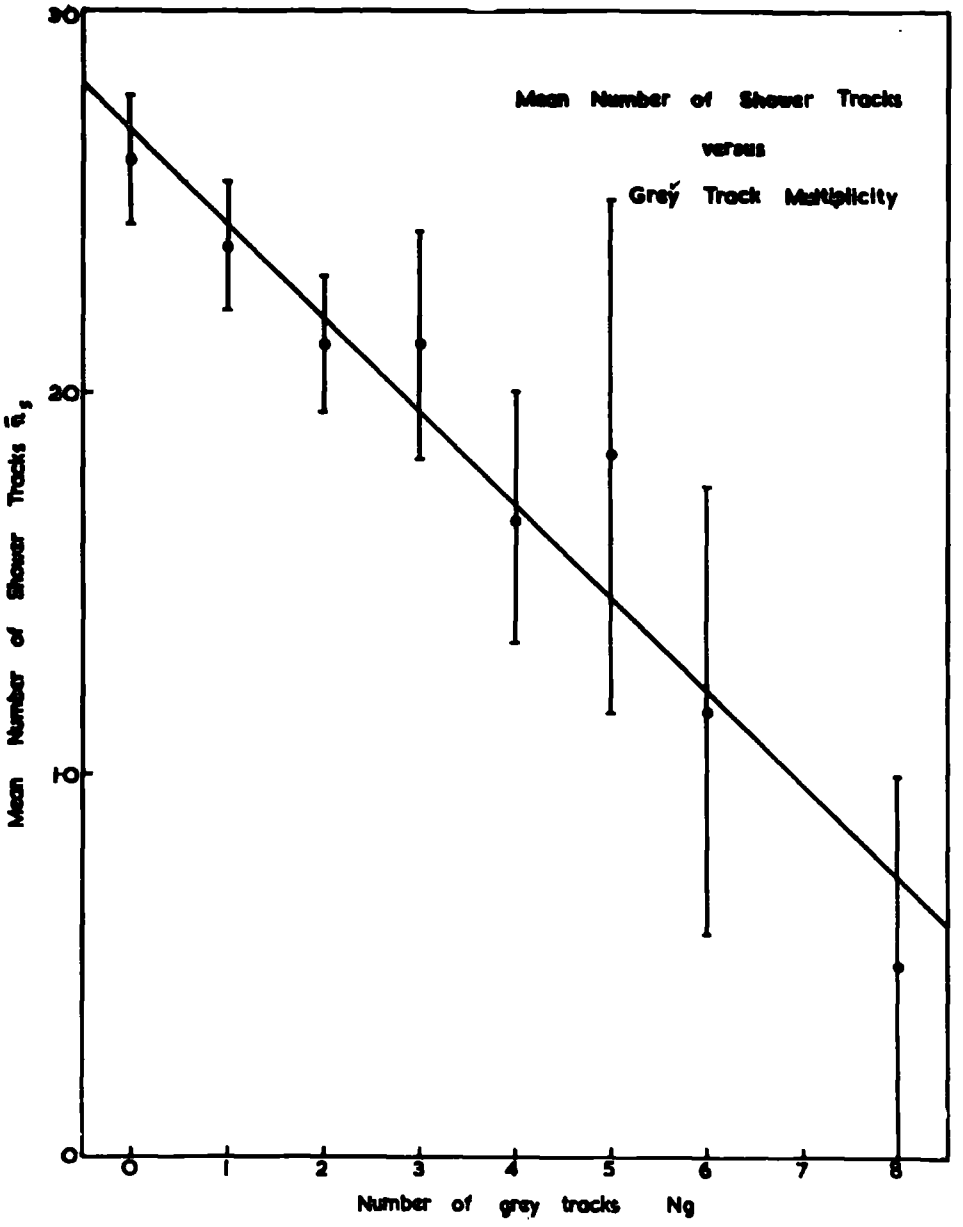

FIG. 13 The variation of the mean number of shower tracks with the grey track multiplicities.

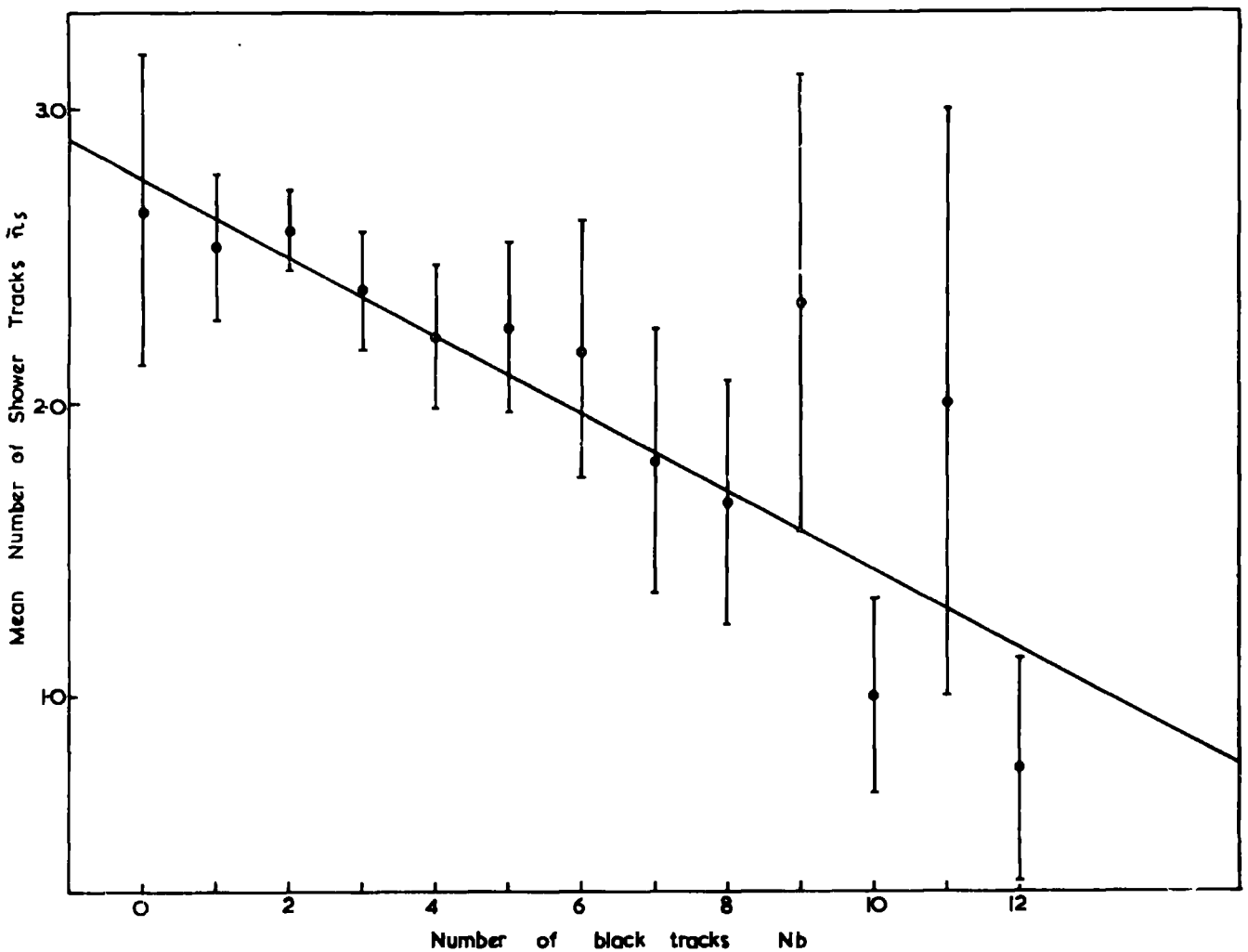

FIG. 14 The variation of the mean number of shower tracks with the black track multiplicities

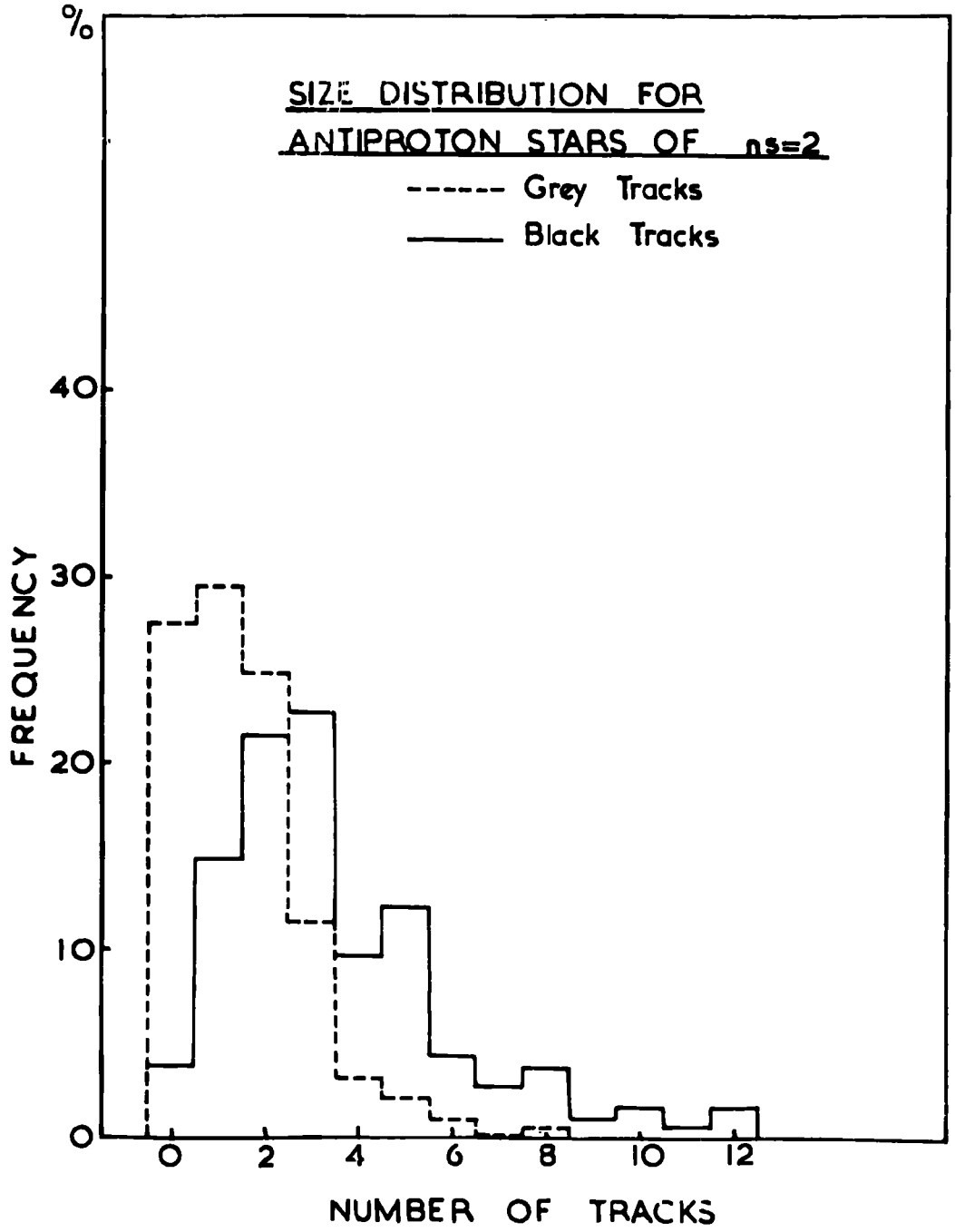

FIG. 15 Size dis^{n} for antiproton stars ns=2

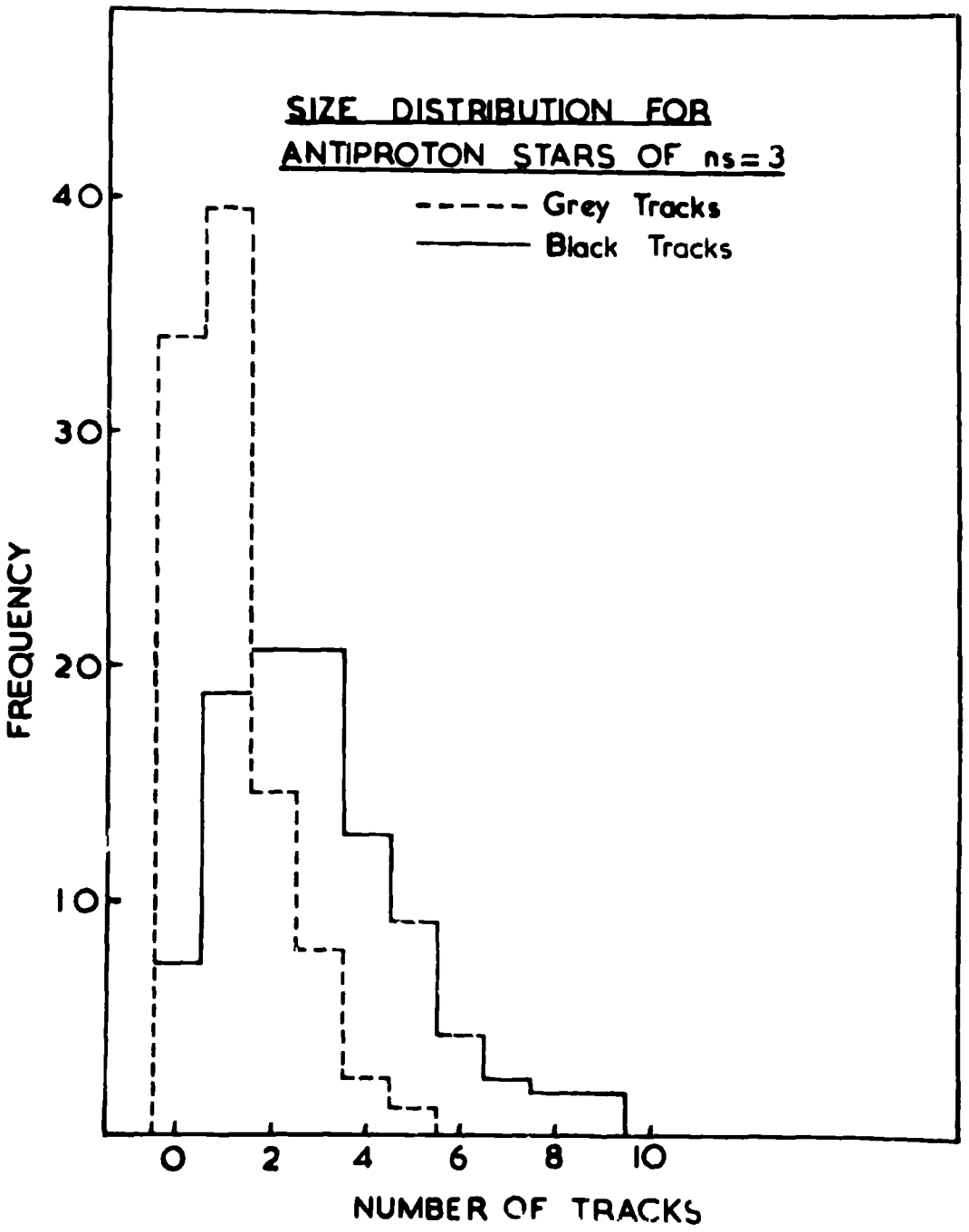

FIG. 16 Size distribution for antiproton stars ns=3

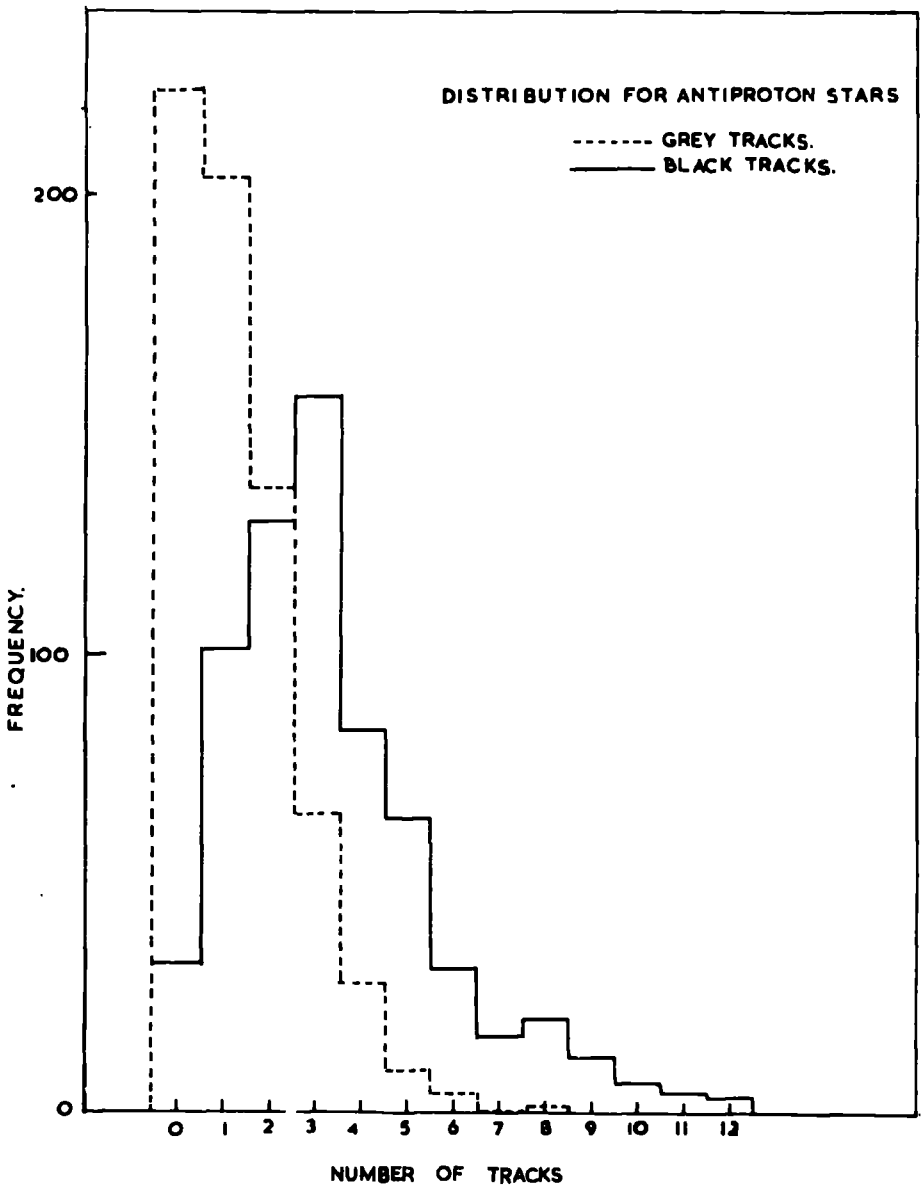

FIG. 17 Size dis^{n} for antiproton stars for all ns

mentioned in the previous sections and are given here since they will be required in Chapter 4 for the analysis of antineutron annihilations. No attempt has been made to measure the energy of heavy prongs, though an initial measurement on a small sample of stars confirms the estimate of Ekspong et al. that about 6% of the total available energy of annihilation is seen in heavy prongs. This estimate of energy carried away by the visible nuclear fragments is multiplied by a factor 2.6 in order to take into account the energy carried by neutrons. The empirical formula used by Chamberlain et al. (1959) is $U = h \cdot \langle \Sigma E_H \rangle$, where U is the energy taken off by the nucleons and h = 2.6.

3.6 Momentum Distribution of Recoiling Nuclei

In Chapter 2 a method is described by which the annihilation of antiprotons at rest in the light elements of nuclear emulsion may be distinguished from the larger number of annihilations in the heavy elements. It is shown that in the light elements carbon, nitrogen and oxygen, there is a high probability that after the annihilation on a target nucleon, the residual nucleus recoils intact since the excitation is low. The momentum of the recoiling nucleus may be determined from the range of the recoiling nucleus.

It is considered that the momentum of the recoiling nucleus is equal and opposite to that of the annihilated nucleon. By examining a large number of annihilations, the distribution in momentum of the target nucleons is determined. In this sense the antiproton is used as a nuclear probe.

There are two main difficulties. Firstly the ranges of the recoil nuclei are only a few microns long and great care has to be exercised in their measurement. The point of origin of the recoil nucleus is determined by the intersection of the lightly ionising secondary particles accompanying the annihilation. The end point of the range is more difficult to decide since the grain size is about 0.55μ and this leads to an average uncertainty of about 0.3μ on the range. Moreover the minimum range that can be determined is about 1μ.

Secondly the identification of the recoiling nucleus is ambiguous. Carbon 12 and oxygen 16 are the predominant light nuclei in the emulsion. On the annihilation of a proton boron 11 or nitrogen 15 is produced; if a neutron is annihilated carbon 11 or oxygen 15 is produced. From the even (or odd) number of mesons accompanying the annihilation it follows that a proton (or neutron) has been annihilated. However, no way has been found to distinguish between the nucleides of mass 11 and mass 15.

Consequently it is necessary to assume that when a proton is annihilated carbon 13 is formed and similarly that nitrogen 13 is formed when a neutron is annihilated. In fact, for the ranges in this experiment a sufficient compromise is to take an average of the various curves of Figure 18. The error associated with this is about 40 MeV/c. The range-momentum relationship (Papineau (1956) and Heckman (1960)) are shown in this figure for the nuclei boron 11, carbon 11 and 13, nitrogen 13 and 15 and oxygen 15.

3.6.1 Measurement of recoil tracks

As mentioned in Chapter 2, a total of 733 stars from the total sample of events were selected which were considered to be annihilations in the light elements. Of these 298 were accompanied by visible recoil tracks. The range of each recoil was measured on a Koristka R.4 microscope under a magnification of X100 x 15 x 1.5.

The distribution in length of the recoil nuclei is given in Table 18. By use of Figure 18 the ranges are converted into momenta and their distribution is given in Table 19, for a momentum interval of 40 MeV/c. Only ranges in excess of 0.8 are considered. In Figure 19 the momentum distribution is expressed as a fraction of the total number of annihilations in light elements which includes those without visible recoils. This latter group will include the annihilations at rest in the

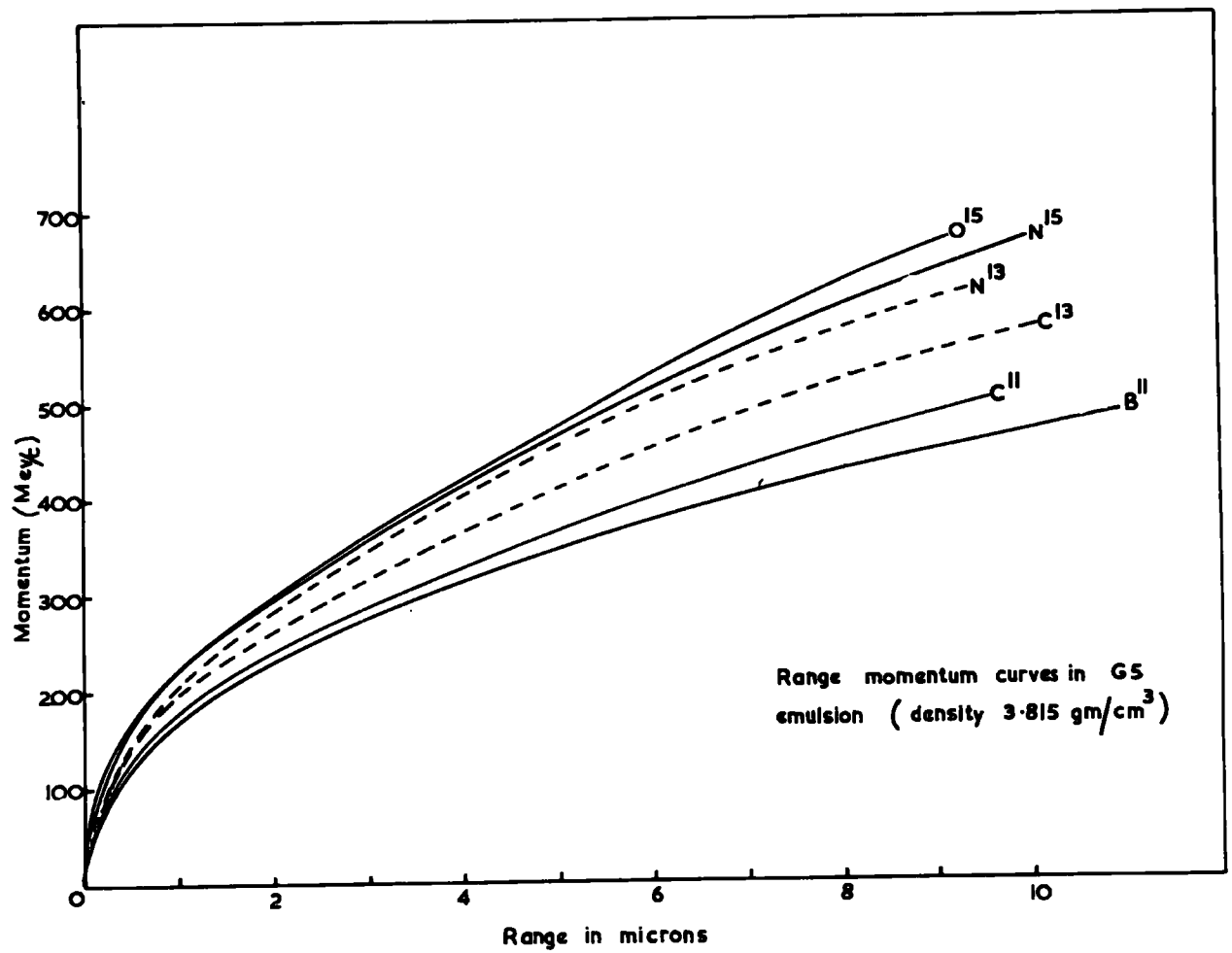

FIG. 18 Range momentum curves for heavy ions in G5 emulsion

Table 18

Frequency Distribution of Track Lengths of Recoiling Nuclei

Length in Divisions	1	2	3	4	5	6	7	8	9	10	11	12	13	14	15	16	17	18
Length in microns	0.274	0.548	0.822	1.096	1.370	1.644	1.918	2.192	2.466	2.740	3.014	3.288	3.562	3.836	4.110	4.384	4.658	4.932
Momentum* MeV/c			190	210	230	240	265	285	300	315	330	345	365	375	392	405	415	430
Frequency		5	24	52	65	56	19	20	10	19	5	6	4	4	2	3	1	3

Total = 298

* Momentum determined from the curves of Papineau and Heckman for light elements of emulsion.

Table 19

Momentum Distribution of Recoiling Nuclei

Momentum Interval	201-240	241-280	281-320	321-360	361-400	401-440
Mean Momentum (MeV/c)	220	260	300	340	380	420
Frequency of Recoils	131	66	40	16	9	7
Percentage Frequency normalised to total number of white stars	0.182 ± 0.016	0.092 ± 0.021	0.056 ± 0.009	0.022 ± 0.005	0.012 ± 0.004	0.0097 ± 0.004

hydrogen of the emulsion. However, in Chapter 2 this number has been shown to be negligible. The errors shown in Figure 19 correspond to the numbers of events in the sample and to the uncertainty on the range.

3.6.2 Discussion and interpretation

The distribution of momenta of protons in light elements has been determined by Gooding and Pugh (1960) and Garron et al. (1962). Similar investigations have been carried out by Hillman et al. (1960) and Pugh and Riley (1961). For carbon 12 (nucleon states $1\,s_{\frac{1}{2}}^{2}\,1\,p_{3/2}^{4}$ for both protons and neutrons) the momenta for the protons in the p and s states have been determined by Garron et al., and it is found that within the range of momentum imposed by the technique (about 0-200 MeV/c), the distributions are given by

$$n(p)dp = \frac{4n_o}{\pi}\ (p/p_o)^2\ \exp\left[-\ (p/p_o)^2\right]\left(\frac{dp}{p}\right)$$

... for s protons,

where $p_o = 160$ MeV/c, and $n_o = 2$ and

$$n(p)dp = \frac{8n_o}{3\sqrt{\pi}}\ (p/p_o)^4\ \exp\left[-\ (p/p_o)^2\right]\left(\frac{dp}{p_o}\right)$$

... for p protons,

where $p_o = 95$ MeV/c and $n_o = 4$.

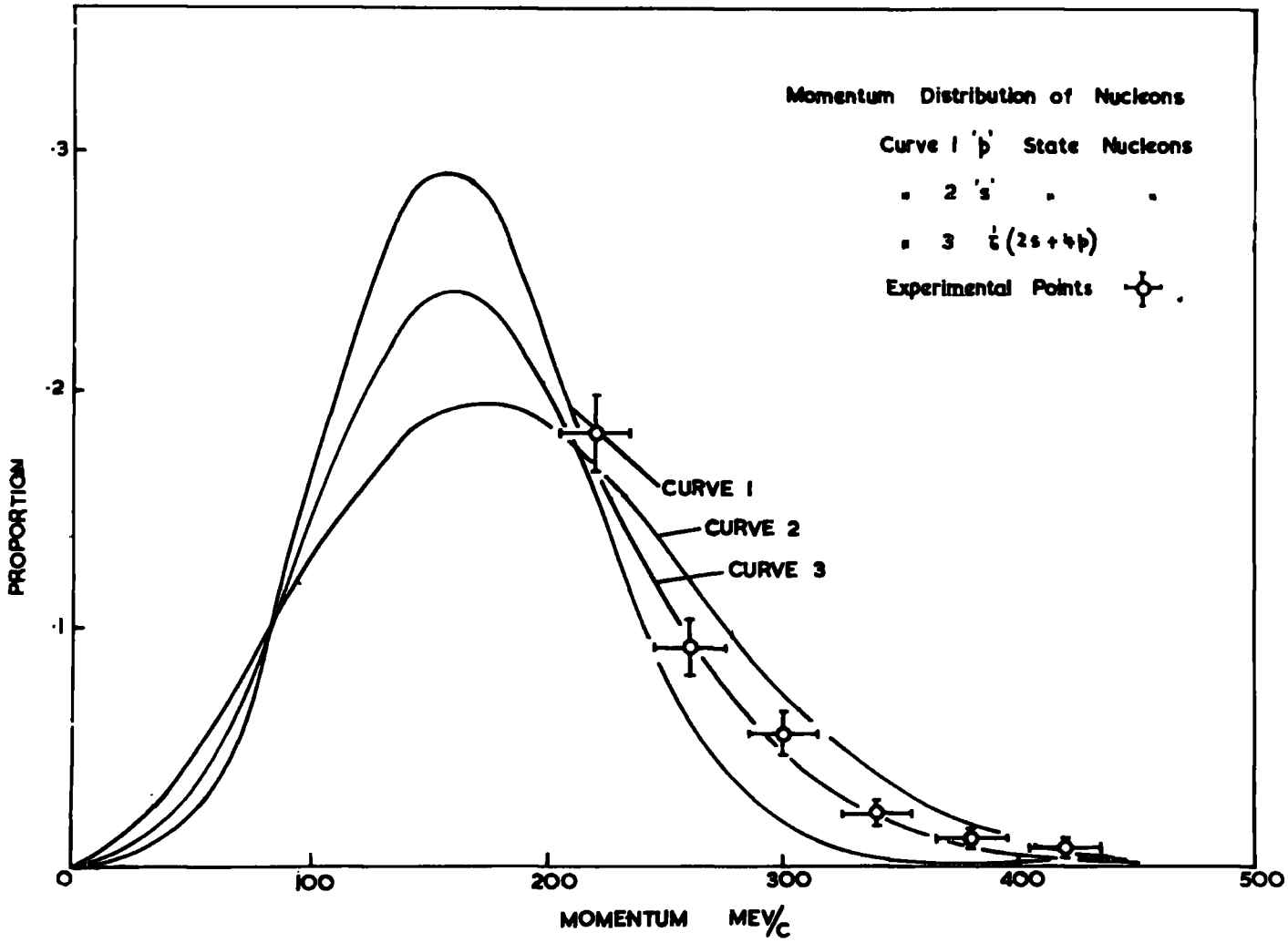

FIG. 19 Momentum distribution of nucleons.

Distributions of these kinds are expected from the harmonic oscillator model. Similar distributions are expected for the s and p nucleons of oxygen ($1\,s_{\frac{1}{2}}^{2}\;1\,p_{3/2}^{4}\;1\,p_{\frac{1}{2}}^{2}$). Since there are no published results for oxygen the distributions are assumed to be identical with those of carbon. These s and p distributions are also plotted in Figure 19, where they can be compared directly with the momenta of the recoiling nuclei and hence with the momenta of the annihilated nucleons. The greatest correspondence appears to be with curve 3 of Figure 19 for a mixing of s and p nucleons in the ratio 1:2, as in carbon. Because of their higher frequency of occurrence, annihilation occurs chiefly on the p-nucleons. A similar result has been found by Chadwick et al. (1958) for K^--meson absorption in the light elements of emulsion.

Scanning criteria may bias the selection of events to those involving p nucleons. From Garron et al. (1962), after the (p,2p) reaction in a light element the residual nucleus is formed in the ground state if a p-proton has been struck or with an excitation of 20 MeV if an s proton has been involved. If similar considerations apply in the annihilation process the break up of the excited residual nucleus might lead to a loss of events involving s-protons. However, it is expected from Ajzenberg and Lauritsen (1955) that de-excitation by γ emission will follow and the recoiling nucleus remains intact.

3.7 Conclusions

It is concluded that:-

a) the momentum distribution of nucleons in light elements is of the form given by Garron et al. for the protons of carbon. This confirms the use of the anti-proton as a nuclear probe. The momenta extend at least to 400 MeV/c,

b) the annihilation appears to take place on p and s-nucleons in the same proportions in which they occur in light nuclei. Since the majority are in the p-state, annihilation is chiefly on the p-nucleons,

c) at annihilation, from the white stars, the mean multiplicity of charged mesons is (2.90 ± 0.03). Allowing for neutral mesons the total multiplicity is (4.92 ± 0.15),

d) in complex nuclei the secondary mesons interact before escaping from the nucleus. The number that interact is estimated to be (1.23 ± 0.25) of which (0.81 ± 0.08) are absorbed. The remainder are scattered or undergo charge exchange,

e) the secondary collisions lead to the knocking out of nucleons and the excitation of the residual nucleus so that correlations exist between the numbers of black, grey and lightly ionising tracks.

CHAPTER 4

The Production and Annihilation of Antineutrons in an Emulsion Stack

4.1 Production

4.1.1 Production in hydrogen

The production of antineutrons by the charge exchange of antiprotons has been described in section 1.4, and the results of various experiments in hydrogen and complex nuclei have been summarised in Table 4. It can be seen from the table that for energies of antiprotons above 150 MeV, the value of the charge exchange cross-section is about 10 mb, whereas at lower energies, in common with the annihilation cross-section, it rises with decreasing energy of the antiproton. Throughout the energy range of these experiments, charge exchange represents about 13% of the total inelastic cross-section. The useful range of antiproton kinetic energy for a copious production of antineutrons in hydrogen is below 80 MeV, where the average value of charge exchange cross-section may be several tens of millibarns.

Hinrichs et al. (1962) have determined, in a hydrogen bubble chamber, the cross-sections for the elastic and inelastic charge exchange production of antineutrons at 930 MeV. It is found that the inelastic charge exchange is less than 20% of the total charge exchange cross-section.

The momentum distribution of the antineutrons has also been determined. It is found that 80% of the annihilating antineutrons have energies between 800 and 930 MeV. The cross-section for annihilation of the antineutron, the mean multiplicity of charged particles and the mean energy of the secondary products are found to be similar to those for antiprotons. Counter experiments of Elioff et al. (1962) and Coombes et al. (1958) substantiate these results so far as cross-sections are concerned though the latter experiments yield no information about the secondary products of the annihilation.

In hydrogen bubble chambers the track of an antiproton may come to a sudden end. If an annihilation star appears at some distance from this end it confirms unambiguously the creation and subsequent annihilation of an anti-neutron. The disadvantage of the technique is that the density of hydrogen is low and the mean free path for the annihilation of antineutrons is long, so that the yield of annihilating antineutrons corresponding to a given beam of antiprotons is small.

4.1.2 Production in complex nuclei

In complex nuclei, the incident antiproton collides with a nucleus and may charge exchange with one of its nucleons. The antineutron thus produced must escape from the parent nucleus before it can be observed. The

probability of such an escape is small since the antineutron may annihilate on a nucleon during its short passage through the nucleus. The beam of antineutrons will thus be strongly attenuated. To what extent this attenuation will act can be judged from the following expression for the charge exchange cross-section for the production of antineutrons in complex nuclei (see Appendix).

$$\sigma_{c.e.} = (\pi f\ Z/A)\ \left\{(1-(1+2KR+K^2R^2)\ e^{-2KR}J/K^2\right\}$$

where f is the fractional yield of antineutrons in hydrogen and K and R are the absorption coefficient and radius of the nucleus. The expression is relatively insensitive to the size of the nucleus. In Figure 20 the cross-section is shown as a function of K, for the known value of f, in carbon, silver and lead. At the estimated value of K, $\sim 3.5\ 10^{12}\ cm^{-1}$ the cross-section lies in the range (8-12)mb. For antiprotons at 430 MeV, the charge exchange cross-sections for carbon and lead have been measured by Button et al. (1957) and found to be $(4.0^{+1.6}_{-1.5})$mb and $(3.8^{+4.2}_{-2.5})$mb respectively. The values for 320 MeV antiprotons in beryllium and carbon are (11^{+4}_{-5})mb and (10^{+6}_{-7})mb. Considering the experimental inaccuracies and the assumptions made in the calculations the agreement between the calculated and the experimental values is good.

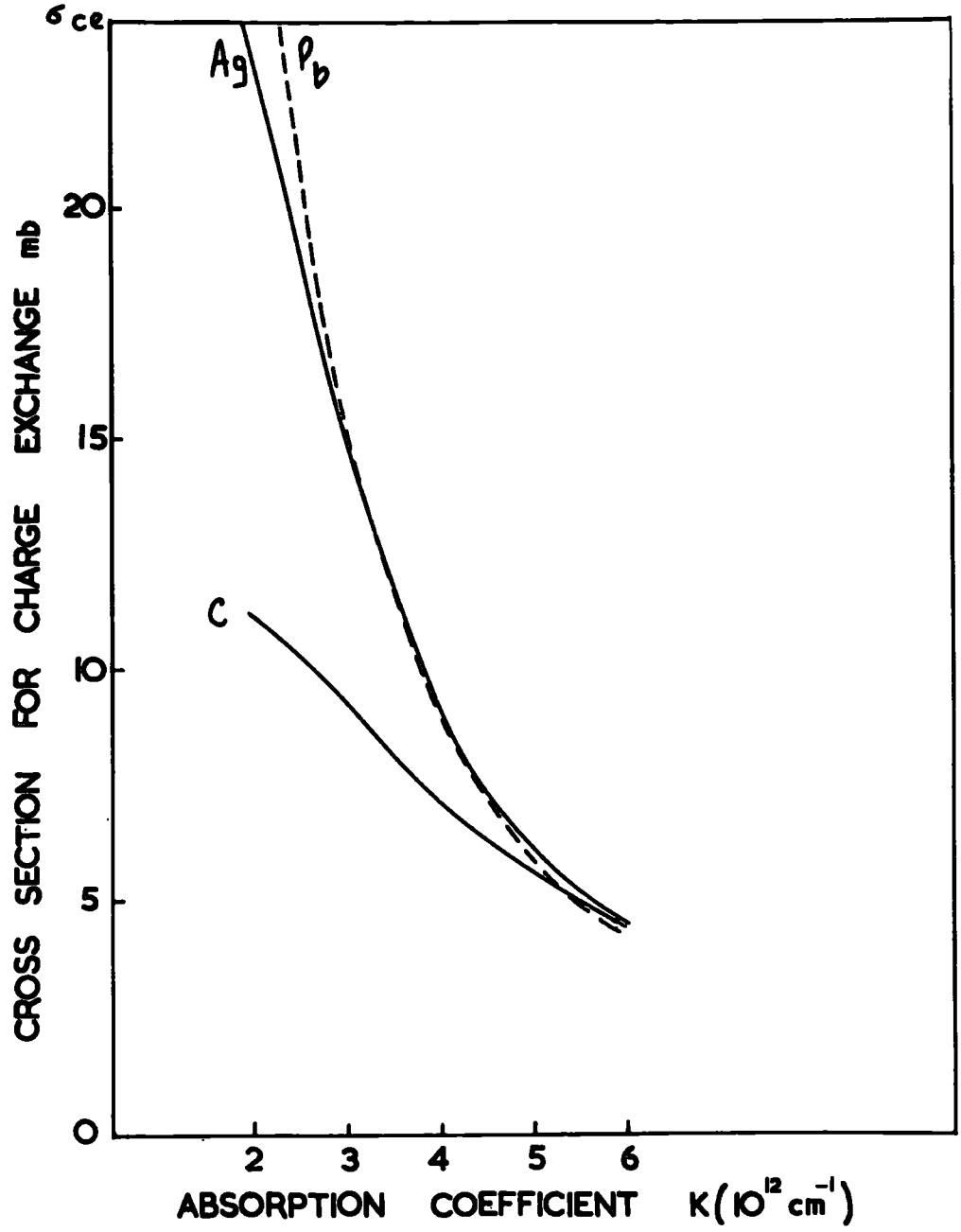

FIG. 20 The variation of charge exchange cross-sections with absorption coefficient

The above considerations justify the use of the expression obtained for the charge exchange of antiprotons in complex nuclei to calculate the cross-section in emulsion. The average cross-section in emulsion is determined by the heavy elements (such as silver) with a cross-section of about 12 mb, by light elements (such as carbon) with a cross-section of 8 mb and by hydrogen with a cross-section which is energy dependent. Hydrogen contributes more than half the charge exchange cross-section in emulsion and hence introduces energy dependence. At the energy (~125 MeV) at which the antineutrons are produced in the present experiment, the calculated cross-section is about 12 mb. From the above it is seen that nuclear emulsion is no more effective in the production of antineutrons than hydrogen. However, since emulsion has greater density than hydrogen, it offers a much shorter mean free path to antinucleons for annihilation with a consequent greater yield of antineutrons followed by their annihilation in a given volume.

4.1.3 Production in the emulsion stack

The exposure of the stack of emulsion to an antiproton beam of momentum 700 MeV/c has been described in section 2.3.1. Antineutrons are produced by charge exchange and in turn are annihilated. In the appendix an approximate calculation is given of the flux of antineutrons at any

point down the antiproton beam, namely,

$$n_{\pi} = P_c \bar{N}_o e^{-x/\lambda}/\lambda$$

Since the range of the antiprotons (~13 cm) is less than the mean free path in emulsion (~18 cms), the flux of antineutrons is a maximum at the end of their range and drops exponentially beyond that range. The density of antineutron annihilation stars will also, therefore, be a maximum and at the end of the antiproton range. It would seem advantageous to search for antineutron annihilation events in this region of the emulsion plate. However, this is also the region in whose proximity the maximum number of antiproton annihilations at rest take place, with the resultant creation of large numbersof pions, some of which travel in the forward direction and may interact with the emulsion nuclei. These interaction events may confuse further the recognition of genuine antineutron stars which already have to be selected against a background of events due to contamination from the beam. A compromise has, therefore, been made by seeking for antineutron events a few centimetres further downstream than just beyond the antiproton range. The background from contamination of the beam can only be reduced by use of selection criteria which enrich the sample in antineutron annihilations.

4.2 Scanning for Antineutron Stars

Area scanning has been carried out between 3 and 10 cms beyond the end of the antiproton range under a magnification of 10 x 15 x 1.5 on Cooke M4000 microscopes. A low value of magnification has been chosen to allow the volume of 48.8 cm^3 to be scanned within a reasonable time. The reduced efficiency of detection of stars on account of the low magnification, is estimated to be about 85%. Since there will be many stars due to 650 MeV pions contaminating the beam or due to 300 MeV pions and low energy neutrons from annihilations of antiprotons, a scanning criterion has been adopted to reduce the acceptance of a large number of these spurious events, namely, an acceptable star should be accompanied by one or more lightly ionising tracks. This discriminates against the low energy neutron stars. Again, if there is only one lightly ionising track it must lie in the forward direction. This discriminates against the pions. The breakdown of the original sample of stars recorded on scanning is given in Table 20.

4.3 Contamination

The stars found by area scanning contain a large proportion of spurious events which arise from different types of contamination, the chief source being the flux of lightly ionising particles, mostly pions, which is as large as one-third of the antiproton flux.

Table 20

Breakdown of original sample of stars recorded on scanning for antineutrons

Number of Shower Tracks	1	2	3	4	5	6	7	8
Frequency of Stars	65	226	54	13	1	2	3	2

Total number = 367

Total Volume scanned = 48.8 cm^3

Number per cm^3 = 7.5 stars/cm^3

(0.17×10^4 per cm^2 against a flux of 0.49×10^4 $\bar{p}/cm^2$). The energy of the pions is about 650 MeV and it is estimated that they will give rise to a maximum number of 10 stars per cm^3. The second major source of contamination are the secondary pions produced as a result of antiproton annihilation in flight and at rest. However, the isotropic emission of these pions leads to a rapid reduction of their intensity beyond the range of the antiprotons so that the density of the pion stars falls quickly. The average of these pions is about 220 MeV and they are expected to produce about 2 stars per cm^3. From the scanning criterion the stars produced by pions from the two sources mentioned above, will be classified as possible antineutron stars of $n_s \geqslant 2$. A large proportion of these will consist of two only lightly ionising particles as the

probability of the creation of a third shower particle is small. The $n_s = 2$ events are, therefore, expected to contain the largest amount of pion interactions. This is confirmed by the number of such stars shown in Table 20.

A third source of contamination arises from a small flux of pions moving in the backward direction through the scanning volume which has resulted from the back scattering of pions further downstream. This consists chiefly of the beam pions which are scattered backward, thus losing about one-half of their energy. They will be absorbed in the emulsion nuclei giving rise to one-shower-track events and may thus be classified as possible anti-neutron stars with $n_s = 1$. Their number is estimated at 0.5 stars per cm^3.

Other sources of contamination include energetic neutrons and K-mesons; these are produced with too low a frequency to introduce any significant contamination.

4.3.1 Contamination from cosmic rays

The stack of emulsion has been transported by air from London to Geneva at an altitude of 18,000 ft., the flight taking about two hours. Some contamination on account of cosmic ray interactions may be present. These interaction events are expected to consist largely of higher shower multiplicities since the energy of the cosmic ray particles will be high. The emulsion stack

was shuffled and the pellicles rearranged before it was exposed to the antiproton beam. Since the tracks from cosmic ray events, (which were produced before the shuffling), cannot cross between adjoining plates, whereas those from the genuine stars produced after the exposure can be followed through the plates, the cosmic ray events can be easily distinguished from the rest. Contamination from this source can, therefore, be eliminated by looking at the final sample of events and tracing the tracks of a star from one plate into the next.

4.4 Selection Criteria

With the exception of cosmic ray interactions, all other sources of contamination discussed in section 4.3 can give rise to stars of low n_s values only. The interactions with high shower track multiplicities ($n_s \geqslant 4$) can safely be taken as genuine antineutron annihilations provided their tracks are traceable into plates adjacent to the one in which a particular event occurred, so as to ensure that it was not a cosmic ray star.

For the lower n_s values, selection criteria have been developed by comparing the distribution of sizes of stars of antiprotons with those of pions which have energies similar to those in the present experiment. It is assumed that the star sizes for the antiproton and antineutron annihilations are similar. By star size, here, is meant

the number of grey and black tracks associated with a star. The data used for this comparison have previously been found in these laboratories in experiments on the interactions of pions and antiprotons in G5 emulsion. The comparison of star sizes can be based on several combinations of the numbers of grey and black tracks and different selection criteria devised. From this variety of criteria, only those have been used which act most preferentially against the background stars. For each value of n_s, therefore, the most selective criterion has been employed as considered below.

(i) $n_s = 1$: in this category, the background events can arise from pions in the beam which have been scattered backward further downstream from the area of scanning. On average their energy will be about 300 MeV and for pions of this energy, previous experiments from these laboratories show the following distribution of star sizes.

Table 21

Star size distribution for 300 MeV pions in G5 Emulsion

$(n_b + N_g + 0)\pi^-$

n_b \ n_g	0	1	2	3	4	Total
0	-	7	2	-	-	9
1	8	4	2	1	-	15
2	8	7	-	1	-	16
3	16	3	1	-	-	20
4	4	6	-	-	-	10
5	6	1	-	-	-	7
6	3	1	-	-	-	4
7	-	1	-	-	-	1
Total	45	30	5	2	-	82

From Table 21 it can be seen that only 9% of the total number of stars which arise from the back scattered pions are expected to be accompanied by two or more grey tracks. Compared to this, 43% of the antiproton stars of $n_s = 1$ have two or more grey tracks as given by Table 22.

Table 22

Size Distribution for Antiproton Stars of $n_s = 1$ in K5 Emulsion

n_b \ n_g	0	1	2	3	4	5	6	Total
0	-	1	3	-	-	-	-	4
1	6	6	2	3	2	-	-	19
2	7	8	5	-	-	1	-	21
3	10	12	6	3	-	-	-	31
4	8	6	3	1	2	-	-	20
5	5	3	6	-	1	-	-	15
6	1	3	4	1	-	-	1	10
7	2	-	3	1	2	-	-	8
8	1	-	-	1	2	1	-	5
9	-	1	1	1	-	-	-	3
10	-	-	1	-	2	-	-	3
11	-	-	1	1	-	-	-	2

From the total number of 65 events with $n_s = 1$, there are only 12 which are accompanied by two or more grey tracks. The comparison of Tables 21 and 22 shows that these must be made up of about 8 antineutron annihilations and 4 pion stars and that the original sample of 65 stars comprises 18 antineutrons and 47 pion stars. Since events with $n_s = 1$ from the backward direction have been rejected at scanning, the above number of annihilations must be doubled to give

the total estimate of about 36 stars in this category.

(ii) $n_s = 2$: there are 226 events in this class. No selective criterion based on star sizes can be chosen for this category as each leaves more pion stars in the selected sample than genuine annihilations. The method applied here is to select stars with both shower particles in the forward direction, since the probability of their production due to back scattered pions is very small. There are 14 such events which are accepted as genuine annihilations. This number must be multiplied by 4 to allow for other orientations, thus obtaining a total of 56 estimated antineutron stars and 170 pion events in this category. In Figures 21 and 22 there are compared the size distributions of selected events with antiproton annihilations of $n_s = 2$. →

(iii) $n_s = 3$: this sample comprises 54 events. Only pions in the beam are energetic enough to give rise to stars of this class. It is, therefore, assumed to be the major source of contamination. Some contamination may arise from the interactions of energetic secondary pions from antiproton annihilations. The selection criterion for this category is based on the relative propertions of events which are accompanied by two or more grey tracks in the interactions of 750 MeV pions and antiproton annihilations in K5 emulsion. For the interactions of 750 MeV pions it has been found (Major, private

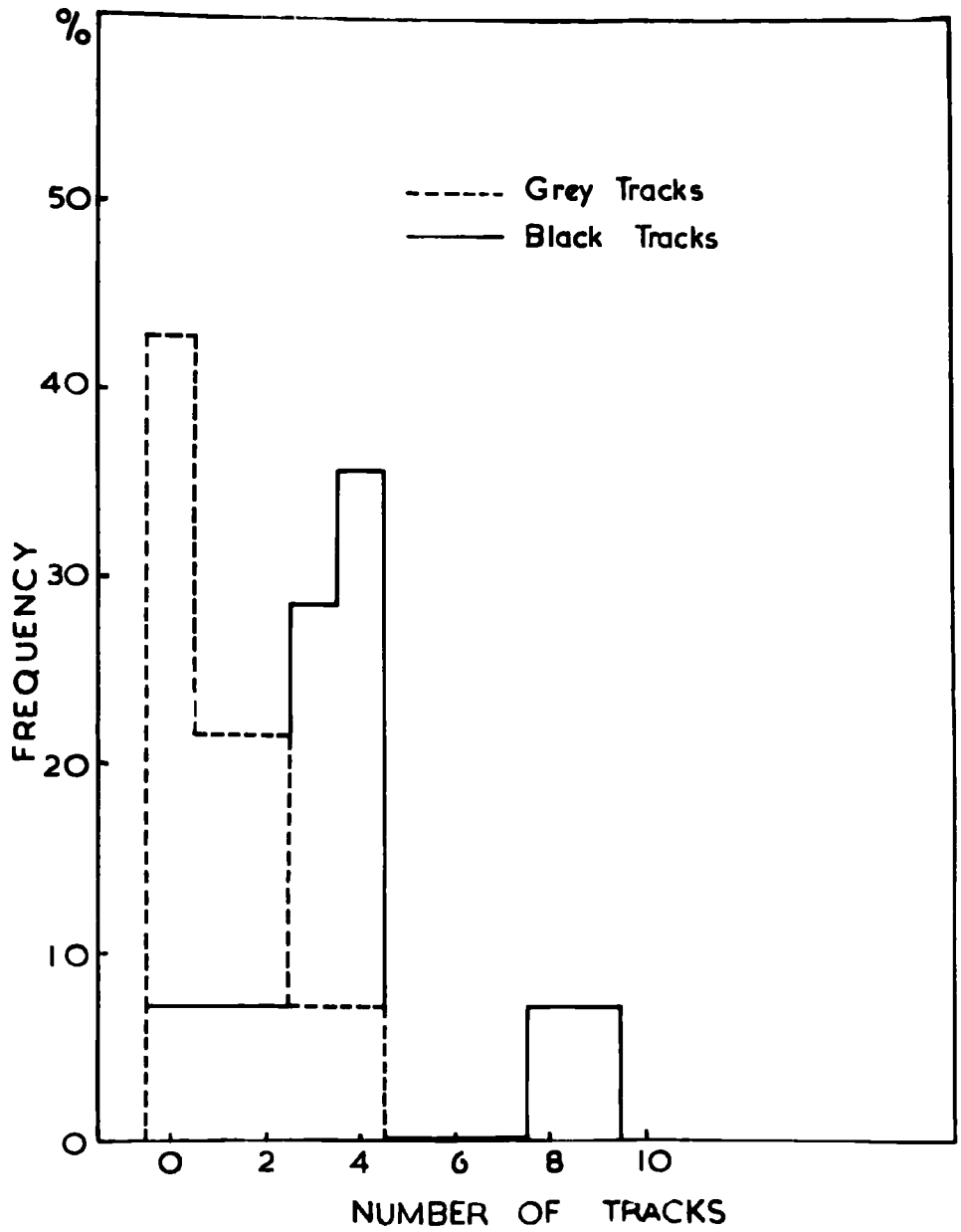

FIG. 21 Size dis[D] for selected antineutron stars ns=2

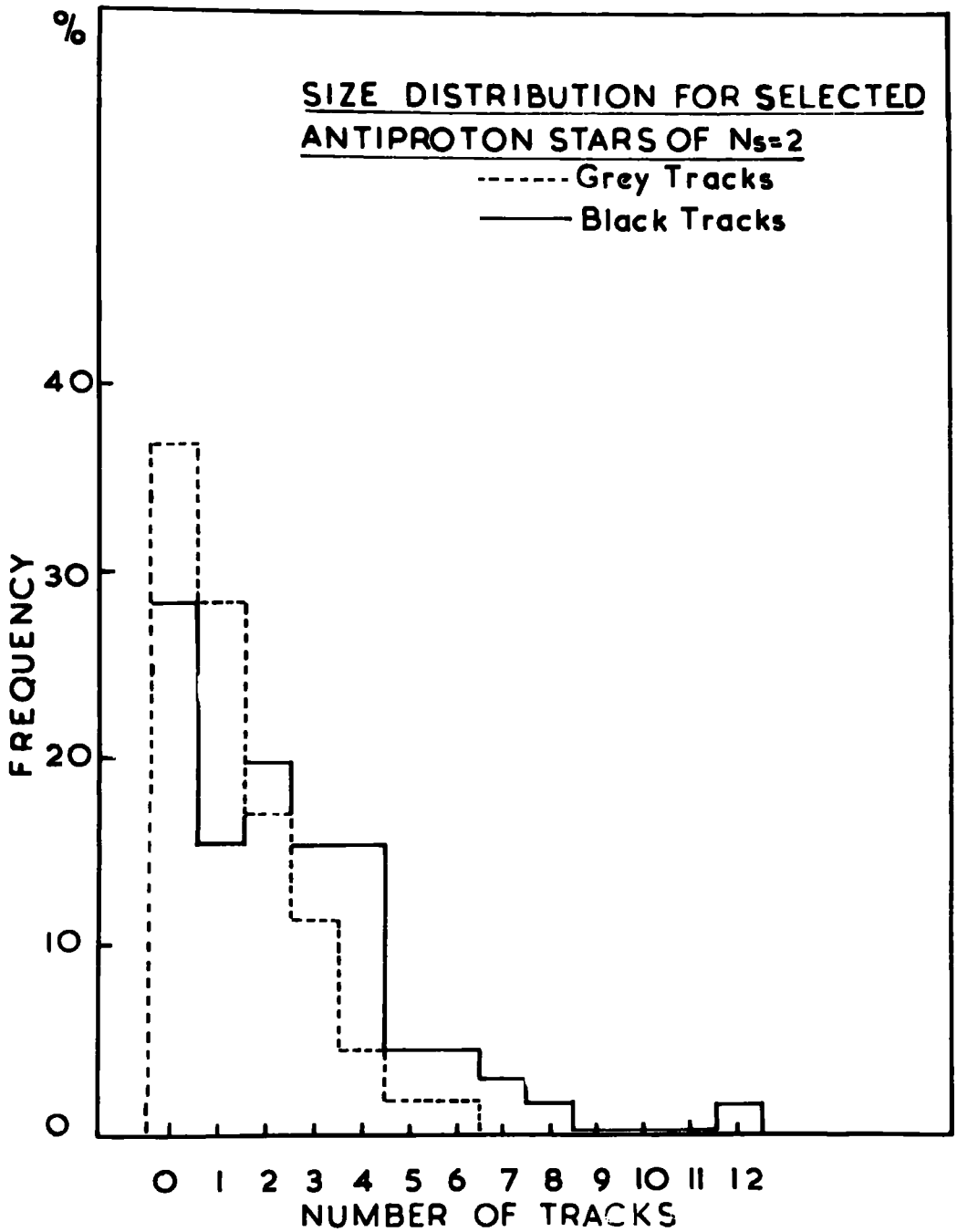

FIG. 22 Size dis^{n} for selected antiproton stars ns=2

communication and Blau and Oliver, 1956) that about one-third are accompanied by one or more grey tracks. The corresponding number for the antiproton annihilations can be estimated from the distribution of star sizes given in Table 23.

Table 23

Size Distribution for Antiproton Stars of $n_s = 3$ in K5 Emulsion.

n_b \ n_g	0	1	2	3	4	5	Total
0	-	8	2	1	-	1	12
1	13	14	4	-	-	-	31
2	17	6	6	5	-	-	34
3	11	17	2	2	1	1	34
4	7	10	3	1	-	-	21
5	2	6	4	2	1	-	15
6	3	2	2	-	-	-	7
7	1	1	1	1	-	-	4
8	2	-	-	-	1	-	3
9	-	1	-	1	1	-	3
Total	56	65	24	13	4	2	164

The number of events with grey tracks equal to or greater than one is 30. Since 66% of the antiproton and 33% of the pion stars are accepted by this criterion, the number fulfilling the condition must comprise 24 annihilations and 6 pion stars. The original sample of 54 is thus made up

of 36 annihilations and 18 pion stars. This number of pion stars agrees approximately with the estimate from class $n_s = 2$ of 12 pion events. The fact that the original sample of $n_s = 3$ is rich in genuine annihilations can be seen from a comparison of Figures 23 and 16 which give the star size distributions for this sample and for the antiproton stars of corresponding category.

(iv) $n_s \geqslant 4$: the 21 events are assumed to be genuine examples of antineutron annihilations.

4.5 Results

There are 76 events which emerge after the application of selection criteria to the original sample of 367 stars. These must be examined for any cosmic ray contamination. Of the 76 events examined only 8 failed to be traced between neighbouring pellicles. Two of these were in the last pellicle and all their tracks passed out of the stack, thus leaving their identity difficult to establish. Nevertheless, since there is some doubt, these events have also been excluded from the final list of accepted events.

After the application of selection criteria and correction for cosmic ray contamination, an enriched sample of 68 events is selected which comprises about 62 amnihilations and 6 pion stars. It is estimated from the considerations of 4.4 that the original sample of 370 stars contains (138 $\pm$ 29) antineutron annihilations.

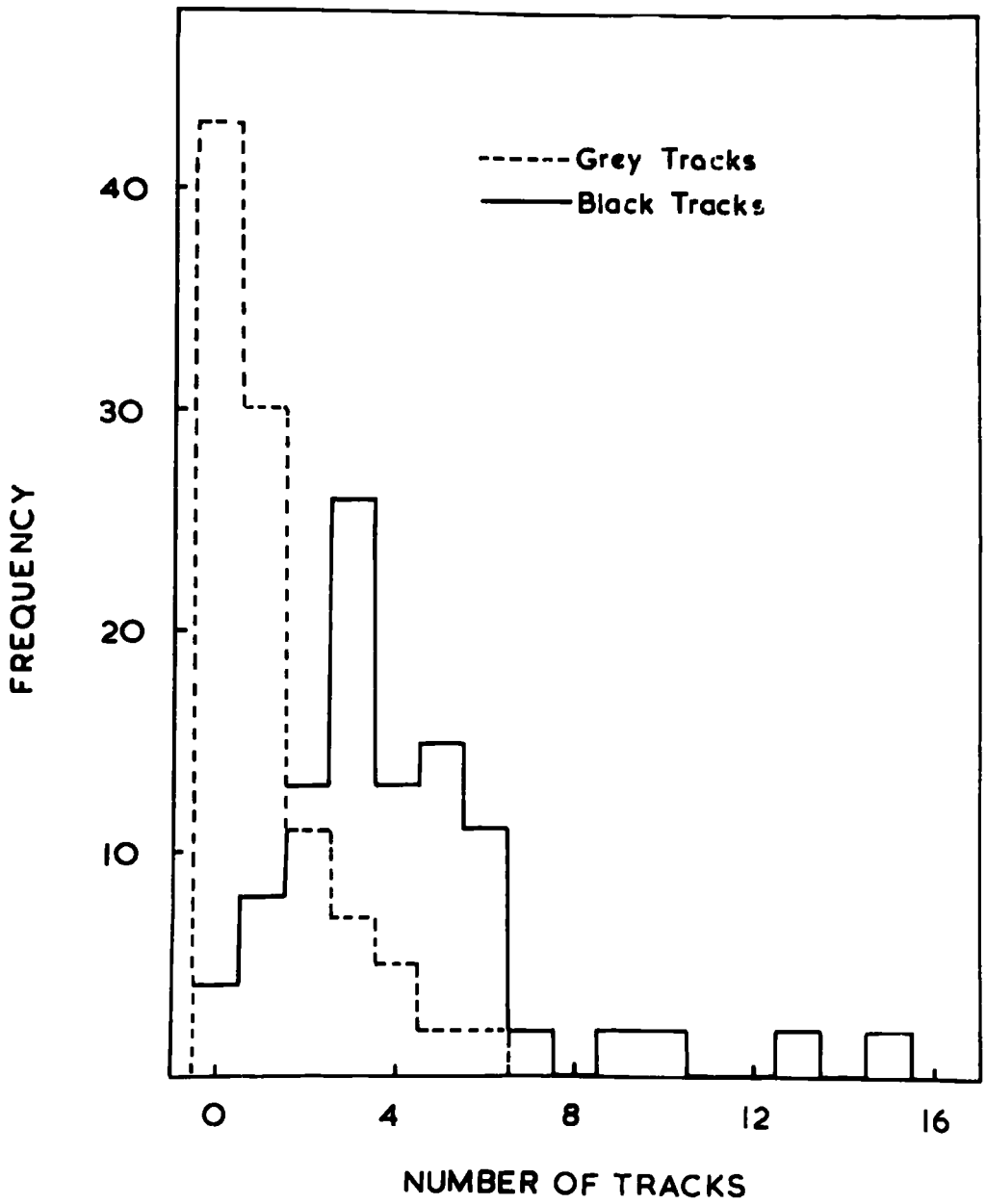

FIG. 23 Size dis[D] for "antineutron" stars ns=3

4.5.1 Multiplicity distribution of antineutron annihilations

From the criterion of demanding at least one lightly ionising track in the forward direction, the events with $n_s = 0$ have been rejected at scanning. The multiplicity distribution can only be estimated for values of $n_s \gg 1$. From section 4.4, the number of antineutron stars in each category of n_s is shown in Table 24. The multiplicities are also represented as percentages and are compared with the corresponding values for antiproton annihilations at rest in emulsion as found in these laboratories and discussed in Chapter 2.

Table 24

Comparison of the multiplicity distributions of mesons from the annihilations of antineutrons and antiprotons

n_s*	1	2	3	4	5	6	7	8
Antineutron Annihilations	(36±14)	(52±14)	(34±21)	11	1	1	2	1
Antineutron %	(26±10)	(38±10)	(25±15)	(8±2)	(4 ± 2)			
Antiproton %	(23±2)	(30±2)	(26±2)	(17±2)	(5 ± 1)			

* only multiplicities $n_s > 0$ are considered.

It can be seen from the table that the annihilations of antineutrons and antiprotons are very similar, thus confirming the method of selection and estimation of the antineutron annihilations. From this similarity the number of antineutron events with $n_s = 0$ is about 8 (6% of all annihilations), leading to a mean multiplicity of (2.2 ± 0.5), which is to be compared with (2.19 ± 0.11), the corresponding figure of Ekspong et al. (1961) for antiproton annihilations in flight at similar energies. The results of Table 24 are displayed in Figure 24.

4.5.2 Measurements in the enriched sample of stars

The characteristics of the enriched sample of 68 stars have been determined, and also of the events rejected on the application of various criteria mentioned before. Comparison is then made between the selected events and the antiproton annihilations in emulsion studied by the various laboratories. The characteristics of the rejected stars are contrasted with those of antineutrons and antiprotons.

(i) Mean energy of the meson secondaries

Scattering measurements have been made on the long flat tracks of low ionisation which are assumed to be due to pions. An average value of (224 ± 37) MeV is obtained. This is to be compared with a mean energy of (216 ± 11) MeV

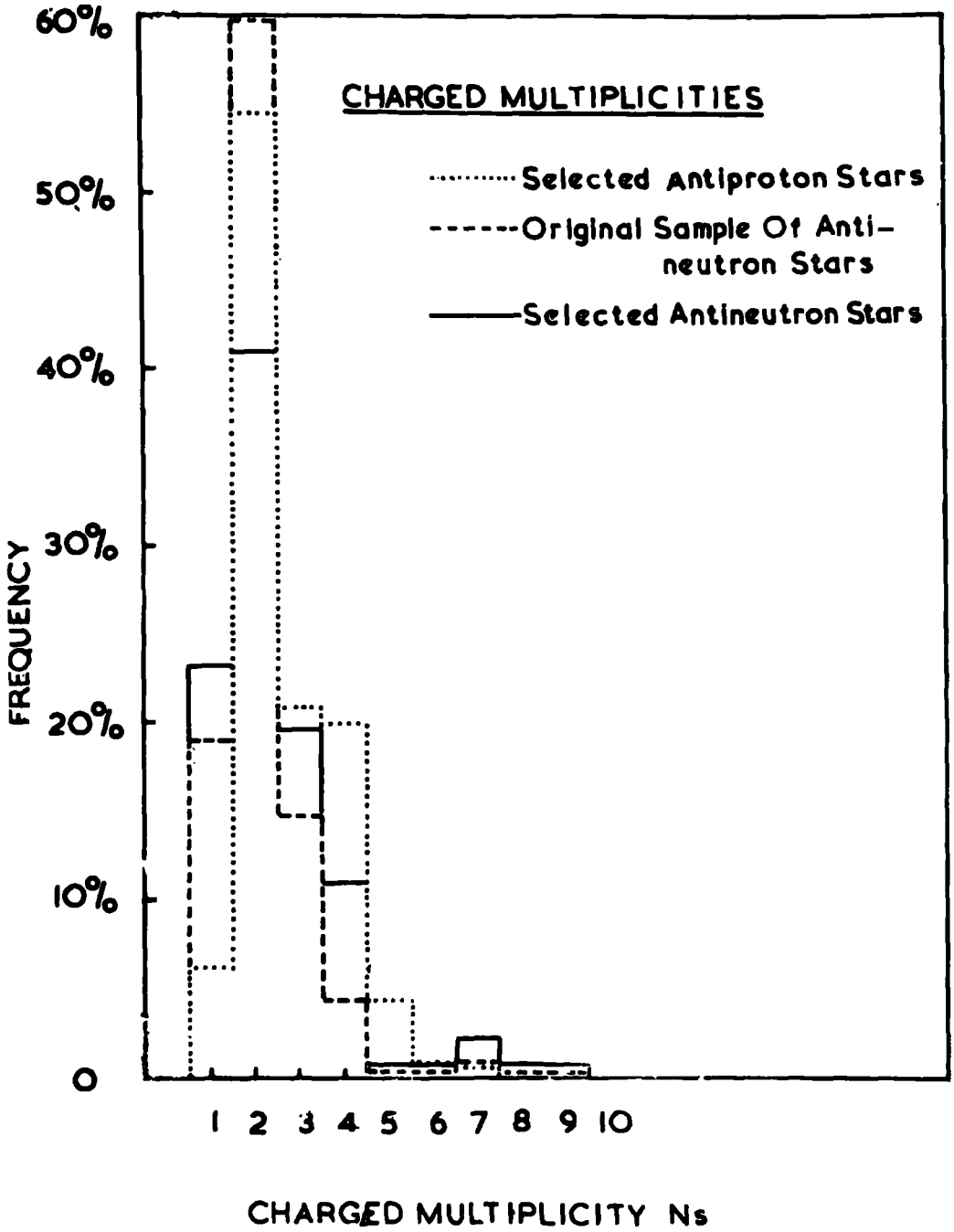

FIG. 24 The comparison of charged multiplicities

found for meson secondaries by the combined results of Uppsala, Berkeley and Rome groups (Ekspong, 1961). For the rejected stars, the mean energy of the shower particles is (360 ± 60) MeV. The energy spectra of mesons from the above mentioned three sources are shown in Figures 25 and 26.

(ii) The star sizes

The mean star-size is represented by the number of black and grey tracks and may be denoted by N_h where h stands for heavily ionising tracks (black and grey). For the final sample, the mean star size is (5.7 ± 0.2), which is to be compared to a value (5.77 ± 0.34) found by Ekspong et al. for antiproton annihilations in the range (0-250) MeV. This range is approximately the same as the range of energies for the antineutron annihilations in the present experiment. Figures 17 and 27 display the distributions of sizes for the antiproton and the selected sample of antineutron annihilations. Since the selection criteria are based on star-sizes, the above mentioned agreement as well as the similarity between the two distributions shown by Figures 17 and 27 may be a consequential result.

4.5 Cross-section for Charge Exchange

As mentioned before the number of antineutron annihilations of $n_s = 0$ are estimated at 8 from the antiproton

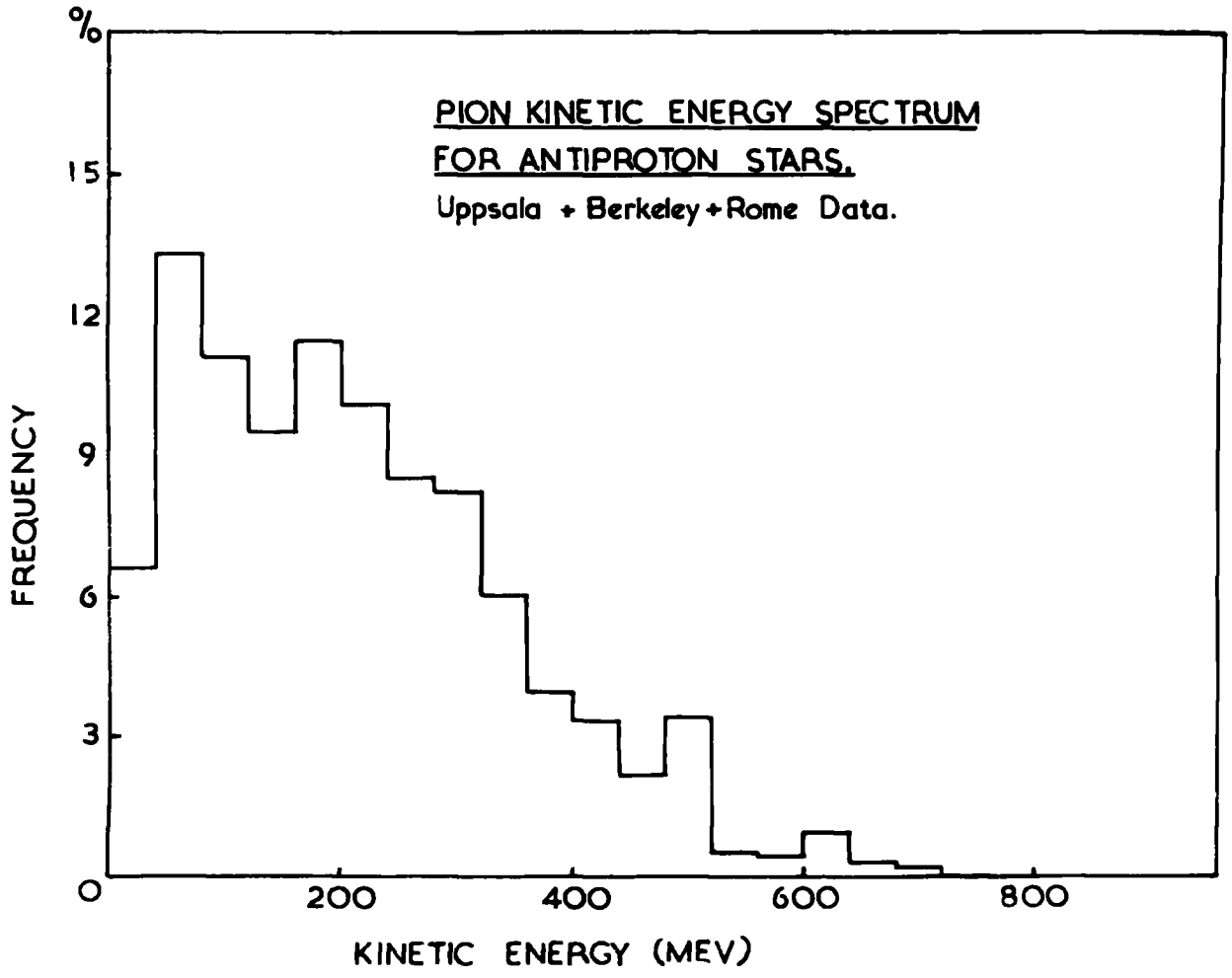

FIG. 25 The kinetic energy spectrum of pions from antiproton annihilation

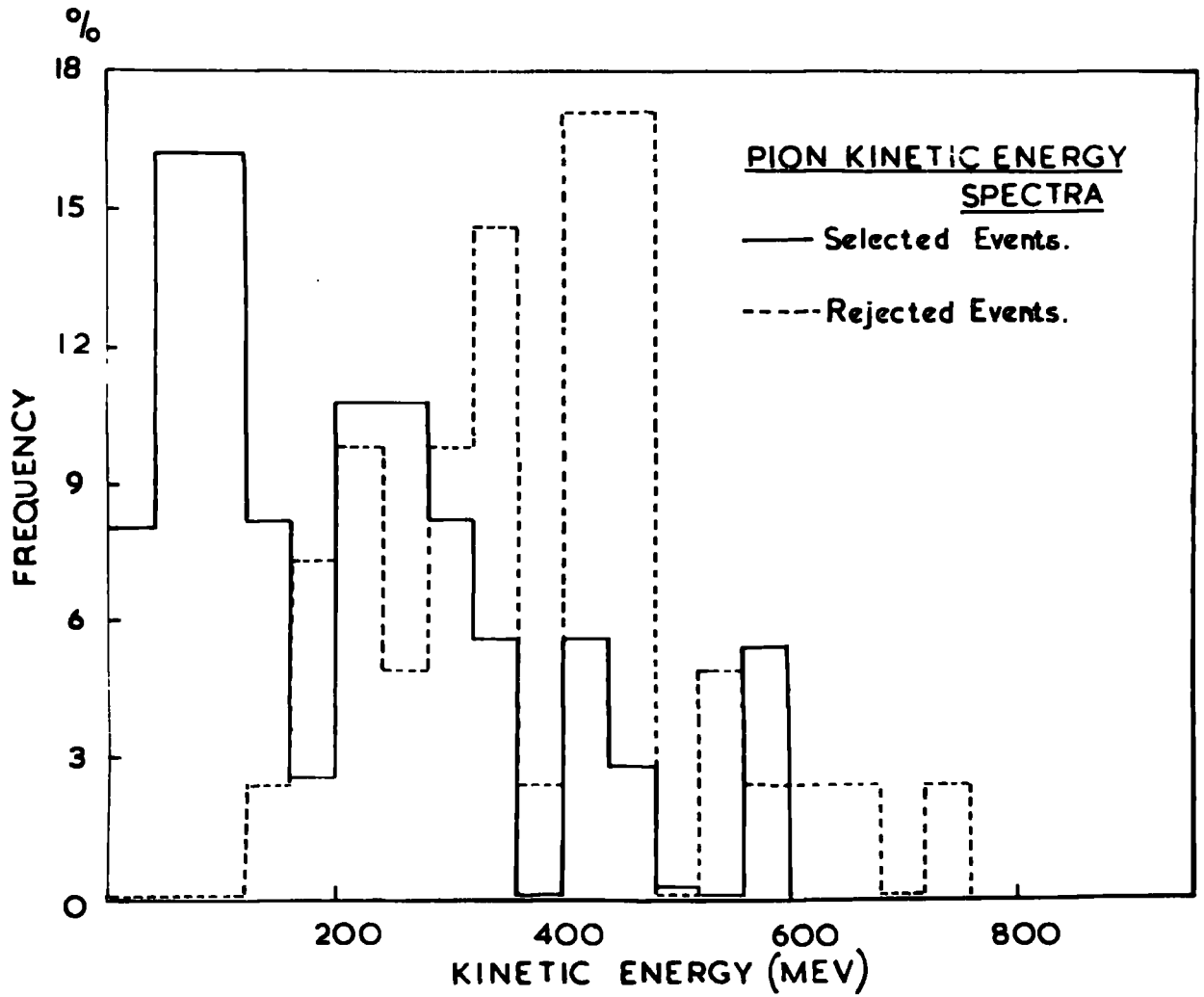

FIG.26 The kinetic energy spectrum of pions from antineutron annihilation

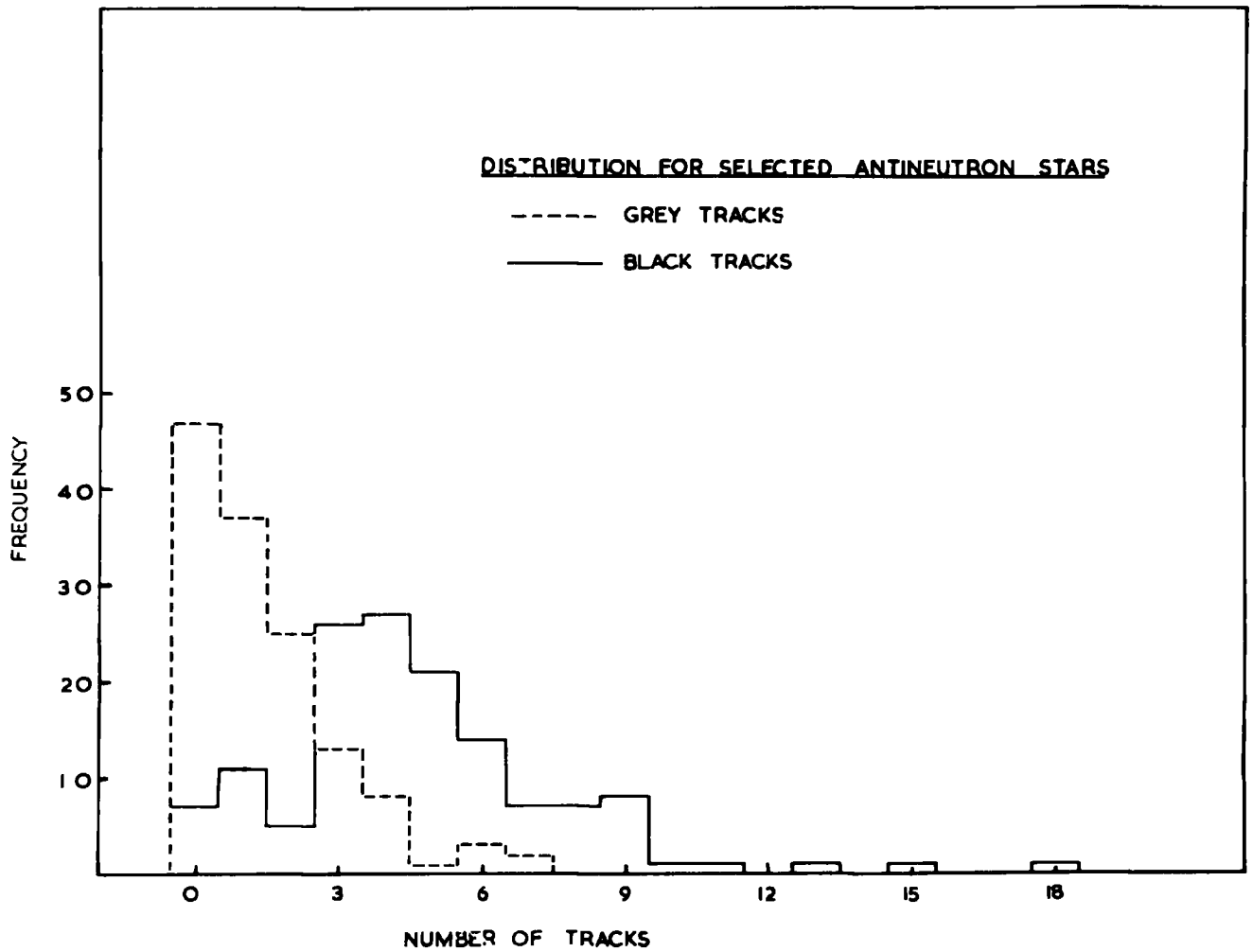

FIG. 27 Size distribution for selected antineutron stars

results of Chapter 2. Including these $n_s = 0$ events, the volume density of annihilations is (3.0 ± 016) per cm^3. From the calculation of this quantity given in the appendix, the mean cross-section for charge exchange of antiprotons by complex nuclei of the emulsion is (17 ± 6)mb. The error does not include any estimate of the accuracy of the calculation. In Figure 28 the cross-sections are plotted as a function of energy of the antiprotons, and both the values for complex nuclei and hydrogen are shown. Also shown is the charge exchange cross-section in emulsion as measured in this experiment.

4.6 Conclusions

If the antiproton beam is free from contamination, (Amaldi et al., 1964) an emulsion stack provides a convenient and suitable way of observing the annihilations of antineutrons produced by the charge exchange of antiprotons.

It is found that the star characteristics for antineutrons are the same as for antiprotons. The charge exchange cross-section for production of the antineutrons has been determined for a mean kinetic energy of 125 MeV for the antiprotons and is found to be (17 ± 6) mb compared to a calculated value of about 11 mb.

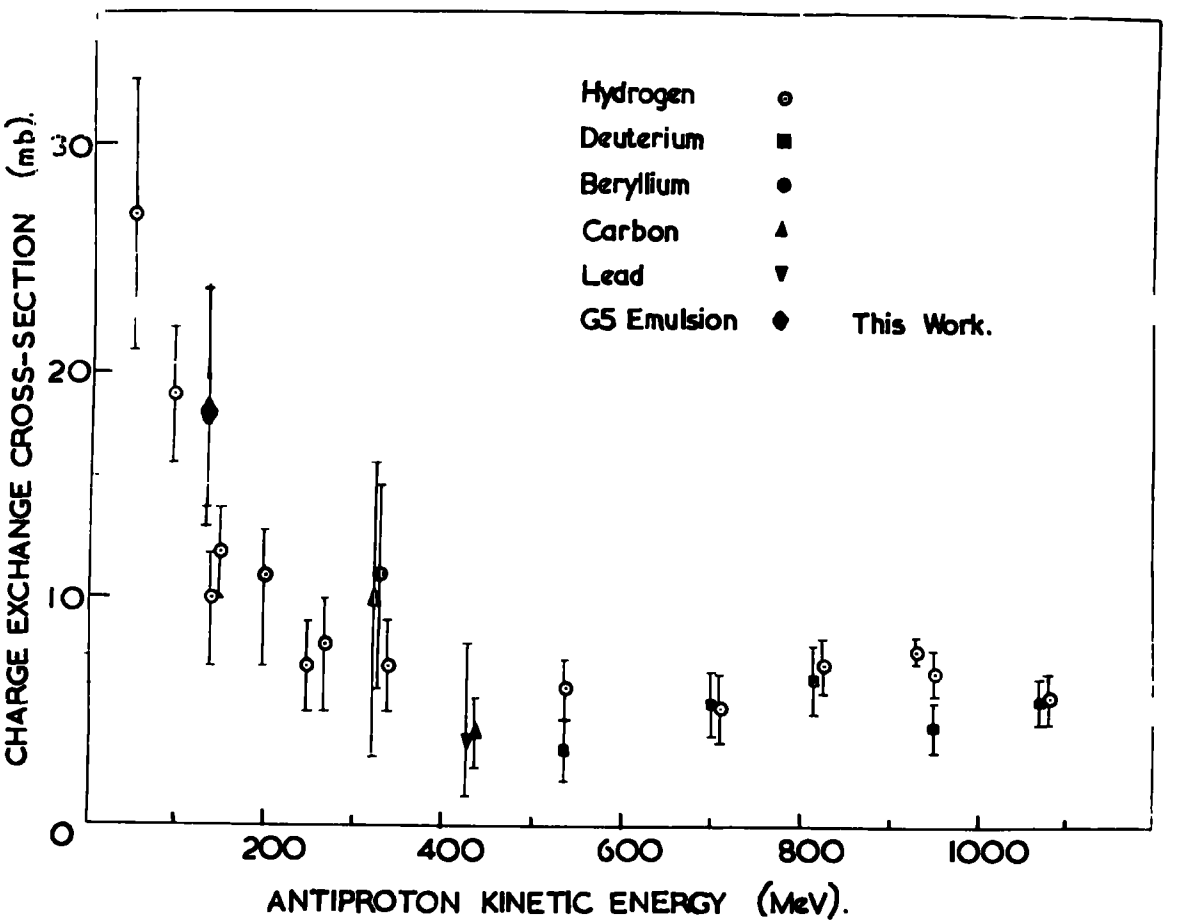

FIG 28 The energy dependence of charge exchange cross - section

CHAPTER 5

Comparison of Meson Multiplicities with Theories of Nucleon-Antinucleon Annihilation

5.1 General Features of Annihilation at Rest

The nucleon-antinucleon annihilation is characterised by the creation of about five mesons. In general these are made up of pions though in about 5% of all annihilations a pair of K-mesons is produced. The multiplicity of mesons ranges from a minimum of two up to about eight for which the charged multiplicity is concentrated in the values 2, 4 and 6. On average there are about 3 charged and 1.5 neutral pions. The production of resonant particles takes place in about 10% of all annihilations.

The models of annihilation must account for the features mentioned above. All are based to some extent on the Fermi statistical model for meson production of which a brief description is given in the following section. This is followed by subsequent modifications to the theory. Experimental results are then compared with the predictions of various models in an attempt to distinguish between them.

5.2 Fermi's Statistical Theory

The statistical theory of Fermi has been successful in accounting for the multiple production of pions in high energy nucleon-nucleon interactions. It can, therefore, be expected to give good results in the similar phenomenon of

nucleon-antinucleon annihilation where large amounts of energy are suddenly released.

It is considered that when two nucleons collide with very great energy in their centre of mass system, this energy will be suddenly released in a small volume surrounding the two nucleons. This energy leads to the creation of mesons and is distributed between them and the original nucleons according to the statistical laws associated with their spins and charge states. The probability of the creation of a certain number of mesons with a given energy distribution can, therefore, be calculated.

The probability of producing a given multiplicity of mesons is the probability of finding the mesons in the volume into which the energy is concentrated. Hence the multiplicity distribution is determined by the size of the volume. Since the pion field surrounding the nucleons extends to a distance of $\hbar/m_\pi c$, the volume into which the energy of the two colliding nucleons is concentrated will also have linear dimensions of this order of magnitude. However, when the two nucleons approach each other with very high energies in the centre of mass system their surrounding pion clouds will be Lorentz contracted and the volume will be correspondingly reduced. The volume is, therefore, taken as energy dependent according to the relationship

$$\Omega = \Omega_o \frac{2Mc^2}{W}$$

where $\Omega_o = \frac{4\pi}{3}\left(\frac{\hbar}{m_\pi c}\right)^3$ is the uncontracted volume.

Fermi obtained good agreement with experimental results of nucleon-nucleon collisions with a volume of radius of the order of the pion Compton wavelength $\frac{\hbar}{m_\pi c}$ i.e. 1.4×10^{-13}cm, but suggested that the choice of the volume was arbitrary and could be changed to improve agreement with experiment. It was also pointed out that the theory was only a rough approach to the actual state of affairs since many factors affecting the statistical equilibrium such as the spin of the particles and the conservation of angular momentum had been ignored.

The statistical theory of Fermi has been applied to the nucleon-antinucleon annihilation. Here, the interaction volume, the only adjustable parameter of the theory, has been found which best fitted experimental results. Thus values of Ω ranging from two to fifteen times the uncontracted volume (Ω_o) have been used to fit the experimental results of charged multiplicities and energy spectra of pions. This is physically unsatisfactory since the interaction range between a nucleon and an antinucleon should be of the order of the Compton wavelength of the pion. Moreover, the theory fails in its prediction for the K-meson production which is much larger than the observed value. The observed K-meson production can be accounted for

only if the interaction volume is about one tenth of the volume required for pion production.

A modification to the statistical theory has been used by Desai (1960 II) who has imposed on the production mechanism the selection rules which follow from the application of the conservation laws of angular momentum (Desai (1960 I) has shown that for protonium the capture takes place from the $^1S_0$ and $^3S_1$ states). The effect is to change the multiplicity distribution of all pions (charged and neutral) by the suppression, largely, of the two-pion annihilation. However, when the multiplicity distribution of charged pions is abstracted, there is little difference between it and the distribution when selection rules are not imposed. This implies once again that an interaction volume of about $10\Omega_0$ is required to account for the observed multiplicities.

In the work of Cerulus (1959), the production of some mesons by resonance formation is introduced into the statistical model. Two resonant states were considered, one with a mass of $4m_\pi$ the other with a mass of $3m_\pi$. Multiplicities were calculated for annihilation at rest for interaction volumes of 0.5, 1 and 2 times Ω_0. Since the work of Cerulus, pion resonances have been observed. The important ones in this connection will be the ρ and ω-mesons with masses of (5-6) m_π. Further calculations are necessary with this mass value before the predictions of the model of Cerulus can be tested by the experimental results.

At finite energies the interaction volume required to interpret the multiplicity of pions decreases with increase in energy. McConnell and Shapiro (1963) analysed the existing data at momenta below 2 GeV/c and of low statistics and determined the energy variation of the volume. Normalising at the "best" experimental result it was claimed that the variation of the interaction volume was consistant with the Lorentz contraction of a rest volume of about $6\Omega_0$. More recent results at 3.25 GeV/c (Ferbel (1963) - thesis) are inconsistent with this.

5.3 The Theory of Koba and Takeda

The difficulty of the statistical model is the large K-meson multiplicity. In the model of Koba and Takeda (1958) this is avoided by considering the production of mesons from two independent sources, the meson clouds surrounding the nucleon and the antinucleon and their cores. The production of K-mesons occurs only in the core-core annihilation so that relative to the total number of mesons, the creation of Kaons is reduced.

The core is supposed to have the following two properties:

i) it acts as a nearly black body for the incoming antiparticle wave, and

ii) its characteristic time for annihilation ($\hbar/2M_Nc^2$) is much shorter than the oscillation period (h/ω_π where ω_π is the energy of the pion) of the outer pion cloud. Upon

overlap of the nucleon-antinucleon cores, annihilation proceeds without changing the state or the number of pions in the cloud. Devoid of their cores the meson clouds then emerge from the interaction contributing from 2 to 3 pions on the average. The core annihilation contributes about 2.2 pions. The latter number is determined by applying the statistical theory to the core annihilation. A total pion multiplicity of 4.8 per annihilation is predicted by this model.

On account of assumption (i), annihilation occurs every time the incoming antinucleon wave hits the core surface. Considering annihilation in flight, therefore, a cross-section of πa^2 is expected for the antinucleon. Here, a is the radius of the nucleonic core. When the distance between the nucleon and the antinucleon is greater than a, a potential due to pion exchanges acts and annihilation occurs if the antinucleonic wave passes through a region within a distance from the core surface, where is the reduced de Brodglie wave length of the antinucleon. The annihilation cross-section thus becomes $(a + \lambda\!\!\!^{-})^2$ instead of the classical value πa^2. Comparing this with the experimental results, Koba and Takeda estimated the radius of the core to be $\frac{2}{3} \times \frac{\hbar}{m_\pi c}$.

This model has successfully explained the high pion multiplicity in annihilation at rest as well as the asymmetry of negative and positive mesons for annihilations

at finite energies. The model, however, does not take into account the resonant mode of production of mesons.

5.4 Summary of the Models of Meson Production

5.4.1 Multiplicity of charged pions in annihilation at rest

The charged pion multiplicities are almost entirely contained in the 2, 4 and 6 pion modes. Because of this, the results of calculations of the various models are best summarised on an equilateral triangular plot (as in a Dalitz plot) where a single point represents the percentage of multiplicities in each pion mode as shown in Figure 29. The lines represent the results of Cerulus based on meson production through the formation of a resonance of mass $3m_\pi$ or $4m_\pi$ respectively, and those of Desai for annihilations in protonium from the $^1S_0$ and $^3S_1$ states with and without the application of selection rules for volumes of 1, 4, 8, 10 and $12\Lambda_0$. The size of the interaction volume is indicated along the curves. Finally, the results of Horwitz et al. (1959) from calculations based on the Koba and Takeda model, are shown.

5.4.2 Variation of mean multiplicities of mesons with the energy of antiprotons

For annihilation in flight, the additional available energy may either increase the average multiplicity or the momenta of pions. A correct model should be able to decide

FIGURE 29

MULTIPLICITIES OF CHARGED PION PREDICTED BY VARIOUS MODELS OF ANNIHILATION

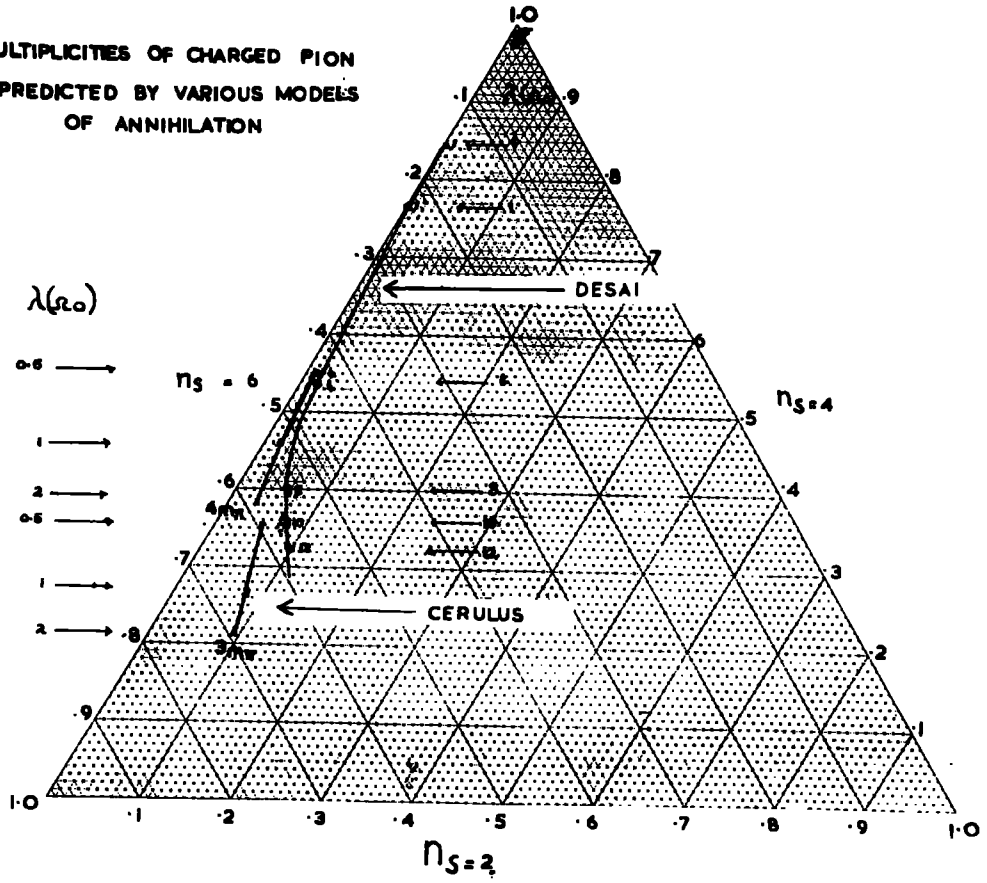

between these two possibilities. The predicted variation of the average pion multiplicity with the antiproton energy has been summarised by Goldhaber et al. (1961) for three different models. This is shown in Figure 30 where the full lines indicate the variation predicted by (a) the statistical theory with a Lorentz invariant interaction volume of ($\Omega = 8\Omega_0$), (b) the same model with Lorentz contraction of the interaction volume, ($\Omega = 8\Omega_0 \times \frac{2M}{W}$) and (c) the Koba and Takeda model. The curves are normalised to an average multiplicity of 4.9 for annihilation at rest.

Also plotted on the figure are the experimental points from some more recent determinations of mean multiplicities.

5.5 Comparison with Experimental Results

In Figure 31 the multiplicities of 2, 4 and 6 charged mesons are compared with the predicted values. The results shown are those of Horwitz et al. (1959), Chadwick et al. (1961), Barnes et al. (1964) and Apostolakis et al. (1965) (this thesis). The first three experiments were conducted in hydrogen or deuterium, the latter in the light elements of emulsion.

For annihilation at rest in hydrogen and deuterium (S-state absorption) the multiplicity distribution is consistent with the statistical theory (with or without selection rules) provided the interaction volume chosen is

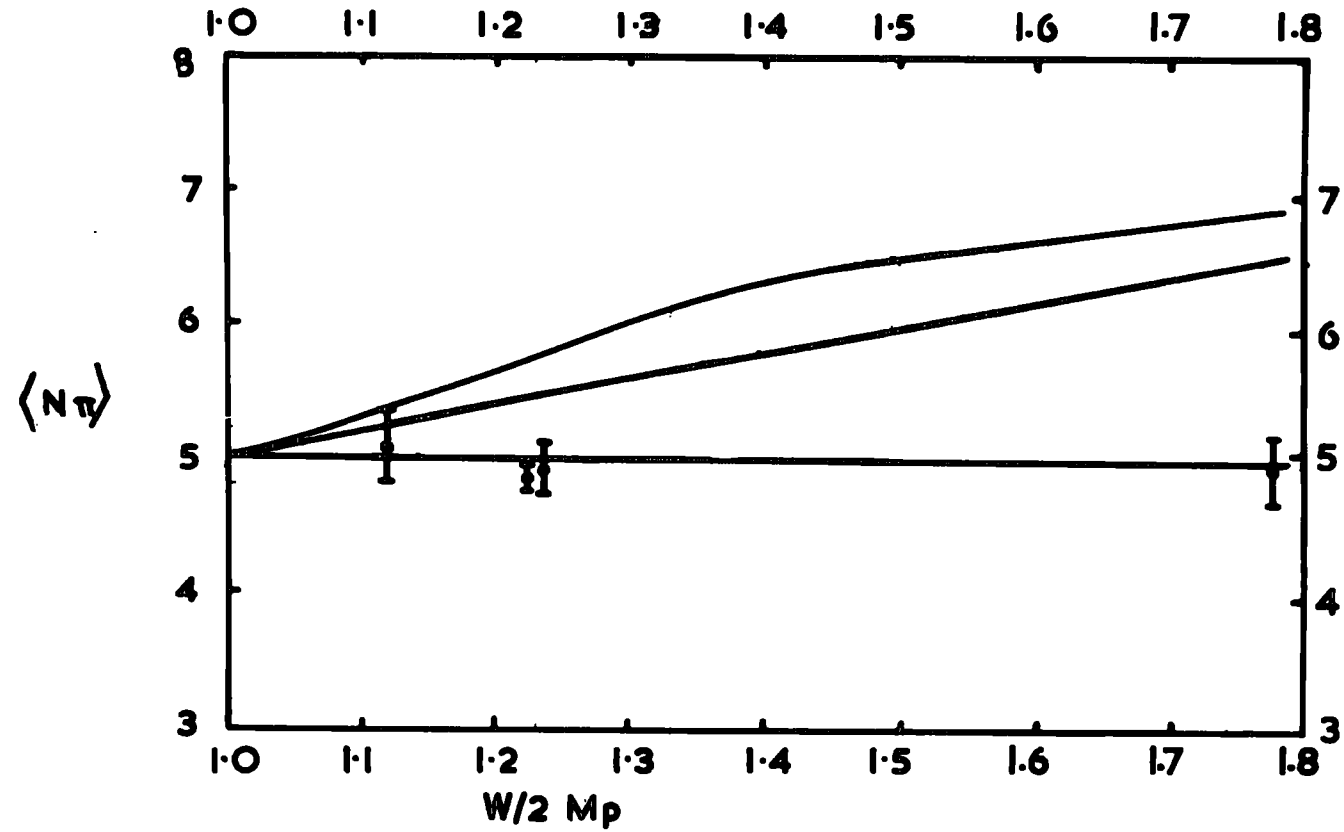

Figure 30. THE VARIATION OF AVERAGE PION MULTIPLICITY WITH W/2MP

FIGURE 81

COMPARISON OF EXPERIMENTAL AND PREDICTED MULTIPLICITIES FOR CHARGED PIONS

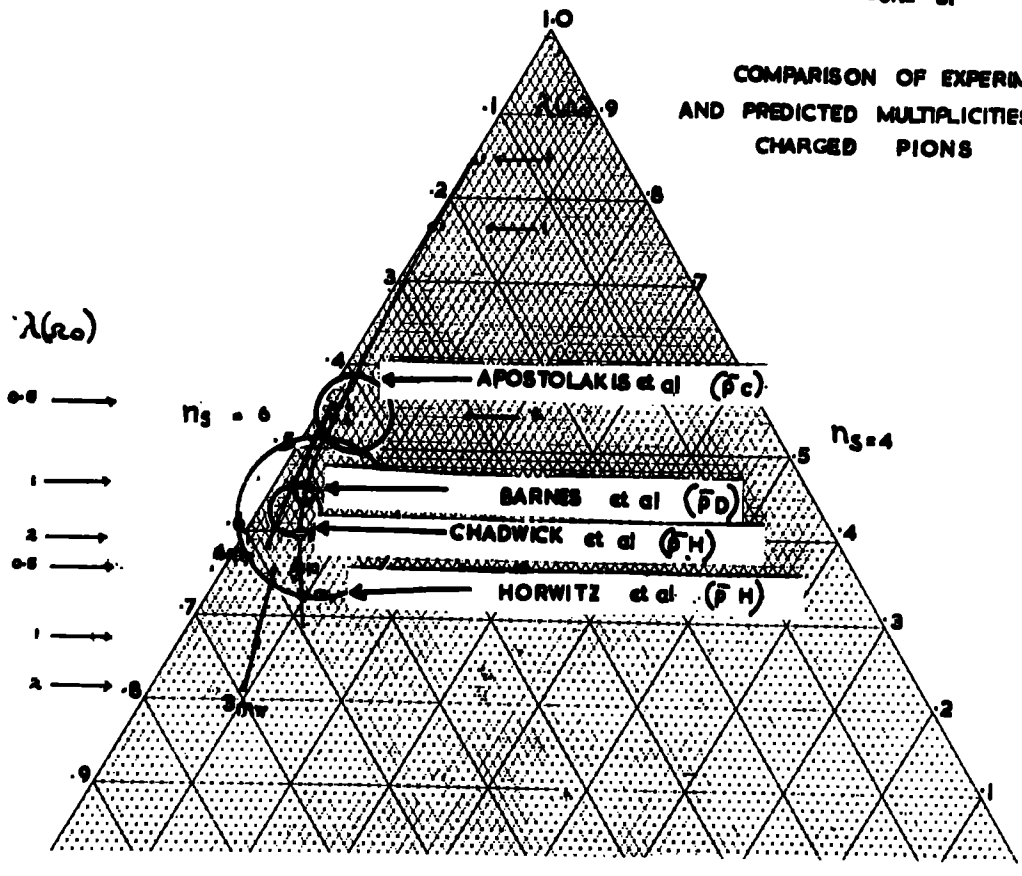

$7\Omega_0$. The results are also consistent with the calculations of Cerulus with resonance production of mass $4m_\pi$ in an interaction volume of Ω_0. However, if the experimentally observed resonances with masses 5-6 times the pion mass are introduced into the calculations an interaction volume of $(3\text{-}4)\Omega_0$ will probably be required.

The multiplicity distribution reported earlier in this thesis (Apostolakis et al.) for annihilation in the light elements of emulsion is seen to be inconsistent with the results from annihilations in hydrogen and deuterium. On the statistical model, these multiplicities are understood by reference to an interaction volume of $4\Omega_0$. Also, the agreement with the Koba and Takeda model is close.

The reason for discrepancy between the two sets of results has not been found. It may be due to the fact that annihilation in protonium occurs from S-state whereas in the light elements such as carbon, annihilation is from higher states. The conservation of angular momentum then leads to a reduction in multiplicity; the equivalent effect is an apparent reduction in the interaction volume.

A similar variation for annihilation in hydrogen in the interaction volume is observed at finite energies (McConnell and Shapiro, 1963). There, the variation is interpreted as a Lorentz contraction of the interacting volume. However, increase in energy is also associated with higher initial angular momentum, which, on the argument

above, would lead to an apparent reduction in the interacting volume.

On the other hand the Durham results are well accounted for by the Koba and Takeda model of annihilation and it is relevant to consider other successes with this model. In Figure 31 the observed variation of mean multiplicity of all mesons is shown and compared with the Koba and Takeda. model and the statistical model with a Lorentz invariant and a Lorentz contracted interaction volume of $7\lambda\!\!\!^{-}_{0}$. The agreement lies with the former model which predicts that multiplicity is independent of energy.

A feature of antiproton annihilation in flight is that the angular distribution of negative mesons is peaked in the forward direction in the centre of mass of the $p\bar{p}$ system and that of the positive mesons in the backward direction. On the Koba and Takeda model there is a natural explanation of this since the core-core annihilation is not supposed to affect the motion of the peripheral pion clouds which are free to proceed in their initial directions. A check of the Koba and Takeda model could be made by examining the centre of mass distribution of mesons from the annihilation of antiprotons in deuterium. On the protons there should be the forward/backward peaking described above, whereas on the neutron there should be forward peaking only.

Finally, whereas on the statistical model the K-meson production can be explained only by reducing the interaction

volume to one-tenth of its size for the pion production, the reduced production of K-mesons follows naturally from the Koba and Takeda model because of the smaller energy available in the smaller core-core annihilation volume.

In general it is concluded that the theory of Koba and Takeda gives a satisfactory picture of the nucleon-antinucleon annihilation.

ACKNOWLEDGMENTS

The author wishes to thank Professor G.D. Rochester for making available all facilities of the laboratory for this work and for his continued interest in its progress.

His grateful thanks are due to his supervisor, Dr. J.V. Major, whose constant guidance and help made this experiment successful and who spent long hours in helpful discussions at all stages of the work. It is a pleasure to thank Dr. A.J. Apostolakis and Mr. G.A. Briggs for their collaboration and many useful discussions. Thanks are due to Dr. A.D. Martin for his helpful criticism of some points in Chapter 2.

Mrs. Elizabeth Errington, Miss Kathleen McLellan, Miss Ann McKellar, Miss Thelma Jopling, Miss Janet Watson and Miss Carole Guyll are thanked for their help in scanning and in the drawing of figures. The help of Mr. R. White and Mr. B. Rowan in photographing the diagrams and of Mrs. P. Brooke in the preparation of the thesis at short notice is gratefully acknowledged.

Finally, the Tālim-ul-Islam College, Rabwah, and the British Council are thanked for study leave and a travel grant.

Appendix

A.1. Interactions of the secondary pions within the parent nuclei

The effect to be considered here is the change of charged multiplicity $n_s = M$, by absorption and charge exchange of charged pions and by charge exchange only of the neutral pions.

If the probability is P that a charged pion undergoes charge exchange or absorption in a nucleus then the probability that r out of M mesons will interact in this way in a single nucleus is given by

$$Pr(r) = {}^{M}C_{r} \left(\frac{P}{Q}\right)^{r} Q^{M}$$

where $Q = 1 - P$.

The charged multiplicity M is accompanied by a mean neutral multiplicity m. To calculate the probability that r neutral mesons will undergo charge exchange in a single nucleus the distribution of the neutral multiplicity for a given M is required. Since this is unknown it is assumed to follow the Poisson distribution. The probability can be shown to be given by

$$pr(r) = \frac{(mp)^{r}}{r} e^{-mp}$$

where p is the probability for charge exchange of a neutral meson in the nucleus.

The charged multiplicity is increased by the charge exchange of neutral mesons and reduced by the charge exchange and absorption of charged mesons. The probabilities that the charged multiplicity changes by $\Delta n_s = 0, \pm 1, \pm 2$ etc. are calculated by combining the probabilities for the two processes above.

The initial multiplicity distribution which is expected when an anti-proton annihilates in a large nucleus is given by mixing the multiplicities

for the odd and even white stars in the ratio of the neutrons to protons for the large nuclei.

The final multiplicity distribution is obtained by taking each charged multiplicity in turn and multiplying it by the probabilities that it will change by Δn_s and summing over all Δn_s and n_s. This is repeated for seceral values of the probabilities of charge exchange and absorption. The odd/even ratio is computed from the final multiplicity distribution. Its variation has been shown in Figure 8. The final multiplicity distribution has been shown already in Figure 9 for the probabilities of charge exchange and absorption expected in the experiment.

Appendix

A.2. Cross-section for charge exchange in a complex nuclei

It is assumed that within the nucleus the antineutrons are produced mainly in the forward direction by the antiprotons. After they are produced the antineutrons are attenuated with an absorption coefficient K in the nucleus and a mean free path λ in the target material. These are assumed to be equal to those for antiprotons.

The number of antiprotons (see Figure 32) entering nuclei of radius R at distance ρ, $\rho+d\rho$ from the centre is given by

$$N_o(\bar{p}) = 2\pi N \rho d\rho/\pi R^2$$

where N is the total number of antiprotons entering the nucleus. These are attenuated so that at distance x along the chord of length 2S the number is

$$N(\bar{p}) = 2N \rho d\rho \; e^{-Kx}/R^2$$

Consequently the number of antineutrons produced in dx is

$$N(\bar{n}) = N g \; 2 \rho d\rho \; K \; e^{-Kx} dx/R^2$$

where g is the probability of charge exchange per nucleon. The number of antineutrons escaping from the nucleus after attenuation along the chord is

$$N(\bar{n}) = 2g \; N \rho d\rho \; K \; e^{-Kx} \; e^{-K(2S-x)} dx/R^2$$

Integrating over the nucleus the number of antineutrons per incident antiproton is

$$F = [1 - (1+2KR + K^2R^2) \; e^{-2KR}] \; g/K^2R^2$$

$$= g \; C/K^2R^2$$

This fraction is also expressed as the ratio of the charge exchange cross-section to the geometrical cross-section. By

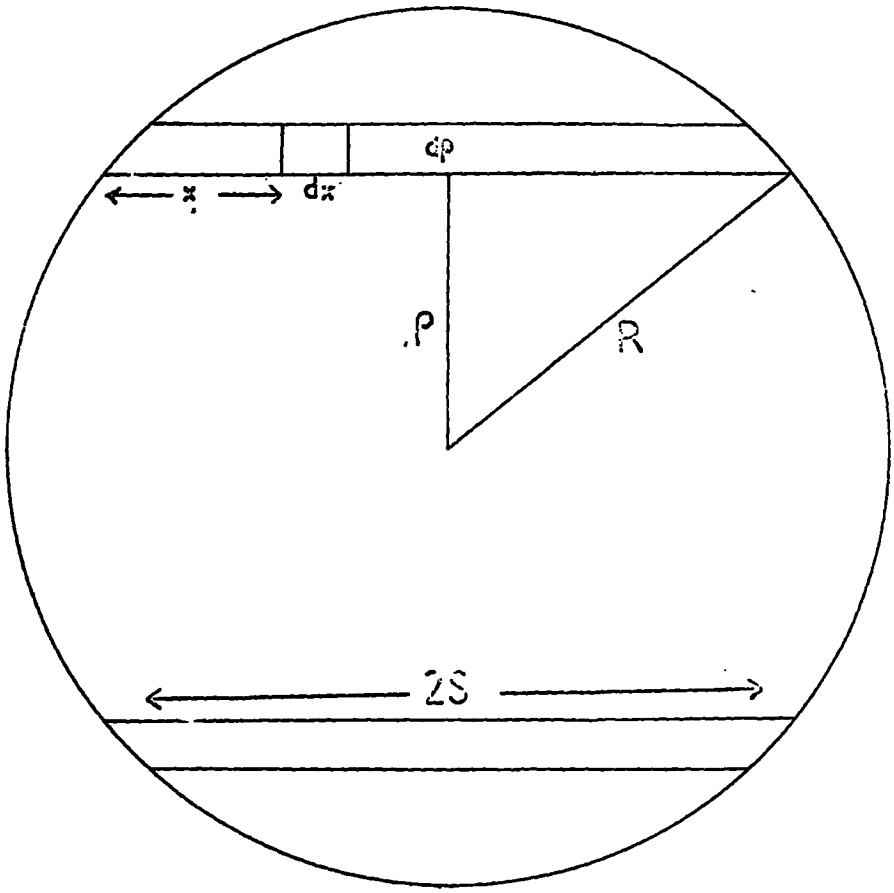

FIG. 32 The parameters of a complex nucleus

$$\text{i.e.} \quad \sigma_{c.e.} = \sigma_g F$$
$$= \pi g C/K^2$$

where $\sigma_g = \pi R^2$.

The probability, g, for charge exchange per nucleon is determined by the ratio of protons to neutrons in the nuclei since the predominant channel for charge exchange occurs on protons. If the probability is f on protons then in the nucleus

$$g = f\ Z/A \text{ to } 5\% \text{ accuracy}$$

so that finally

$$\sigma_{c.e.} = \pi f C Z/A K^2$$

This cross-section for carbon, silver and lead is plotted in Figure 20 for a range of values of the absorption coefficient K. The radii of nuclei have been assumed to be $r_o A^{\frac{1}{3}}$ where r_o is 1.35 fermis. The probability f, for charge exchange on the proton is 0.13 (from the literature) over a wide band of energies.

The relevant value of the absorption coefficient is calculated from

$$K = 3A\sigma/4\pi R^2 = 3\sigma/4\pi r_o^3$$

where σ is the cross-section for inelastic interaction of antiprotons in hydrogen. However according to Ball & Chew (1960), the inelastic cross-section in hydrogen is large by the "finite size" effect represented by the reduced de Broglie wavelength λ and the cross-section is $\pi (a_o + \lambda)^2$. Over the energy range (0 - 1) GeV a_o is constant at $1.08\ 10^{-13}$ cm (from a survey of the literature). Using πa_o^2 for the cross-section above the absorption coefficient is $3.6\ 10^{12}\ cm^{-1}$.

For this value of K, the cross-section for charge exchange in carbon

and in lead are 8.0 and 12 mb respectively. Experimental values are difficult to determine and few measurements have been made. However for antiprotons at 430 MeV, Button et al. (1957), the cross-sections in carbon and lead are $(4.0 \pm {}^{1.6}_{1.5})$ mb and $(3.8 \pm {}^{4.2}_{2.5})$ mb respectively. At 320 MeV, (Wenzel (1962)) the values in beryllium and carbon are (11^{+4}_{-5}) mb and (10^{+6}_{-7}) mb. Considering the experimental inaccuracies and the simplifying assumptions of the calculations, there is reasonable agreement between calculation and experiment. Consequently the calculations can be used to estimate the cross-section for charge exchange in the complex medium of nuclear emulsion.

To the extent that the absorption coefficient is constant the cross-sections for charge exchange in the complex nuclei of the elements in the emulsion are independent of energy. What energy dependence there is of the average cross-section arises from that of the hydrogen in the emulsion. At the mean energy of 125 MeV at which antiproton interactions take place in the present experiment the expected cross-section is 12 mb. In an inelastic interaction in emulsion this cross-section corresponds to a probability, P_c, that charge exchange will take place, of 3.1%. It is made up of 1.6% from the hydrogen of the emulsion, 0.7% from the other light elements (C ≡ N ≡ O) and 0.8% from the heavy elements (S, Br, Ag, I).

Appendix

A.3. Flux of antineutrons in the emulsion stack

If the energy dependence of the cross-section for charge exchange is ignored, the flux of antineutrons, N_x, at distance x down the antiproton beam in the emulsion is given by

$$N_x = P_c N_o x e^{-x/\lambda}/\lambda$$

where λ is the m.f.p. for interaction of the antinucleons. Since the cross-section for charge exchange increases towards the end of the range of the antiprotons (i.e. at low energies), N_x is an underestimate of the antineutron flux.

Appendix

A.4. Density of antineutron annihilations

At distance y beyond the end of the range, r, of the antiprotons, the number of antineutron annihilations per cm^3 is given by

$$N_{ann} \geq P_c \, N_o \, r \, e^{-r/\lambda} e^{-y/\lambda} / \lambda^2$$

where the inequality refers to the underestimation of flux in A.2. Substituting for P_c and the known values for this experiment

$$N_{ann} \sim 2 \text{ stars}/cm^3$$

in the region of scanning.

REFERENCES

Agnew, L., Elioff, T., Fowler, W.B., Lander, R., Powell, W.M., Segre, E., Steiner, H., White, H., Wiegand, C., Ypsilantis, T., 1960, Phys. Rev., 118, 1371.

Amaldi, E., Baroni, G., Bellettini, G., Castagnoli, C., Ferro-Luzzi, M., Manfredini, A., 1959, Il Nuovo Cimento, 14, 977.

Ajzenberg, F., and Lauritsen, T., 1955, Rev. Mod. Phys., 27, 77.

Amaldi, U., Fazzini, T., Fidecaro, G., Ghesquiere, C., Legros, M., Steiner, H., 1963, Il Nuovo Cimento, 30, 973.

Amaldi, U., Fazzini, T., Fidecaro, G., Ghesquiere, C., Legros, M., Steiner, H., 1964, Il Nuovo Cimento, 34, 825.

Apostolakis, A.J., Briggs, G.A., Khan, N.A., Major, J.V., 1965, Il Nuovo Cimento.

Armenteros, R., Combes, C.A., Cork, B., Lambertson, G.R., Wenzel, W.A., 1960, Phys. Rev., 119, 2062.

Ashmore, A., Cocconi, G., Diddens, A.M., and Wetherell, A.M., 1960, Phys. Rev. Letters, 5, 576.

Baker, G.A., 1960, Phys. Rev., 117, 1130.

Ball, J.S., Chew, G.F., 1958, Phys. Rev., 109, 1385.

Barbaro-Galtieri, A., Smith, F.M., Patrick, J.W., 1963, Phys. Letters, 5, 63.

Barkas, W.H., 1957, Il Nuovo Cimento, 8, 201-214.

Barkas, W.H., Birdge, R.W., Chupp, W.W., Expong, A.G., Goldhaber, G., Heckman, H.H., Perkins, D.H., Sandweiss, J., Segre, E., Smith, F.M., Stock, D.H., Van Rossum, L., Amaldi, E., Baroni, G., Castagnoli, C., Franzinetti, C., Manfredini, A., 1957, Physical Review, 105, 1037.

Barnes, V., Lai, K.W., Anninos, P., Gray, L., Haggerty, P., Harth, E., Kalogeropoulos, T., Zenoe, S., Bizzarri, R., Dore, V., Gialanella, G., Moneti, G., Guidnni, P., 1964, Private Communication.

Blair, J.S., 1958, Nuclear Phys., 6, 348.

Blau, M., and Oliver, A.R., 1956, Phys. Rev., 102, 489.

Button, J., Elioff, T., Segre, E., Steiner, H.M., Weingart, R., Wiegand, C., and Ypsilantis, T., 1957, Phys. Rev., 108, 1557.

Button, J., Eberhard, P., Kalbfleisch, G.R., Lannutti, J.E., Lynch, G.R., Maglic, B.C., Stevenson, M.L., Xuong, N.H., 1961, Physical Review, 121, 1788.

Cerulus, F., 1959, Nuovo Cimento, 14, 1959.

Chadwick, G.B., Durrani, S.A., Jones, P.B., Wignall, J.W.G., and Wilkinson, D,H., 1958, Phil. Mag., 3, 1193.

Chadwick, G.B., Davies, W.T., Derrick, M., Hawkins, C.J.B., Mulvey, J.H., Radojicic, D., Wilkinson, C.A., 1963, Physical Review Letters, 10,

Chadwick, G.B., Davies, W.T., Derrick, M., Hawkins, C.J.B., Mulvey, J.H., Radojicic, D., Wilkinson, C.A., Crest, M., Limentani, S., Santangelo, R., 1962, Proceedings High-Energy Physics Conference.

Chamberlain, O., Goldhaber, G., Jauneau, L., Kalogeropoulos, T., Segre, E., Silberberg, R., 1959, Physical Review, 113, 1615.

Condo, G.T., Hill, R.D., Martin, A.D., 1964, Physical Review, 133, A1280.

Cook, L.F., 1959, UCRL, 8841.

Coombes, C.A., 1958, UCRL, 8279.

Coombes, C.A., Cork, B., Galbraith, W., Lambertson, G.R., Wenzel, W.A., 1958, Phys. Rev., 112, 1303.

Cork, B., Lambertson, G.R., Piccioni, O., and Wenzel, W.A., 1956, Phys. Rev., 104, 1193.

Cork, B., Lambertson, G.R., Piccioni, O., Wenzel, W.A., 1957, Phys. Rev., 107, 248.

Cork, B., Dahl, O.I., Miller, D.H., Tenner, A.G., and Wang, C.L., 1962, Nuovo Cimento, 25, 497.

Dalitz, R.H., 1963, Annual Review of Nuclear Science, 13, 339.

Desai, B.R., 1960, Physical Review, 119, 1385. Ibid 1390

Ekspong, A.G., Frisk, A., Nilsson, S., Ronne, B.E., 1961, Nuclear Physics, 22, 353.

Ekspong, A.G., Ronne, B.E., 1959, Il Nuovo Cimento, 13, 27.

Elioff, J., Agnew, L., Chamberlain, O., Steiner, H.M., Wiegand, C., Ypsilantis, T., 1962, Physical Review. 128, 869.

Ferbel, T., 1963, Ph.D. Thesis, Yale University.

Fermi, E., 1950, Progress of Theoretical Physics, 5, 570.

Foley, K.J., Lindenbaum, S.J., Love, W.A., Ozaki, S., Russel, J.J. and Yuan, L.C.L., 1963, Phys.Rev.Letters, 10, 376.

Fulco, J.R., 1958, Physical Review, 114, 374.

Garron, J.P., Jacmart, J.C., Riou, M., Ruhla, C., and Teillac, J., 1962, Nuclear Physics, 37, 126.

Goldhaber, G., Fowler, W.B., Goldhaber, S., Hoang, T.F., Kalogeropoulos, T.E., Powell, W.M., 1959, Physical Review, 3.

Goldhaber, S., Goldhaber, G., Powell, W.M., Silberberg, R., 1961, Physical Review, 121, 1525.

Gooding, T.J., and Pugh, H.G., 1960, Nucl. Physics, 18, 46.

Heckman, M.H., Perkins, D.H., Betty, L., Sinon, W.G., Smith, F.M., Barkas, W.H., 1960, Phys. Rev., 117, 544.

Hillman, P., Tyrev, H., Maris, T.A.J., 1960, Phys. Rev. Lett., 5, 107.

Hinrichs, C.K., Moyer, B.J., Poimer, J.A., Ogden, P.M., 1962, Physical Review, 127, 617.

Horwitz, N., Millar, D., Murray, J., Tripp, R., 1959, Physical Review, 115, 472.

Kalbfleisch, G., 1961, UCRL, 9597.

Kalogeropoulos, T., 1959, UCRL, 8677.

Koba, Z., Takeda, G., 1958, Progr. Theor. Phys., 19, 269.

Lee, T.D., Yang, C.N., 1956, Il Nuovo Cimento, 3, 749.

Lindenbaum, S.J., Love, W.A., Niederer, J.A., Ozakis.,
Russel, J.J., Yuan, L.C.L., 1961, Physical Review, 7.

Longo, M.J., Helland, J.A., Hess, W.N., Moyer, B.J.,
Perez-Mendez, U., 1959, Phys. Rev. Letters, 3, 568.

Lynch, G.R., 1961, Reviews of Modern Physics, 33, 395.

McConnell, J., and Shapiro, J., 1963, Il Nuovo Cimento, 28,
1272.

Maglic, B.C., Kalbfleisch, G.R., Stevenson, M.L., 1961,
Physical Review, 7.

Martin, A.D., 1963, Il Nuovo Cimento, 27, 1359.

Nilsson, S., Frisk, A., 1958, Ark. . Pysik, 14, 277.

Papineau, A., 1956, J. Phys. Radium, 17, 566.

Pugh, H.G., Riley, K.F., 1961, Rutherford Jubilee Int. Conf.,
(Manchester).

Schwartz, M., 1961, Phys. Rev. Letters, 6, 556.

Segre, E., 1958, Annual Review of Nuclear Science, 8, 127.

Von Dardel, G., Frisch, D.H., Mermod, R., Milburn, R.H.,
Piroue, P.A., Vivargent, M., Weber, G., Winter, K.,
1963, Internal Report.

Wenzel, W.A., 1962, Proc. Aix-en-Provence Conference.

Xuong, N., Lynch, G., Hinrichs, C.K., 1961, Phys. Rev.,
124, 575.

Youtz, B., 1958, Ann. J. Phys., 26, 202.

PUBLICATIONS BY THE AUTHOR

The Annihilation of Antiprotons on Protons and Neutrons
(Nuovo Cimento 1965, in the press)
with A.J. Apostolakis, G.A. Briggs and J.V. Major.

The Production and Annihilation of Antineutrons in an Emulsion Stack
(submitted to Nuovo Cimento for publication)
with J.V. Major.

The Antiproton as a Nuclear Probe
(being submitted for publication)
with A.J. Apostolakis, G.A. Briggs and J.V. Major.